

Doctoral thesis

Doctoral theses at NTNU, 2023:271

Tanzima Habib

Image Appearance Reproduction Framework Using 2.5D Techniques

NTNU
Norwegian University of Science and Technology
Thesis for the Degree of
Philosophiae Doctor
Faculty of Information Technology and Electrical
Engineering
Department of Computer Science



Norwegian University of
Science and Technology

Tanzima Habib

Image Appearance Reproduction Framework Using 2.5D Techniques

Thesis for the Degree of Philosophiae Doctor

Gjøvik, September 2023

Norwegian University of Science and Technology
Faculty of Information Technology and Electrical Engineering
Department of Computer Science



Norwegian University of
Science and Technology

NTNU

Norwegian University of Science and Technology

Thesis for the Degree of Philosophiae Doctor

Faculty of Information Technology and Electrical Engineering
Department of Computer Science

© Tanzima Habib

ISBN 978-82-326-7242-4 (printed ver.)

ISBN 978-82-326-7241-7 (electronic ver.)

ISSN 1503-8181 (printed ver.)

ISSN 2703-8084 (online ver.)

Doctoral theses at NTNU, 2023:271

Printed by NTNU Grafisk senter

Abstract

Light plays a crucial role in the perception of the world around us, as it interacts with objects and stimulates our eyes to create visual images. Appearance is the result of human visual perception of the interaction of light with the surface of objects and is defined as the aspect of visual perception by which objects are recognised. One of the most easily quantifiable aspects of appearance is colour, which is represented by the CIE tristimulus values. This is the sum of the product of the spectral power distribution of light, the colour matching functions, and the reflectance or transmittance of an object. However, this limited perception of colour due to the response of only three types of cone cells in the retina can lead to metamerism, that is, when two objects with different reflectances can match in colour under one illuminant but not under another. Spectral reproduction is a solution to this issue, but spectral data is not always available, making spectral estimation an important area of research.

Understanding and measuring appearance attributes such as colour, gloss, translucency, and texture are important to control printer attributes that enable accurate object creation or accurate soft proofing. A generic 2.5D printing pipeline includes having a 3D surface model and its corresponding colour map and height map to print. The 3D surface structure is first printed primarily with white deposit, then colours are printed on top as the final layer with half-toning using ink deposition and drying by UV curing. The elevation of the surface is achieved by assigning the height map corresponding to the original 3D model. The number of ink layers required to print the elevated 3D structure layer by layer from the bottom to the top is quantified by slicing. The final colour printed on top uses the colour map and an ICC profile that converts the colour map values to printer colours through the ink separation employed, as is traditionally done for 2D printing. Colour management is currently carried out using a flat colour target that is printed, measured, and mapped to the printer colours, and this mapping is encoded inside the ICC profile. Such an ICC profile is also used for soft proofing in 2D printing.

The aim of this work is to establish a strong framework for spectral estimation as a means of reducing metamerism and its integration into existing colour management workflows and to design an appearance reproduction framework for 2.5D printing using the current colour management architecture called iccMAX.

Sammendrag

Lys spiller en avgjørende rolle i oppfatningen av verden rundt oss, da det interagerer med objekter og stimulerer øynene våre til å skape visuelle bilder. Utseende er resultatet av den menneskelige, visuelle oppfatningen av samspillet mellom lys og overflaten til objekter, og det defineres som aspektet av visuell oppfatning der objekter gjenkjennes. En av de lettest målbare aspektene ved utseendet er farge, som representeres av CIE-tristimulusverdier. Dette er summen av produktet til spektral-distribusjonen til lys, fargeblandingsfunksjonene og refleksjonen eller gjennomsiktigheten til et objekt. Alikevel kan denne begrensede oppfatningen av farge som resultat av responsen til bare tre typer tappceller i netthinnen føre til metameri, det vil si når to objekter med forskjellige refleksjoner kan ha samme farge under ett belyningsforhold, men ikke under et annet. Spektral reproduksjon er en løsning på dette problemet, men spektrale data er ikke alltid tilgjengelige, noe som gjør spektral estimasjon til et viktig forskningsområde.

Å forstå og måle egenskaper av utseende som farge, glans, gjennomskinnelighet og tekstur er viktig for å kontrollere printerattributter som muliggjør nøyaktig objektsjenkaping eller nøyaktig 'softproofing'. En generisk 2,5D-utskriftspipeline inkluderer en 3D-overflatemodell og dens tilhørende fargekart og høydekart for utskrift. 3D-overflatestrukturen blir først primært printet ut med hvitt materiale, deretter printes farger oppå som den siste laget med halvtone ved bruk av blekkskriver og tørking ved UV-herding. Høydeøkningen av overflaten oppnås ved å tildele høydekartet som samsvarer med den opprinnelige 3D-modellen. Antallet blekklag som kreves for å printe ut den forhøyede 3D-strukturen lag for lag fra bunnen til toppen, kvantifiseres ved 'slicing'. Den endelige fargen som skrives ut på toppen, bruker fargekartet og en ICC-profil som konverterer fargekartverdiene til printerfarger gjennom den brukte blekkskillerprosessen, slik det tradisjonelt gjøres for 2D-utskrift. Fargehandtering utføres for øyeblikket ved hjelp av en flat fargereferanse som printes ut, måles og tilordnes printerfargene, og denne tilordningen er kodet inne i ICC-profilen. En ICC-profil brukes også for 'softproofing'.

Målet med dette arbeidet er å etablere en solid ramme for spektral estimasjon som et middel for å redusere metameri og integrere det i eksisterende arbeidsflyter for fargehandtering, samt å utforme et rammeverk for gjengivelse av utseende for 2,5D-utskrift ved bruk av den nåværende fargehandteringsarkitekturen kalt iccMAX.

Acknowledgements

I am profoundly grateful for the invaluable guidance, support, and encouragement I have received throughout the course of my doctoral journey. This thesis would not have been possible without the contributions of numerous individuals, each of whom played a significant role in shaping both my academic and personal growth.

First and foremost, I extend my heartfelt gratitude to my main supervisor, Prof. Phil Green, whose unwavering dedication to research excellence has been a constant source of inspiration. Your insightful feedback, thoughtful discussions, patient guidance, and consistent availability for discussing new problems have been instrumental in shaping the direction of this research.

I also deeply appreciate the guidance provided by my NTNU co-supervisor, Associate Prof. Peter Nussbaum. Your expertise and insightful perspectives have significantly enriched my research, and I am sincerely grateful for the impromptu discussions you have generously shared.

I want to sincerely thank my co-supervisors Associate Prof. Daniel Nyström and Markus Barbieri for their valuable contributions and guidance during this research. Your expertise and willingness to engage in discussions have greatly influenced the depth and quality of this work.

I am incredibly thankful to my friends and family, who have provided unwavering support throughout this journey. Your encouragement, patience, and understanding have been my pillars of strength. I extend my heartfelt appreciation to my dear Mom and Dad for their boundless love and encouragement. My sister, Iffa, and brother, Sanu, have always been my sources of motivation and inspiration. I am also grateful to their better halves, Ashish and Snehal, for being a part of our family and contributing positively to my life.

To my nephews, Ryan and Kian, whose laughter and innocence provided moments of respite, thank you for reminding me of the joys in life. And to my cousin, Shaba, your constant support and words of encouragement have meant a lot to me.

I would also like to thank my friends and colleagues from the Colour Lab and ApPEARS group. To Greg, Agnese, Dipendra, Hilda, Fereshteh, Mekides, Vlado, Michele, Irina, Olga, Mathieu, Raed, Markus, Anuja, Federico, Siamak, Ali and so many more, especially some of whom have been enduring me since our COSI days, Aldo, Yoko, Luvin, Majid, Yen Ting, and honorary members David and Ram

for engaging in discussions, debating ideas, pondering about both life and work, helping in time of need and most importantly, sometimes 'wasting' time together. Special thanks to my friend Dona, whose patient management of the demanding and extended sessions of measurement acquisition is deeply valued.

To my childhood friends, Sush and Sonu, who have been with me through thick and thin, thank you for your constant friendship and for always keeping me grounded. To Shubhra, Anu & Anu and Gwari for always being there regardless of the distance or the time.

Finally, I would like to express my deepest gratitude to everyone who has touched my life in ways big and small.

Contents

Abstract	i
Sammendrag	iii
Acknowledgements	v
Contents	vii
Figures	xi
Tables	xiii
Code Listings	xv
Acronyms	xvii
1 Introduction	1
1.1 Motivation	2
1.2 Research Objectives and Research Questions	4
1.3 List of Publications	6
1.4 Thesis Organisation	7
2 Background	11
2.1 Colour Management in Printing	11
2.1.1 ICC version 5	13
2.2 Spectral Reproduction	14
2.2.1 Spectral Data Acquisition	14
2.2.2 Spectral Estimation Methods	16
2.3 Chromatic Adaptation	19
2.3.1 Sensor Adjustment Transforms	20
2.4 Appearance Reproduction in Printing	23
2.4.1 Bi-direction Reflectance Distribution Function	24
2.4.2 BRDF Data Acquisition	24
2.4.3 BRDF Models	25
2.5 Evaluation Metrics	26

3	Summary of the Included Articles	29
3.1	Core Contributions	29
3.1.1	Article II: Spectral Estimation: Evaluation and Application	29
3.1.2	Article III: Spectral Estimation: As a Sensor Adjustment Transform	32
3.1.3	Article VII: Colour Management of Material Appearance .	34
3.1.4	Article VIII: 2.5D Printing: A Framework for Appearance Reproduction of Printed 3D Surfaces	36
3.2	Supplementary Contributions	38
3.2.1	Article I: Spectral reproduction: drivers, use cases and workflow	38
3.2.2	Article IV: Estimation of BRDF Measurements for Printed Colour Samples	40
3.2.3	Article V: BRDF rendering by interpolation of optimised model parameters	42
3.2.4	Article VI: Implementing directional reflectance in a colour managed workflow	45
3.2.5	Article IX: A weighted goodness-of-fit metric for comparison of spectra	47
4	Research Contributions	49
4.1	Fundamental Contributions to the Field of Research	49
4.2	Additional Contributions to the Field of Research	50
5	Discussion and Conclusion	53
5.1	Research Objective: Spectral Reproduction	53
5.2	Research Objective: Rendering Material Appearance	57
5.3	Research Objective: Appearance Reproduction Framework	58
5.4	Conclusion	59
5.5	Future Scope	61
	References	65

Included Papers

Article I	77
Article II	83
Article III	101
Article IV	115
Article V	123

Article VI	131
Article VII	137
Article VIII	161
Article IX	183
Appendix A Oral Contributions	193
A.1 Spectral Reproduction	193
A.2 iccMAX BRDF Implementation	199
A.3 Calculator Element Programming	205
Appendix B iccMAX Profiles in XML	213
B.1 iccMAX Profiles for Spectral Estimation	213
B.2 iccMAX Profile for BRDF Rendering	215
Appendix C Additional Documents	217
C.1 Requirements Document	217

Figures

1.1	Diagrammatic representation of thesis organisation	8
1.2	Deliverables planned in the Ph. D. proposal at the initial stage . .	9
1.3	Courses planned in the Ph. D. proposal at the initial stage	10
1.4	Trainings planned in the Ph. D. proposal at the initial stage	10
2.1	2D printer pipeline	12
2.2	2.5D printer pipeline	12
2.3	2.5D printed colour samples.	13
2.4	Metamerism	14
2.5	Corresponding colour match	20
2.6	Bidirectional Reflectance Distribution Function	24
3.1	A practical appearance reproduction framework for 2.5D printing.	37
3.2	iccMAX Appearance Rendering Workflow	47
4.1	The official cover of the book, <i>Fundamentals and Applications of Colour Engineering</i>	50
5.1	Appearance reproduction framework for 2D printing	59
5.2	Appearance reproduction framework for 2.5D printing	59
5.3	Status of deliverables that were planned in the Ph. D. proposal at the initial stage	62
5.4	Status of courses that were planned in the Ph. D. proposal at the initial stage	63
5.5	Status of trainings that were planned in the Ph. D. proposal at the initial stage	63

Tables

2.1	Polynomial expansion	18
3.1	Description of spectral reflectance datasets	30
3.2	Colour difference in appearance reproduction framework	37
5.1	Results of Spectral Estimation Methods as a MAT	55
5.2	Results of the spectral estimation methods and other SATs in predicting corresponding colours.	57

Code Listings

B.1	A2B and B2A Tags of an iccMAX Profile for Spectral Estimation using PCA	213
B.2	A2B and B2A Tags of an iccMAX Profile for Spectral Estimation using Third Order Polynomial	214
B.3	M2B Tag of an MVIS iccMAX Profile for encoding isotropic inplanar BRDF model	215

Acronyms

- ASTM** American Society for Testing and Materials. 3
- BRDF** bidirectional reflectance distribution function. ix, xv, 3–6, 15, 23–26, 35–38, 40–47, 49–51, 57–63, 215
- BTF** bidirectional texture function. 4
- CAT** chromatic adaptation transform. 20, 22, 23, 32, 33, 49, 54–56, 60
- CI** Combined Index. 48, 50
- CIE** Commission Internationale de l'Éclairage. *Glossary:*
- CIE** Commission internationale de l'éclairage. 3, 15, 26, 33
- CII** Colour Inconstancy Index. 27, 48
- CSEM** Swiss Center for Electronics and Microtechnology. 1
- HVS** human visual system. 3, 19
- ICC** International Color Consortium. 4–6, 8, 12–14, 20, 23, 24, 31, 34, 35, 38, 43–46, 50, 51, 54, 58–62
- MAT** material adjustment transform. 20, 22, 32–34, 49, 54–56, 60
- MCS** Multiplex Connection Space. 35, 46, 58
- MID** Multiplex Identification. 35, 36, 46
- MVIS** Multiplex Visualisation. 35, 36, 46
- NRMSD** normalised root mean square difference. 42, 57, 58
- OBA** optical brightening agents. 31, 33, 54
- PCA** principal component analysis. xv, 16, 17, 30, 31, 213

PCS profile connection space. 5, 11–13, 31, 34, 43, 46, 53, 54, 60, 61

RMSE root mean square error. 27, 30, 31, 48

SAT sensor adjustment transform. 7, 20, 32, 34, 54, 56

SCI Spectral Comparison Index. 27, 48

SI Smoothness Index. 27, 48

SPD spectral power distribution. 16, 17

UV Ultraviolet. 4, 14, 15

Chapter 1

Introduction

Printing technology has evolved significantly over the past century, with the advent of digital printers such as dye sublimation, laser, and inkjet printers. These 2D printing technologies have been gradually developing since the 1920s. In the 1980s, around the same time as inkjet printers, additive manufacturing emerged as a new technology for creating 3D objects through the deposition and fusion of material layer by layer. 3D printed objects are complex in geometry and are mainly used to create functional parts rather than to create fine textures with mixed colours [1]. However, recent developments in 3D printing technology, such as Mimaki [2] and Stratasys' [3] full-colour 3D printers and printing processes, have enabled the creation of more detailed and visually appealing 3D printed objects. While 3D printing has revolutionised the manufacturing industry, it is primarily used for creating functional parts with complex geometries, rather than for reproducing fine textures with mixed colours. In addition, 2.5D printing technology has emerged as a viable option for reproducing textures and tactile images on flat substrates, such as reproducing artwork. One potential advantage of such technologies is that they can help reduce production costs and material waste by creating objects on demand and with customised designs and dimensions. Thus, apart from printed products being functional, it is also essential to achieve accurate colour and appearance for their aesthetic value.

In 2.5D printing, the colourful 3D surface is created on a substrate only to a small height of around 1-10mm. Canon Océ uses this method of inkjet printing in which UV curing of resins/inks is carried out along each pass, and the variable surface is created using information from a height map [4]. Mofrel, the 2.5D printer introduced by Casio, is a 16 million-colour inkjet that prints on digital sheets containing a layer of micropowder between the inkjet layer and the paper [5, 6]. The Swiss Center for Electronics and Microtechnology (CSEM) team developed a method that prints lines with smoother features and at a specific height by depositing the ink in spherical droplets, called pinning caps, which then form liquid bridges made of ink [7]. Mimaki introduced the JFX200 series, in which its texture-maker software is used to create a smoother surface with stepped layers of the printed surface [8]. There are also case studies where the printing

apparatus could be modified to replicate textures that mimic a brush stroke or wood grain rather than creating the shape with ink dots. An example of such 2.5D printing used for appearance reproduction is a study in which trials have been carried out to reproduce an image of a waterlily based on how an artist will paint the waterlily with different brush strokes [9]. This was achieved by vector-driven 2.5D printing, where vectors are analogous to brush strokes, along with nonphotorealistic rendering, where computational methods are used to process and segment a digital image and render it with an artistic expression.

The appearance of printed objects can vary depending on the technology used. Factors such as the number of cured ink layers, substrate properties, white and black points, ink mixing process, number of passes, halftoning process, and more, all play a role in determining the final appearance quality and durability. As a result, there is a challenge to improve the existing colour management architecture that has been used in 2D printing for so long, in order to develop a 2.5D appearance printing framework. The primary challenge is characterising changes in appearance with respect to changes in slope. In recent years, research focused on matching/improving the appearance of 2.5D printing has gained momentum, with the goal of using the technology to manufacture products where aesthetics and appearance perception are crucial. Likewise, this project aims to develop a framework for appearance reproduction in 2.5D printing.

This Ph.D. project is part of the ApPEARS project funded by the European Union and hosted by the Norwegian University of Science and Technology, Gjøvik, with participation from several beneficiaries. FOGRA in Munich provided 2D printed samples and assisted with measurements, while Canon is one of the partner organisations that contributed to the printing of 2.5D samples. Additionally, Barbieri Electronic snc/OG in Italy and Linköping University in Sweden are other partners and beneficiaries, respectively, who are co-supervising this Ph.D. programme. The project aims to explore a framework for appearance reproduction in 2.5D printing and to identify ways to integrate it into the existing colour management system.

This chapter sets the narrative of the work and introduces briefly the research carried out through the Sections 1.1 Motivation, 1.2 Research Aims and Research Questions, 1.3 List of Publications, and 1.4 Thesis Organisation.

1.1 Motivation

"Such is the importance that light is the only human response that has an associated SI Unit, the candela."

Pointer's quote [10] above emphasises the importance of light and its role in illuminating objects and how it bounces and stimulates our eyes, thus letting us perceive the world around us. Appearance is the result of human visual perception

of the interaction of light with the material surface. It is defined by ASTM and CIE as the aspect of visual perception by which objects are recognised [11, 12]. The appearance of an object, in general, implies the colour of an object, which is the most easily quantifiable aspect of appearance. Colour represented by the CIE tristimulus values is the sum of the product of the spectral power distribution of light, the colour matching functions, and the reflectance or transmittance of an object. This simulates and quantifies our colour perception, which is limited to the response of the three types of cone cells found in the retina. This limitation in turn leads to metamerism, i.e. two objects with different reflectances can match in colour under one illuminant but mismatch under another illuminant. Metamerism is a major issue in any colour reproduction workflow where an image reproduced should match the original under different lighting conditions. Therefore, there has always been interest in the handling of colour workflows through spectral reproduction [13–17]. In a spectral reproduction workflow, the most essential component is spectral data which is not always available. Hence, the first motivation for this work is to establish a strong framework for spectral estimation as a means of reducing metamerism and its integration into existing colour management workflows.

However, in reality, appearance is a complex product of many attributes. Therefore, the concept of total appearance has been introduced, which comprises measurable visual attributes to define the appearance of an object [10]. In addition to colour, important attributes or optical properties that are measurable to a certain degree, as recognised by the CIE, are gloss, translucency, and texture [18]. The simplest and most frequently used method to measure gloss is using a gloss metre that quantifies the amount of light reflected from a surface at a particular specular angle [18]. After colour, gloss has been extensively studied and understood. Modelling the bidirectional reflectance distribution function (BRDF) of a material surface can also give information about gloss by studying the specular lobe. Although there are known methodologies to characterise gloss, it is not yet standardised, and linking gloss measurements with gloss perception is an ongoing topic [19–21]. Both translucency and surface texture are optical properties that are challenging to define and measure. Translucency is the property that makes an object fall between the extremes of opacity and transparency [18]. Due to subsurface scattering, how an object reflects, transmits and scatters light and the relationship among these three mechanisms [10] affect the appearance of colour and result in the perception of translucency. Gigilashvili et al. carried out a comprehensive review of the current state of understanding translucency and highlighted that the visual cues by which the human visual system (HVS) decodes translucency are fundamentally different for see-through objects (more transparent) and highly scattering objects (more translucent) [22]. Over the years, multiple factors have been identified that contribute to translucency perception, but tying them together into a unified translucency framework is a far too challenging task [22]. The texture of the surface of an object is related to perceived spatial variation [23]. Various factors such as homogeneity, uniformly

arranged smaller structures or patterns, locally variable reflectance, resolution scale, region, etc. of an object give rise to the perception of surface texture [24]. Therefore, texture has to be measured over an area where the smaller patterns that create the sensation of a particular texture are encompassed. Spatially varying BRDF or bidirectional texture function (BTF) are used to capture and model the surface texture [24–26]. These appearance attributes influence each other and are important to understand and measure to characterise and control printer attributes that enable accurate object creation or accurate soft proofing.

A generic 2.5D printing pipeline includes having a 3D surface model and its corresponding colour map and height map to print. The 3D surface structure is first printed primarily with white deposit, then colours are printed on top as the final layer with half-toning using ink deposition and drying by UV curing. Elevation of the surface is achieved by assigning the height map corresponding to the original 3D model. The number of ink layers required to print the elevated 3D structure layer by layer from the bottom to the top is quantified using slicing [27]. The final colour printed on top uses the colour map and an ICC profile (defined by the International Color Consortium (ICC)) that converts the colour map values to printer colours through ink separation employed, as is traditionally done for 2D printing. That is, colour management is currently carried out using a flat colour target which is printed, measured, and mapped to the printer colours, and this mapping is encoded inside the ICC profile. Such an ICC profile is also used for soft proofing in 2D printing, where, by applying the ICC profile to the input image, the pixel values are mapped to the printer colours within the gamut. Soft proofing in 2D printing is already well established and has defined standards such as ISO 3664, ISO 12646 and ISO 14861 [28–30]. But soft proofing of a 3D surface requires more than just mapping diffuse colours of flat targets. The colour management process has to take into account the possible change in the appearance of colours printed on a 3D surface having different slopes or surface normals where different printing parameters are affected by the stacking of stepped layers to create these slopes. To generate a more realistic soft proof for the viewer, rendering solutions using colour management have to also consider how the appearance of colour is changing based on the direction of the light and the view to the surface normal of the 3D structure. Well-designed soft proofs of printed objects can help the viewer preview and adjust to the desired look, visualise the limited printable gamut, reduce material waste and the cost of production. Therefore, the second motivation is to design an appearance reproduction framework using the current colour management architecture called iccMAX [31].

1.2 Research Objectives and Research Questions

The two main goals as discussed in the previous section are to establish a framework for spectral estimation as a means to handle metamerism in existing colour management workflows and to design a colour management integrated frame-

work of appearance reproduction for 2.5D printed surfaces. To accomplish these goals, the following research objectives have to be addressed.

- **Investigate the efficacy of various spectral estimation methods in handling metamerism and develop a framework for spectral estimation in a colour management workflow.**

Twenty years ago, Rosen explored spectral reproduction and the possibility of a spectral colour management system [32]. Over the years, many spectral reproduction workflows have been developed, e.g., for ink separation, gamut mapping, image reproduction, etc. [14, 33, 34]. But until now, the requirements for spectral reproduction in colour management have not been standardised or realised. This is partly due to the fact that until recently ICC colour management could only use colorimetric PCS, allowing only one standard viewing condition [35]. ICC.2 has now made it possible to have ICC profiles with a spectral PCS and the possibility of including variable viewing conditions [31]. Moreover, a spectral reproduction workflow depends on spectral data. However, spectral data are not readily available and, therefore, require spectral estimation of available colorimetric data. Therefore, finding a suitable spectral estimation method is essential with the aim of integrating it into colour management. Another requirement is to evaluate the accuracy of the reconstructed spectra and its role in minimising metameric mismatch.

- **Investigate rendering of material appearance in 2.5D printing.**

Material appearance of a 3D or elevated surface created by 2.5D printing is affected by different printer attributes such as type of inks used, layering of the inks, ink droplet size, half-toning and ink separation algorithms, curing time of the inks, printmode, etc. [36, 37]. We limit the scope of this work to investigating two material appearance attributes - colour and gloss, and how they are affected because of 3D surface creation with different ink mixes and along different slopes in 2.5D printing. There are many empirical or physical optics-based models available to characterise the material appearance of a surface [38, 39]. Measurement and modelling of BRDF of a surface give important information on how the colour appearance and specular highlight (related to surface roughness) change in different lighting and viewing directions. Such a model can be exploited to characterise the appearance of a 2.5D printed surface that spatially varies in colour of ink mixes and slopes.

- **Design an appearance reproduction framework for 2.5D printing using the current colour management architecture, iccMAX.**

ICC.2 also provides BRDF support to communicate the necessary information related to the appearance of a surface [31]. It also allows us to include texture information in an ICC profile in the form of a height map or a normal map. However, this information is included so that external software can use and process the information. To render appearance through an ICC profile, a new appearance reproduction framework must be developed, where the BRDF

information is processed and the output is rendered under the desired lighting conditions. In this work, we develop the framework to render the appearance of 2.5D printed surfaces which will serve as soft proofing through colour management in 2.5D printing.

We then ask the following research questions related to each of the research objectives:

1. Why is spectral reproduction of colour important and what are its use cases and requirements? How to obtain spectral data required for spectral reproduction from easily available colorimetric data? What is the performance of spectral estimation methods in minimising metameric mismatch? How can spectral processing be achieved through the current colour management architecture?
2. How to model the material appearance for a 2D printed surface? Can a workflow be developed to predict the appearance of any given mix of inks in 2D printing? Can a similar workflow be developed to predict appearance of a 2.5D printed surface where it also spatially varies in height? What is the performance of this workflow in reproducing colour and gloss?
3. How to define a BRDF model inside an ICC profile? How can the appearance reproduction framework of a 2.5D printed surface be integrated into colour management? What are the requirements of a data exchange format for such a framework?

1.3 List of Publications

This work includes four core articles, **Articles II, III, VII and VIII**, highlighted in bold in List 1.3, which address all research objectives and find answers to the research questions stated above. Articles I, IV, V, VI, and IX are supplementary contributions that relate to an intermediate requirement of the above research objectives. All articles play a crucial role in the overall discourse of this work, and their order of narration as shown in List 1.3 below corresponds to the manner in which the supplementary articles support and lead to the core contributions that result in the attainment of each research objective. The overview of these articles in relation to the research objectives is shown in figure 1.1 and this is explained in the next section 1.4. The summary of each of these articles can be found in Chapter 3. The core contributions, articles II, III and VIII are under review in scientific journals, and article VII is a chapter in ‘Colour Engineering: Fundamentals and Applications’, under production. Articles I, IV, V, VI, and IX are published in the conference proceedings.

- Article I: T. Habib, P. Green and P. Nussbaum, ‘Spectral reproduction: drivers,

- use cases and workflow,' *Electronic Imaging*, vol. 32, pp. 1–6, 2020
- **Article II: T. Habib, P. Green and P. Nussbaum, 'Spectral estimation: Evaluation and Application (Under Review),' *Optics Express*, 2023**
 - **Article III: T. Habib, P. Green and P. Nussbaum, 'Spectral estimation: As a Sensor Adjustment Transform (Under Review),' *Optics Express*, 2023**
 - Article IV: T. Habib, P. Green and P. Nussbaum, 'Estimation of BRDF Measurements for Printed Colour Samples,' vol. 29, pp. 123–128, 2021
 - Article V: T. Habib, P. Green and P. Nussbaum, 'BRDF rendering by interpolation of optimised model parameters,' in *Color and Imaging Conference*, Society for Imaging Science and Technology, vol. 28, 2020, pp. 162–168
 - Article VI: T. Habib, P. Green and A. Sole, 'Implementing directional reflectance in a colour managed workflow,' in *London Imaging Meeting*, Society for Imaging Science and Technology, vol. 1, 2020, pp. 119–123
 - **Article VII: T. Habib, 'Colour Management of Material Appearance,' in *Colour Engineering: Fundamentals and Applications (Under Production)*, P. Green, Ed., John Wiley & Sons, 2023**
 - **Article VIII: T. Habib, P. Green and P. Nussbaum, '2.5D Printing: An Appearance Reproduction Framework for Printed 3D Surfaces (Under Review),' *Journal of Imaging Science and Technology*, 2023**
 - Article IX: T. Habib, P. Green and P. Nussbaum, 'A weighted goodness-of-fit metric for comparison of spectra,' in *Sensing Colour; Proceedings of the International Colour Association (AIC) Conference 2022*, International Colour Association, 2022, pp. 397–404

1.4 Thesis Organisation

Figure 1.1 is a diagrammatic representation of the articles included in this work and how they are related to the research objectives. The articles are divided into two groups; Articles I-III answer research questions related to spectral reproduction, and Articles IV-VIII answer research questions related to appearance reproduction in 2D and 2.5D printing. The oval shape represents a framework, and rectangular shapes are the essential components of the framework. Components that are useful to another component are connected by an arrow. Articles are shown with shaded boxes that contain the components or frameworks to which they contribute.

Article I reviews spectral reproduction in the field of colour imaging and highlights different components required in a spectral reproduction system, e.g. spectral data and spectral estimation. **Articles II & III** evaluate various existing spectral estimation methods and show that a priori knowledge-based spectral estimation methods can be used to minimise metameric mismatch and produce a comprehensive comparison of their performance as a SAT.

Articles IV and V investigate BRDF data or measurement estimation, and BRDF modelling, and describe a workflow to predict BRDF parameters for ink mixes or

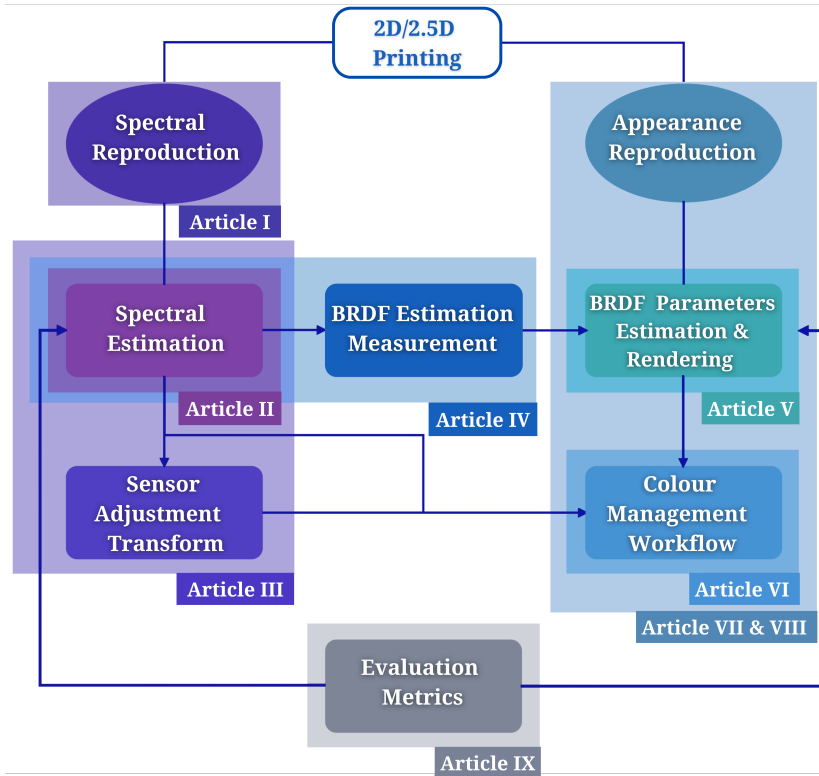


Figure 1.1: Diagrammatic representation of thesis organisation

colours in 2D printing. Article VI shows a paradigm for encoding and processing BRDF in an ICC profile and obtaining a rendered output. **Article VII** is a chapter on *Colour Management of Material Appearance* that culminated as a result of all theoretical and experimental studies carried out related to the material appearance reproduction and its application using the current ICC colour management architecture. **Article VIII** uses the knowledge gained so far and extends it to answer the complexities of rendering a 2.5D surface appearance and proposes an appearance reproduction framework for 2.5D printing.

Article IX proposes a new metric that is an adjustable composition of existing spectral and colorimetric metrics to assess the quality of results from spectral estimation methods. The existing metrics mentioned in the article are also essential for evaluating spectral estimation methods and for the optimisation and evaluation of BRDF models.

Figures 5.3, 5.4 and 5.5 summarise the tasks I planned to carry out during this Ph. D. work. They are divided into deliverables, courses and trainings to complete.

Their status will be addressed in Chapter 5 where I summarise the conclusions of this work.

Work Plan No.	Goal	Deliverable	Dissemination
WP1	Literature study	<ul style="list-style-type: none"> Documenting review on chromatic adaptation transforms and spectral reproduction methods and use cases. "Spectral reproduction: Drivers, use cases, and workflow.", paper submission to Electronic Imaging 2020. 	Yes
WP2	Spectral estimation method and evaluation	<ul style="list-style-type: none"> New method to evaluate the accuracy of a spectral estimation method. Paper submission about spectral estimation method for colour management in a conference. 	Yes
WP3	Appearance modelling using iccMAX and evaluation	<ul style="list-style-type: none"> Reflectance models and other appearance attribute models implementation using iccMAX. Paper on implementing and visualising reflectance models using iccMAX and submission to London Imaging Meeting 2020. 	Yes
WP4	Appearance reproduction framework and colour management	<ul style="list-style-type: none"> An appearance reproduction framework for 2.5D printing. Evaluation of reproduction using psychophysical experiments and objective quality metrics. Paper submission on topic of 2.5D appearance reproduction framework to a journal. 	Yes
WP5	File format for 2.5D appearance reproduction framework	<ul style="list-style-type: none"> Introduction of file format to store spectral data, and appearance attributes in the colour management system. 	—
WP6	Thesis writing	<ul style="list-style-type: none"> Documentation of the prototypes created, and final PhD thesis compiled. 	Yes

Figure 1.2: Deliverables planned in the Ph. D. proposal at the initial stage

Chapter 2 provides the theoretical and methodological background used in the research conducted to achieve the objectives of this work. In Chapter 3, a summary of each article is presented, including its purpose, methods, and results. Chapter 4 highlights the research contributions made throughout the course of this Ph.D. study. Furthermore, Chapter 5 discusses the results and analysis of these articles, explaining how they address the research objectives and answer the research questions. This chapter also presents the conclusions drawn from the research conducted in these articles and the future scope of this work.

Course Name	ECTS	Level	Semester	Location
Research Ethics	2.5	Ph. D.	S 2020	Gjøvik
Colour Science	5	Ph. D.	S 2020	Gjøvik
Colour Imaging	7.25	Ph. D.	S 2020	Trondheim
Scientific Communication	5	Ph. D.	S 2022	Gjøvik
Four training schools as part of ApPEARS	10*	Ph. D.	S 2020 to A 2022	Gjøvik, Darmstadt, Paris, Bristol

1. S 2020 = Spring semester 2020 2. A 2022 = Autumn semester 2022

Figure 1.3: Courses planned in the Ph. D. proposal at the initial stage

Code	Course Name	Partners	ECTS	Location
TE1	Imaging and quality – from colour to appearance	NTNU	4	Gjøvik
TE2	Material appearance workflow	FHG	2	Darmstadt
TE3	Metrology for appearance	CNAM	2	Paris
TE5	Printing innovation and applications	UWE	2	Bristol

1. FHG = Fraunhofer-Gesellschaft 2. CNAM = National Conservatory of Arts and Crafts
3. UWE = University of the West of England

Figure 1.4: Trainings planned in the Ph. D. proposal at the initial stage

Chapter 2

Background

2.1 Colour Management in Printing

Colour management in an imaging pipeline is important for consistent and accurate colour reproduction of a target image through different devices such as camera, scanner, printer, projector, monitors, etc. It is defined as the means of controlling and adjusting colours through hardware, software, and processes across multiple devices within an imaging pipeline [49]. Each colour imaging device has its own characteristic way of reproducing colours and is limited by the extent of unique colours they can reproduce. This variability among devices is efficiently handled by modern colour management by creating colour profiles for each device that allow them to communicate through a device independent colour space called the profile connection space (PCS) which is either CIELAB or CIE XYZ. The colour management of a device requires two important steps, calibration and characterisation. Calibration is the adjustment of the device to a known state so that a consistent and reproducible device colour response is achieved. It helps correcting for system drifts and manufacturing variations. It is the essential first step. Colour characterisation is the mapping between the device colours and the PCS. In printing, this mapping can be achieved by physical models (e. g., Neugebauer, Murray-Davies, Kubelka-Munk), empirical models (e. g., polynomial transforms, neural network) and look-up tables [50]. The forward characterisation model maps the device colours to the PCS while the inverse characterisation model maps the values of the PCS to the device colours. In this case, gamut mapping is also essential to ensure that out-of-gamut colours are adjusted to colours within the gamut of the device. A generic inkjet printer pipeline consists of converting image colours to device colours through the PCS. As shown in Figure 2.1, colour separation, linearisation, and halftoning are applied to the device colours to lay the final pattern of ink drops on the substrate. The ink layers are dried to harden them firmly to the substrate.

The 2.5D printing pipeline, instead of printing in monolayers of inks, has to build a 3D structure on the flat substrate with layers of voxels of white deposit and

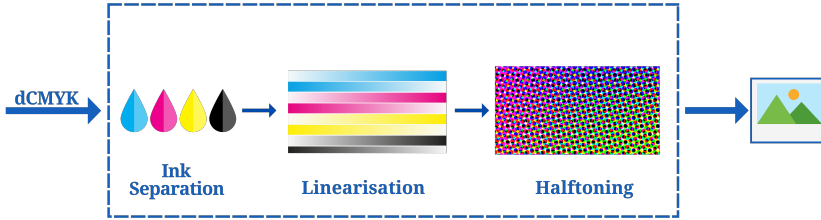


Figure 2.1: A 2D printing pipeline.

then apply the halftoned ink to create colour on the final layer. A generic 2.5D printing pipeline is shown in Figure 2.2 where the slicer uses the 3D model of the object, height map, colour map, and ICC profile to decide the number of layers required to build the base structure including the final colour layer on top using halftoning. After the colour is printed, an optional varnish layer can be applied. In this case, the printer colour characterisation step is similar to 2D printing where a flat colour target is printed, measured and modelled.

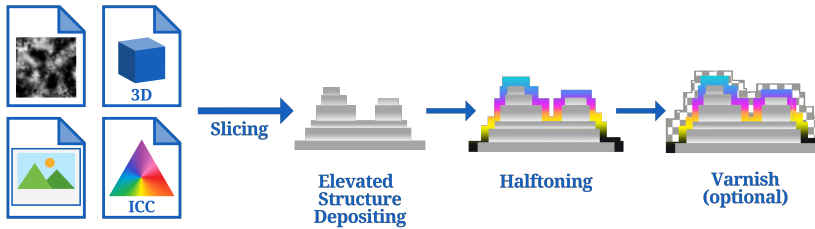


Figure 2.2: A 2.5D printing pipeline.

In Article VIII, the colour samples were printed using a 2.5D inkjet printer on a flat substrate and four different slopes with angles of 15° , 30° , 45° , and 60° . On each slope including the flat target, a total of 72 colour patches of the FOGRA Media Wedge CMYK V3.0 were printed, as illustrated in Figure 2.3. Details of the printed samples are given in Requirements Document in Appendix C.

The International Color Consortium (ICC) is responsible for defining the PCS framework and outlines standards and guidelines for colour management. ICC specification document describes the structure and format of colour profiles [49]. ICC profiles perform two distinct functions. The first is the coordinate transformation, which relates the colour code values of a device to colorimetric code values in the PCS. The second is colour rendering or re-rendering, which changes the colorimetry of an original to better suit a particular reproduction medium [51]. ICC v4 profiles have gained broad usage in the graphic arts industry where the main purpose is to match the CIELAB colorimetry of one print to another, while maintaining the same viewing conditions, in order to achieve the desired visual outcome. Another common use case is specifying colour separation, which involves converting the PCS usually CIELAB, to device-dependent colours such



Figure 2.3: 2.5D printed colour samples.

as CMYK or CMYKOGV [52].

Another application of ICC v4 profiles is in soft proofing, a procedure where a digital version of a printed image is displayed on a monitor, following specific viewing conditions. Achieving accurate soft proofing entails matching the colour appearance of the print to that of the monitor, which can be challenging because of the difference between the media, i.e. reflective vs. emissive. Softproofing in printing is similar to applying the inverse model a printer profile to get the in-gamut device values and then applying its forward model to get the PCS values to display them on a monitor through the monitor profile. Despite their widespread use, the v4 profiles have some limitations. First, they rely on D50 and CIE 1931 2° colour matching functions, producing suboptimal outcomes when viewed under non-D50 lighting. Second, v4 profiles may pose challenges for handling photographic images and extended process printing systems that have seven or more inks due to their size. Third, the v4 profiles cannot anticipate colour shifts due to the fluorescence of paper and inks when objects are exposed to different lighting environments [52].

2.1.1 ICC version 5

ICC Version 5 also called the iccMAX format an extension of the ICC v4 profile format, maintaining the same header and tag structure. However, it introduces novel data types and features, including non-D50 PCS, spectral PCS, fluorescence support, procedural algorithm embedding, tagless ICC profiles, and directional colour appearance [52].

The new capabilities of iccMAX have various practical uses. They can predict the appearance of the colour under different lighting conditions using spectral

colour data, which is useful in colour workflows. iccMAX can also incorporate information about optical brightening agents, allowing accurate reproduction of colour appearance under different lighting conditions, including UV light [52]. Additionally, iccMAX enables the embedding of procedural algorithms in profiles through calculator elements, leading to more compact profiles. Calculator elements are a component that uses stack-based programming, which is Postfix Notation [53]. The resulting profiles are more precise and flexible, suitable for use in colour-managed workflows. This study uses iccMAX to encode spectral and rendering frameworks in ICC profiles for accurate colour management of printed objects.

2.2 Spectral Reproduction

Spectral reproduction in colour imaging is a method to achieve colour reproduction goals based on the spectral reflectance properties of an object or scene mainly to handle metamerism. As illustrated in Figure 2.4, metamerism is the phenomenon when two objects having different spectral characteristics might match in colour appearance under one lighting condition but not under another. Spectral reproduction helps improve the accuracy and consistency of colour reproduction, especially for materials with complex spectral characteristics, and is important in fields where colour accuracy is prime. There are many examples of spectral reproduction workflows used in printing, such as spectral printer characterisation [54, 55], spectral gamut mapping [56], spectral colour separation [33, 57–59], and soft proofing [37, 60]. This is discussed in Article I. Spectral data drives a spectral reproduction workflow. Spectral data can be acquired by measuring colour samples or by estimating spectral data from colorimetric data which will be discussed in the next two Subsections 2.2.1 and 2.2.2.

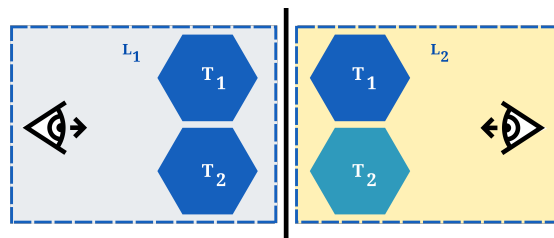


Figure 2.4: Metamerism.

2.2.1 Spectral Data Acquisition

Spectral data can be acquired using a spectrophotometer or a telespectroradiometer. In printing, spectrophotometers are more commonly used to acquire

the surface reflectance of a printed sample. These instruments can be a hand-held device making a spot measurement or a scanning device making measurements of a large number of colour patches. Spectrophotometers use a diffraction grating that splits light coming from the surface of a sample into its spectral components or spectrum. CIE has defined different measurement geometries for illumination and detection. They are three versions of $45^\circ:0^\circ$, $0^\circ:45^\circ$, $d:0^\circ$, $0^\circ:d$, $de:8^\circ$, and $di:8^\circ$ [61, 62]. The $45^\circ:0^\circ$ geometry illuminates the sample at a 45° angle and views it at a normal angle, and it is opposite in $0^\circ:45^\circ$. The $d:0^\circ$ geometry uses diffuse illumination at an angle of no more than 10° from the normal and views it at a normal angle. The $di:8^\circ$ geometry uses diffuse illumination and normal detection with the specular component included, and $de:8^\circ$ has the same geometry, but the specular component is excluded. Diffuse illumination is achieved by using an integrating sphere. There are four measurement modes M0, M1, M2, and M3 defined by ISO 13566 [63] for such measurement devices. M0 is a legacy mode and commonly allows for a tungsten lamp, M1 uses the D50 illuminant that includes the measurement of Ultraviolet (UV) light from the measurement system, while the M2 mode excludes UV light from the system. M3 is the polarising mode [49].

In this work, the reflectance data of the 2D printed colour samples used in **Articles II & III** and Article IX were obtained from standard online databases or internal datasets from the industry. The reflectances of 2.5D printed colour samples used in **Article VIII** have been measured using GON 360 goniometer equipped with a CAS 140CT array spectrophotometer with variable measurement geometry as part of BRDF acquisition including $45^\circ:0^\circ$ and $0^\circ:45^\circ$.

Reflectance measurements in practical applications often differ from the CIE recommended spectral range of 360nm-830nm in steps of 1nm for tristimulus value calculations, often obtained in truncated ranges and larger intervals, such as 10nm [64]. The spectral data used in **Articles II & III** and Article IX were measured in different ranges and intervals, (380nm-780nm in 5nm and 10nm intervals), (380nm-730nm in 10nm interval) and (400nm-700nm in 10nm interval). The use of the 400nm-700nm range for tristimulus value calculations can lead to significant errors when compared to the recommended procedure. Therefore, the reflectance measurements of narrow ranges were extrapolated to the 380nm-730nm range using linear interpolation recommended by CIE [65]. To ensure that the tristimulus values were accurately calculated, optimum weighting tables with a 10nm interval were generated using CIE illuminant and observer functions [64, 66]. These weighting tables are bandpass corrections applied to the weighting factors, which are essentially the products of the illuminant and observer functions. It should be noted that narrow peak illuminants, such as some fluorescent illuminants, cannot be accurately interpolated from 1nm to 10nm without significant errors [64, 67]. Therefore, the use of these optimum weights is crucial to obtain accurate tristimulus values, and they can be directly applied to the reflectances.

2.2.2 Spectral Estimation Methods

The simplest spectral estimation method is a least squares solution, i.e., pseudoinverse method [68, 69]. However, the most commonly used method is PCA [70–73]. Fairman and Brill proposed an efficient PCA-based method for estimating reflectance from tristimulus values, which was further modified by Agahian et al. to weight the training reflectances based on minimising the colorimetric difference from the test value. Other methods include using Cohen’s matrix R theory to calculate fundamental stimuli and metameric black [74], the Wiener estimation method [75], and methods that impose a non-negativity constraint on estimated spectra [76, 77]. Dupont studied the spectral estimation of colorimetric values using different optimisation methods, including genetic algorithms, and used a metric that minimises the colour difference under two different lights [78]. In addition, there are spectral estimation algorithms that use optimisation to minimise spectral and colorimetric errors [79, 80], as well as methods that use interpolation [81–83]. Spectral estimation methods can also be applied to achieve colour-constant estimated spectra [84]. van Trigt proposes a spectral estimation method that always creates a generic reflectance curve for a tristimulus value, achieved by generating the least variation or the smoothest reflectance for a tristimulus value [85, 86]. In this work, some of the spectral estimation methods using least squares fit are used to find a suitable method that can be integrated into colour management. They are discussed next.

The task of least-squares fit is to find a solution to an overdetermined set of equations by minimising residuals. This is done by finding a solution x to $Ax \simeq b$ by minimising the residuals $\|Ax - b\|$, where A and b are known matrices [87]. This equation can be rewritten to obtain spectral estimates from the tristimulus values, as shown in Equation 2.3. In this case, r is the spectral reflectance, n is the number of wavelengths, T is the tristimulus value, and M is the linear mapping that minimises residuals. To estimate spectral reflectance from a test tristimulus value, we need to determine the matrix M first using a training dataset with the number of samples j . The size of the matrix r is, therefore, $n \times l$ that holds the training reflectances, and the size of the matrix T is $3 \times l$ that holds the corresponding training tristimulus values in Equation 2.1. M can then be used to recover the spectral reflectance \hat{r} from any test tristimulus value T as shown in Equation 2.2.

$$r = MT \tag{2.1}$$

$$\hat{r} = MT \tag{2.2}$$

The XYZ tristimulus value T is obtained by multiplying the illuminant spectral power distribution (SPD) E , the colour matching functions O , and the surface reflectance r at each wavelength and summing the products. Weighted colour matching functions A^T can be obtained by multiplying the transposed colour

matching functions O^T with a diagonal matrix $diag(E)$ of the illuminant SPD and normalising with a constant k . The tristimulus values can be represented in matrix form using A^T and r as shown in Equation 2.3.

$$T = A^T r \quad (2.3)$$

The simplest way to determine the matrix M is the pseudoinverse method. This involves determining M using Equation 2.4, by finding the inverse of matrix T in Equation 2.3. As T is not a square matrix, its inverse cannot be calculated directly, and instead the Roger-Penrose inverse, or the pseudoinverse method, must be used.

$$M = r T^T (T T^T)^{-1} \quad (2.4)$$

Using the Wiener inverse is another spectral estimation method that uses a correlation matrix μ to determine the matrix M as shown in 2.5. μ can be the correlation matrix of the training spectral reflectance r [75]. Using a straightforward method to determine spectral similarity, this method produces estimates of spectral reflectance that are relatively unaffected by the illuminant [88].

$$M = \mu A (A^T \mu A)^{-1} \quad (2.5)$$

Fairman and Brill introduced a classical mean-centred PCA method for spectral reflectances. This involves determining the mean reflectance V_0 of the training dataset r , calculating the first three eigenvectors V from the mean-centred spectral reflectance of the training dataset $(r - V_0)$, and determining the $C \in R^3$ that contains the principal component coordinates [71], as shown in Equation 2.6. Using principal components this method maximises the variance in the dataset by determining a projection matrix. Therefore, in this case, the tristimulus value constrained principal component coordinates C have to be determined to find the spectral reflectance estimate \hat{r} using Equation 2.7.

$$r = VC + V_0 \quad (2.6)$$

$$\hat{r} = V_0 + VC \quad (2.7)$$

C can be calculated by substituting Equation 2.6 into 2.3 and rearranging for C as shown in Equation 2.8, where T is the test tristimulus value.

$$C = (A^T V)^{-1} (T - A^T V_0) \quad (2.8)$$

Agahian et al. proposed a weighted approach to the PCA spectral estimation method that calculates the weighted reflectance $r' = rW$ using the weight matrix

W in Equation 2.9. The authors obtained the weighted coordinates C using Equation 2.7 first by computing the principal components V and the mean reflectance V_0 from r' , leading to a more accurate reflectance estimate compared to classical PCA. Babaei et al. also aimed to increase the accuracy of pseudoinverse spectral estimation by weighting the training tristimulus values based on their similarity or dissimilarity to the test tristimulus values. The new weighted basis M is calculated by replacing T and r in Equation 2.4 with weighted tristimulus values $T' = TW$ and weighted reflectances $r' = rW$, respectively. The weight matrix W in Equation 2.9 is a diagonal matrix where j is the total number of samples in the training dataset and $e = 0.01$ is a small constant to prevent division by 0.

$$W = \begin{bmatrix} \frac{1}{\Delta E_{ab,1}^* + e} & 0 & \dots & 0 \\ 0 & \frac{1}{\Delta E_{ab,2}^* + e} & 0 & \vdots \\ \vdots & 0 & \ddots & 0 \\ 0 & \dots & 0 & \frac{1}{\Delta E_{ab,j}^* + e} \end{bmatrix} \quad (2.9)$$

The method of pseudo-inverse spectral estimation can be changed to use a polynomial fit. To use a polynomial, the tristimulus value (represented as $T = (X, Y, Z)$) must be expanded according to the chosen polynomial order, as specified in Table 2.1. The expanded tristimulus values are then used in Equation 2.4 to generate the basis matrix M . This matrix can be used to estimate the spectral reflectance, where the test tristimulus value also needs to be expanded in Equation 2.2 according to the polynomial order. However, it is crucial to keep the number of terms significantly lower than the number of samples, as increasing the polynomial order too much can result in overfitting.

Table 2.1: Polynomial expansion

Sl. No.	Order	Terms
1.	Second	$1, X, Y, Z, XY, XZ, YZ, X^2, Y^2, Z^2$
2.	Third	$1, X, Y, Z, XY, XZ, YZ, X^2, Y^2, Z^2, XY^2, XZ^2, X^2Y, X^2Z, Y^2Z, YZ^2, XYZ, X^3, Y^3, Z^3$

The Waypoint method, as proposed by Derhak, employs spectral reflectance decomposition to represent spectral reflectance as a sum of scaled non-selective reflectance and characteristic reflectance [89]. The non-selective reflectance is a vector that reflects the same amount of light at every wavelength, making it invariant to wavelength. Meanwhile, the characteristic reflectance, which is the wavelength-selective component, is obtained by normalising a reflectance vector such that the minimum value becomes 0 and the maximum value becomes 1. This is known as the primary reflectance, according to Chau.

In this method, the tristimulus values are first converted to Waypoint (Wpt) coordinates (W, c, h) using the Wpt normalising matrix determined for the source observing conditions. The Waypoint hue (Wpt h) is then used to determine

its corresponding characteristic reflectance. Although Munsell reflectances are typically used to determine characteristic reflectances, they can also be obtained from other measured reflectances. These characteristic reflectances are divided into groups with constant hues, forming a hue-plane. From this group, one of the characteristic reflectances is selected to represent the hue-plane. The Wpt coordinates (W, c, h) of the characteristic reflectances and non-selective reflectance are then calculated.

To determine the scalar of spectral whiteness (g) and the scalar of spectral saturation (s), the W and c coordinates of the characteristic reflectance and the W coordinate of the non-selective reflectance are used. Finally, a reflectance vector is estimated by scaling the non-selective reflectance with g , scaling the characteristic reflectance with s , and then combining them, as described in [90].

2.3 Chromatic Adaptation

The way we perceive colour is heavily influenced by the lighting conditions under which we observe objects. Different lighting conditions can alter the colours of objects. But due to colour constancy we perceive object colours as being relatively constant under varying lighting conditions, which enables us to identify objects and recognise them under these different lighting conditions. Colour constancy is achieved by one of the important sensory processes called chromatic adaptation [91]. Thus, chromatic adaptation is the mechanism by which the HVS adjusts to these variations induced by different lighting conditions to preserve the appearance of object colours [92].

The basis for modelling chromatic adaptation was established by von Kries, who assumed that HVS adapts to changes in the spectral composition of light by adjusting the sensitivity of its three types of photoreceptors, generally known as cones [93]. This can be mathematically obtained by scaling factors applied to cone excitations based on the ratio of the destination whitepoint and the source whitepoint in the cone space as shown in Equation 2.10, where (X_1, Y_1, Z_1) and (X_2, Y_2, Z_2) are the tristimulus values under the source illuminant and the destination illuminant, respectively, (L_{w1}, M_{w1}, S_{w1}) and (L_{w2}, M_{w2}, S_{w2}) are the cone excitations of the source illuminant whitepoint and the destination illuminant whitepoint respectively, and M is the matrix to linearly transform the tristimulus values to the cone space. Over the years, many different models have emerged where the transformation matrix M is optimised in different ways to fit the corresponding colour data. Corresponding colours are two different stimuli that match in colour appearance under two different illuminants [92]. That is, a pair of tristimulus values $T1$ under the source illuminant and $T2$ under the destination could be perceived as the same colour as illustrated in Figure 2.5. Corresponding colour data is obtained through different experiments, such as haploscopic matching, memory matching, or magnitude estimation.

$$\begin{bmatrix} X_2 \\ Y_2 \\ Z_2 \end{bmatrix} = M^{-1} \begin{bmatrix} \frac{L_{w2}}{L_{w1}} & 0 & 0 \\ 0 & \frac{M_{w2}}{M_{w1}} & 0 \\ 0 & 0 & \frac{S_{w2}}{S_{w1}} \end{bmatrix} M \begin{bmatrix} X_1 \\ Y_1 \\ Z_1 \end{bmatrix} \quad (2.10)$$

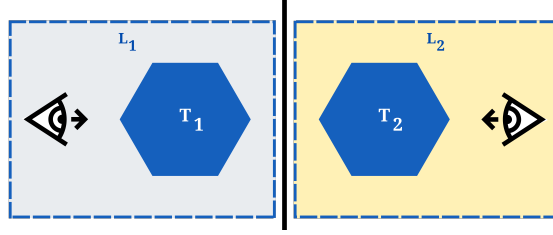


Figure 2.5: Corresponding colour match.

In this work, the term sensor adjustment transform (SAT) defined by Derhak is followed, which is an umbrella term to define a transform that adjusts cone excitations without considering the specific method or intent behind the transform. A SAT is further divided into a chromatic adaptation transform (CAT) and material adjustment transform (MAT)[94]. This is discussed in the next section.

2.3.1 Sensor Adjustment Transforms

Two goals can be realised through a SAT, colour constancy, or material constancy. Material constancy can be said to be attained when the colour appearance of an object under an illuminant is predicted based on the spectral property such as surface reflectance of the object, i.e. keeping the material properties constant. A SAT that tries to achieve colour constancy is called a CAT and a SAT that tries to achieve material constancy is called a MAT [94]. Most CATs try to predict corresponding colour data. The well-known CATs used in this work are discussed next.

The ICC v4 specification recommends using the Linear Bradford CAT for chromatic adaptation, which is based on the Bradford CAT developed by Lam, but with a non-linear correction in the blue region which is removed [95]. Finlayson et al. compared the performance of Bradford CAT, and linear Bradford CAT against a sharp adaptation transform that uses spectral sharpening and showed that Bradford transform performs no better than the sharp adaptation transform [96]. To obtain the chromatically adapted destination tristimulus value (X_2, Y_2, Z_2) , the source tristimulus value (X_1, Y_1, Z_1) , source illuminant whitepoint (X_{w1}, Y_{w1}, Z_{w1}) , and destination illuminant whitepoint (X_{w2}, Y_{w2}, Z_{w2}) in Equation 2.10 are first converted to the cone excitation space by replacing M with M_{LBFDF} given in Equation 2.11.

$$M_{L_{BFD}} = \begin{bmatrix} 0.8951 & 0.2664 & -0.1614 \\ -0.7502 & 1.7135 & 0.0367 \\ 0.0389 & -0.0685 & 1.0296 \end{bmatrix} \quad (2.11)$$

CIE TC8-01 [97] proposed the CIECAM02 colour appearance model, which uses CAT02 for chromatic adaptation. To convert the tristimulus values (XYZ) to sharpened cone responses (RGB), the transform matrix M_{CAT02} as shown in Equation 2.12 is used. Considering full adaptation, CAT02 can be calculated similarly to the von Kries transformation, as shown in Equation 2.13, where (R_{w1}, G_{w1}, B_{w1}) and (R_{w2}, G_{w2}, B_{w2}) are the sharpened cone responses of the source and destination whitepoints, respectively, while (X_1, Y_1, Z_1) and (X_2, Y_2, Z_2) are the source tristimulus value and the destination tristimulus value, respectively.

$$M_{CAT02} = \begin{bmatrix} 0.7328 & 0.4296 & -0.1624 \\ -0.7036 & 1.6975 & 0.0061 \\ 0.003 & 0.0136 & 0.9834 \end{bmatrix} \quad (2.12)$$

$$\begin{bmatrix} X_2 \\ Y_2 \\ Z_2 \end{bmatrix} = M_{CAT02}^{-1} \begin{bmatrix} \frac{R_{w2}}{R_{w1}} & 0 & 0 \\ 0 & \frac{G_{w2}}{G_{w1}} & 0 \\ 0 & 0 & \frac{B_{w2}}{B_{w1}} \end{bmatrix} M_{CAT02} \begin{bmatrix} X_1 \\ Y_1 \\ Z_1 \end{bmatrix} \quad (2.13)$$

Li et al. developed CAT16 to address the computational challenges caused by CAT02. They optimised the CAT16 transformation matrix M_{CAT16} as shown in Equation 2.14 with several corresponding colour datasets. Similarly to Equation 2.13, a chromatically adapted tristimulus value can be obtained for full adaptation when the luminance of the source and destination illuminants are equal. However, in this case, the matrix M_{CAT02} is replaced by M_{CAT16} [98].

$$M_{CAT16} = \begin{bmatrix} 0.401288 & 0.650173 & -0.051461 \\ -0.250268 & 1.204414 & 0.045854 \\ -0.002079 & 0.048952 & 0.953127 \end{bmatrix} \quad (2.14)$$

Li et al. also developed a two-step CAT16 transformation based on the CAM02 model, which used illuminant E as an intermediate or reference illuminant [99]. This two-step process involves a transformation to and from illuminant E. To adapt a source tristimulus value (X_1, Y_1, Z_1) to a destination tristimulus value (X_2, Y_2, Z_2) , where full adaptation is considered and the luminance of the illuminants matches each other, Equation 2.15 can be used.

$$\begin{bmatrix} X_2 \\ Y_2 \\ Z_2 \end{bmatrix} = M_{CAT16}^{-1} \begin{bmatrix} \frac{R_{w2}}{R_{wE}} & 0 & 0 \\ R_{wE} & \frac{G_{w2}}{G_{wE}} & 0 \\ 0 & 0 & \frac{B_{w2}}{B_{wE}} \end{bmatrix} \begin{bmatrix} \frac{R_{wE}}{R_{w1}} & 0 & 0 \\ R_{w1} & \frac{G_{wE}}{G_{w1}} & 0 \\ 0 & 0 & \frac{B_{wE}}{B_{w1}} \end{bmatrix} M_{CAT16} \begin{bmatrix} X_1 \\ Y_1 \\ Z_1 \end{bmatrix} \quad (2.15)$$

A MAT uses least dissimilar colour matching proposed by Logvinenko to achieve material constancy under changing illuminants. It is based on the concept that the appearance of a stimulus changes when the illuminant varies, but the human visual system can still identify the material to some extent because of a secondary mechanism. Following Logvinenko's proposal, Derhak et al. proposed the Waypoint transform, which maps the colour of an object to Waypoint coordinates (W, p, t), where W , p , and t represent perceptive lightness and perceptive chromaticness, respectively. It is a colour equivalency representation used to navigate between the source and destination colour viewing conditions. The aim of deriving a colour equivalency representation is to achieve orthogonality between lightness and chromaticness, with linear loci of constant hue and circular contours of constant chroma if possible. Equations 2.16 and 2.17 provide optimised Waypoint-based material adjustment transform matrices from source colorimetry CIE 1931 2° Standard Observer and illuminants D65, D50, A, and F11, respectively, to Waypoint representation. [94].

$$M_{2^\circ, D65} = \begin{bmatrix} 0.02964 & 0.97487 & -0.00280 \\ 4.83916 & -4.73122 & 0.12117 \\ 0.54248 & 1.30671 & -1.67368 \end{bmatrix}, M_{2^\circ, D50} = \begin{bmatrix} -0.06265 & 0.03839 & 0.02669 \\ 4.68561 & -4.82563 & 0.37293 \\ 0.28350 & 1.50053 & -1.15101 \end{bmatrix} \quad (2.16)$$

$$M_{2^\circ, A} = \begin{bmatrix} -0.33810 & 1.30006 & 0.20048 \\ 4.40232 & -5.32134 & 1.36425 \\ -0.41103 & 2.17849 & -4.85343 \end{bmatrix}, M_{2^\circ, F11} = \begin{bmatrix} -0.12366 & 1.05659 & 0.10608 \\ 4.38611 & -4.63611 & 0.32299 \\ 0.37476 & 1.29098 & -2.59413 \end{bmatrix} \quad (2.17)$$

Oleari developed a method for CAT by optimising the conversion of tristimulus values under various viewing conditions to an ABC reference frame. This ABC reference frame has three independent primaries A , B , and C that have mutually dependent chromatic opponency, and it is obtained by mixing and transforming LMS cones. The method assumes complete illuminant adaptation and perfect colour constancy under a set of illuminants, and an adaptation matrix is derived that converts the cone space to the ABC space [100]. These matrices are available in their article [100]. This approach ensures that colour constancy is maintained, meaning that different cone excitations under different illuminants and observers produce the same perceived colour. However, Derhak contends that Oleari's CAT are actually MAT because they optimise cone excitations. In this work, these transforms are regarded as Oleari's MAT.

Burns proposed a new method for CAT that uses spectral estimation without relying on the corresponding colour datasets for training. The method is an

improvement over traditional CATs, ensuring that the tristimulus values rendered under a destination illuminant do not fall outside of the spectral locus. Burns modified Van Trigt's approach to spectral estimation [85], which uses optimisation of the minimum slope squared integrated over the wavelengths of the visible range to find the unique reflectance curve that produces the source tristimulus value. Burns performed this optimisation in the log space of the reflectance curve to create a strictly positive reflectance curve. Two spectral power distributions are estimated to represent the source and destination whitepoints. Using these illuminants, the estimated reflectance curve and colour matching functions, the source tristimulus value and the destination tristimulus value are calculated. The destination tristimulus value is further adjusted to preserve its chromaticity while matching the relative luminance Y value of the source tristimulus value. This adjusted tristimulus value is the predicted corresponding colour. In this work, Burns' method are regarded as a CAT because it aims to predict the corresponding colours well without achieving material constancy.

MAT is especially important in colour reproduction, where the spectral reflectance or transmittance of the material used can affect the final product's colour appearance. These transforms are critical to ensure accurate colour reproduction across different devices and materials, which is important in many fields such as photography, printing, and colour science.

2.4 Appearance Reproduction in Printing

The accurate reproduction of appearance is crucial for various applications in printing, including softproofing. Softproofing is a critical tool in the graphic arts industry for accurately controlling print properties such as colour, glossiness, and texture. It is a widely used practice in 2D digital printing that allows users to preview and adjust the appearance attributes of an object before printing, ensuring that the final product meets their specifications. Although it mainly strives in reproducing appearance of diffuse colour. Softproofing in 2.5D and 3D printing is less common, and it requires surface appearance reproduction of non-planar surfaces. HP has developed a 3D printing softproofing system that uses an Appearance Reference Object (ARO) to demonstrate the printing system's colour capabilities using 3D sub-objects [101]. Additionally, a 2.5D softproofing approach based on a four-flux theory colour prediction model has been shown to be effective for relief prints in 2.5D printing [37]. However, this system only takes into account colour prediction and not appearance, which involves the prediction of colours changing under different light and viewing directions. BRDF is vital to model the appearance of objects under different light and viewing directions. Current colour management allows the incorporation of material appearance information into ICC profiles which has paved the way for appearance management.

2.4.1 Bi-direction Reflectance Distribution Function

The bidirectional reflectance distribution function (BRDF), is a mathematical function that characterises the reflection of light from a surface. Specifically, it determines the amount of light reflected in various directions based on incidence and viewing angles $(\theta_i, \phi_i, \theta_v, \phi_v)$ as shown in Figure 2.6. A BRDF model has to follow two important properties: energy conservation to ensure that it is impossible for a surface to reflect more light than was incident on it and Helmholtz reciprocity, which means that the BRDF must be unchanged when the angles of incidence and exitance are swapped. BRDF is essential to accurately model surface appearance under different lighting conditions, particularly in computer graphics, 3D printing, and virtual reality applications. Incorporating BRDF data into ICC profiles is critical in managing material and surface appearance information[39, 102].

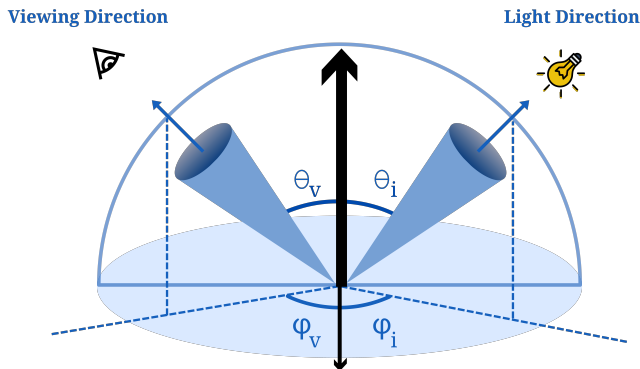


Figure 2.6: Bidirectional Reflectance Distribution Function.

2.4.2 BRDF Data Acquisition

BRDF data acquisition involves measuring the BRDF of a surface, that is the light reflected from the surface at different angles and wavelengths. The BRDF is measured by illuminating a flat surface with a collimated light beam with direction (θ_i, ϕ_i) and measuring the spectral radiance reflected in an output direction (θ_v, ϕ_v) as shown in Figure 2.6. An isotropic BRDF has a reduced angular domain whose dimension is less by one $(\theta_i, \theta_v, \phi_i - \phi_v)$. The BRDF can only be measured over finite spatial and angular intervals because it is a derivative quantity. A gonireflectometer is a classic device for measuring anisotropic BRDF. The detector is linked to a spectroradiometer or other optical assembly that allows the recording of dense spectral measurements for each configuration of the source and detector. While this method provides high angular resolution, precision, and

repeatability, it is also time-consuming [103, 104]. If acquisition is limited to isotropic BRDFs, acquisition time and equipment cost can be reduced. The next method involves a dome-shaped frame with multiple detectors and light sources that can capture the full BRDF at once without moving any component [105, 106]. However, this system is expensive and bulky. To address this issue, Ben-Ezra et al. have developed a smaller dome-shaped system that uses light-emitting diodes as both emitters and detectors [106]. Alternatively, an image-based system has been developed that uses a digital camera, a light source, and a spherical sample to acquire BRDF measurements [107–109]. However, this method does not provide spectral data, which is necessary to analyse material characteristics with accuracy.

In Article V, 17 colour samples were printed on a flat glossy paper using a 2D printer and in Article VIII, 23 colour patches printed using a 2.5D printer for each type of surface, including flat, 15°, 30°, 45°, and 60° slopes. BRDF measurements were carried out for a total of 65 reflectance measurements for each colour patch using a GON 360 goniometer with a CAS 140CT array spectrophotometer. Measurements were taken at incidence angles (θ_i) of 0°, 15°, 30°, 45°, and 60°, with viewing angles (θ_r) ranging from 30° to -65° in 5° intervals with respect to the incidence angle space.

2.4.3 BRDF Models

This section will cover some simple BRDF models. According to Montes et al. [39], a BRDF model can be described empirically or physically. Empirical models, such as the Blinn-Phong and Ward models, are straightforward, while the Cook-Torrance model is a physical model. The parameters of these models can be obtained by fitting the BRDF measurements.

The simplicity of the Blinn-Phong model has made it a popular choice for rendering systems. The diffuse reflection component, expressed as tristimulus values or spectral values, is represented by $\frac{k_d}{\pi}$. This model is a modification of the Phong model, in which the dot product between the viewing direction and the direction of perfect reflection of incident light is replaced by $N \cdot h$ to estimate specular reflection. The distance of a surface from the direction of perfect reflection is determined by $N \cdot h$ or the cosine of θ_h , where N is the surface normal and h is the half-angle vector between the incidence direction ω_i and reflection direction ω_r . The sharpness of the specular lobe is determined by the value of α , and the specular reflection component is represented by k_s . The specular lobe is responsible for creating the appearance of shininess on a surface [110]. The Blinn-Phong model is represented in equation 2.18.

$$f_r(\omega_i, \omega_v) = \frac{k_d}{\pi} + k_s(\cos\theta_h)^\alpha \quad (2.18)$$

The Ward model is an empirical model that can be used to fit BRDF measurements.

This model is elegant in its simplicity, using three parameters k_s , α_x , and α_y to create an anisotropic specular lobe with a Gaussian distribution. The α terms control the sharpness of the lobe in the x and y directions of anisotropy. Equation 2.19 represents the isotropic Ward model. In an isotropic BRDF, the object's appearance remains the same when it is rotated around the surface normal, while keeping the light and viewing directions fixed. This is achieved in the Ward model when $\alpha_x = \alpha_y = \alpha$ [111].

$$f_r(\omega_i, \omega_v) = \frac{k_d}{\pi} + \frac{k_s}{4\pi\alpha^2\sqrt{\cos\theta_i\cos\theta_v}} e^{-\frac{\tan^2\theta_h}{\alpha^2}} \quad (2.19)$$

The Cook Torrance model is a BRDF model based on the theory of microfacets that is grounded in physics. This model assumes that only the microfacets oriented towards the half-angle vector contribute to the final reflection. To generate the specular term, three essential concepts are used: a term D describes the distribution of microfacets, a Fresnel term F determines how light is reflected off each microfacet, and G is the geometric attenuation factor that determines how light is affected due to shadowing and masking of one microfacet onto another [112]. The Fresnel term can be determined using Schlick' approximation as shown in equation 2.21 where n is the refractive index of the material. Typically, a Gaussian distribution with the α term is used to describe D . [39] as shown in equation 2.22. The Cook Torrance model is represented in equation 2.20.

$$f_r(\omega_i, \omega_v) = \frac{k_d}{\pi} + \frac{k_s}{\pi\cos\theta_i\cos\theta_v} FDG \quad (2.20)$$

$$R_o = \left(\frac{1-n}{1+n}\right)^2, \quad F = R_o + (1-R_o)(1-\cos\theta_i)^5 \quad (2.21)$$

$$D = \frac{\exp\left[-\frac{\tan^2\theta_h}{\alpha^2}\right]}{\alpha^2\cos^4\theta_h}, \quad G = \min\left\{1, \frac{2\cos\theta_h\cos\theta_i}{n.v}, \frac{2\cos\theta_h\cos\theta_v}{n.v}\right\} \quad (2.22)$$

2.5 Evaluation Metrics

In a colour reproduction or spectral reproduction workflow, it is important to evaluate the quality of the output. To evaluate colour reproduction, the most commonly used metrics are CIE recommended colour differences such as ΔE_{ab}^* , ΔE_{00}^* . The ΔE_{ab}^* equation is a simple colour difference equation that takes into account the differences in lightness (L^*), chroma (C^*), and hue angle (h^*) between two colours. The ΔE_{00}^* equation is an advanced colour difference equation that considers the non-uniformity of the CIELAB colour space and is more accurate than the ΔE_{ab}^* . Manufacturers often want their products to look the same under

different lighting sources. Therefore, Colour Inconstancy Index (CII) measures how much the colour of an object changes when viewed under different lighting conditions. To calculate CII, the colour of an object is measured under a reference light source and then under a test light source. The tristimulus value obtained under the test light source is chromatically adapted to the reference light, i.e. its corresponding colour is predicted. The difference between the measured colour and the predicted corresponding colour under the reference light is the CII [113].

To evaluate spectral data or estimated reflectances, root mean square error (RMSE) is most often used to find the error between the reference and estimated reflectance curves or metameric difference is used by calculating the tristimulus values of the reflectance curves under two different illuminants and then adding their absolute difference under each illuminant. But visual colour difference and curve fitting approaches are insufficient on their own to provide accurate information, and the relative importance of these two approaches may vary depending on the application [114]. To address this issue, Nimeroff and Yurow developed a metameric difference that correlates well to the chromaticity spread among observers [115]. This difference is a weighted sum of the absolute difference between two spectra. Similarly, Viggiano developed Spectral Comparison Index (SCI), which derives weights according to the CIELAB values of the observed spectrum [116]. This metric considers both human vision and the difference between light and dark colours. In a study of non-metameric pairs, it was found that the SCI assumed values around 2.6 times that of the total colour difference of CIELAB. According to Imai et al., the advantage of this metric is that it considers both colorimetric and spectral differences, although its resulting unit may be less intuitive. López-Álvarez et al. proposed a metric that calculates both spectral and colorimetric similarity using annealing search algorithms, but it has limited and specific application. Green has developed a method to measure the smoothness of a colour transform, which involves calculating the second derivative of points on a curve and then determining the median of these values [117]. This same approach can be used to assess the smoothness of a reflectance spectrum, and is referred to in this work as Smoothness Index (SI).

Chapter 3

Summary of the Included Articles

This chapter presents an overview of the articles in sequence of summarising the core contributions first and then the supplementary contributions that constitute this thesis. Among them, **Articles II, III, and VIII** have been submitted to scientific journals, while **Article VII** is a chapter included in a book that is currently in press [46] and they form the core contributions of this work. Articles I, IV, V, VI, and IX are conference proceedings and they are the supplementary contributions.

3.1 Core Contributions

This section outlines the core contributions presented in the thesis, which include **Articles II, III, VII and VIII**.

3.1.1 Article II: Spectral Estimation: Evaluation and Application

T. Habib, P. Green and P. Nussbaum, ‘Spectral estimation: Evaluation and Application (Under Review),’ *Optics Express*, 2023

The aim of this article is to evaluate different existing spectral estimation methods and different training datasets to determine their performance and precision in estimating the reflectance from tristimulus values. The paper aims to answer two main questions: first, whether a training dataset selected based on material similarities with the test dataset can increase the accuracy of spectral estimates, and second, what is a suitable spectral estimation workflow that can be easily integrated into colour management.

The spectral estimation methods were used to estimate reflectance or emission spectra from tristimulus values obtained under D50 illuminant and CIE 1931 2° Standard Observer colorimetry. Tristimulus value calculations, according to CIE

recommendations, should use a spectral range of 360 nm-830 nm with a step size of 1 nm [64]. However, in practical applications, measurements are often obtained in truncated ranges and larger intervals, which can result in errors. In addition, narrow-peak illuminants, such as certain fluorescent illuminants, cannot be interpolated to 10 nm from 1 nm without creating large errors [64, 67]. Therefore, reflectance measurements with a narrow range were extrapolated to the range of 380nm-730nm using linear interpolation [65], and optimum weighting tables of 10nm intervals were generated using respective CIE illuminant and observer functions to ensure accurate calculations [64, 66]. These tables can be applied directly to reflectances to obtain tristimulus values.

The spectral estimation methods evaluated are Wiener estimation, Classical PCA, Weighted PCA, Pseudo Inverse, Weighted Pseudo Inverse, Second-Order Polynomial, Third-Order Polynomial, and Waypoint methods as given in Section 2.2.2. Seven spectral datasets were selected to evaluate the spectral estimation of surface reflectance from tristimulus values; they are Munsell [118], FOGRA51 [119], web offset print on lightweight coated, cold-set offset on newsprint, and digital print on textile datasets. These datasets belong to different printing conditions and cover the printable gamut as described in Table 3.1.

Table 3.1: Description of spectral reflectance datasets

Dataset	Substrate (L*, a*, b*)	No. of samples	Spectral range	Use
Munsell glossy colour chip (M1)	-	1600	380nm-780nm interval 5 nm	Training
Offset litho on premium coated (F1)	(95, 1.5, -6)	1617	380nm-730nm interval 10 nm	Training
Web offset on lightweight coated (W1)	(88.8, -0.18, 3.7)	1600	400nm-700nm interval 10 nm	Training
Cold-set offset on newsprint (N1)	(81.9, -0.79, 5.08)	1485	380nm-730nm interval 10 nm	Training and test
Cold-set offset on newsprint (N2)	(82.9, 0.31, 4.45)	1485	380nm-730nm interval 10 nm	Training and test
Digital print on textile (T1)	(87, 4.55, -19.33)	1485	380nm-780nm interval 10 nm	Training and test
Digital print on textile (T2)	(94.52, 2.26, -14.7)	1485	380nm-780nm interval 10 nm	Training and test

Three tests were conducted. Test 1 divided each spectral reflectance dataset in Table 3.1 into training and test datasets using k-fold cross-validation with $k = 5$. Each spectral estimation method was evaluated by calculating the mean and maximum values of RMSE and ΔE_{ab}^* between the estimated reflectances and the reference reflectances for each dataset. This test evaluated spectral estimation methods when the training and test data belonged to the same dataset. In Test 2, the spectral estimation methods were evaluated when the training and the test belonged to different datasets, for example, the training data is M1 and the test data is W1 in Table 3.1. Nine different combinations of training and test datasets were evaluated using the eight spectral estimation methods, and the mean and maximum of RMSE and ΔE_{ab}^* were reported. The aim was to understand how close the material match of a training dataset must be to minimise metameric mismatch under different lighting conditions. Tests 1 and 2 showed that when a training dataset was used with similar material components, such as similar primary colourants and substrate (and therefore having similar reflectance curves), the RMSE errors and metameric differences under different illuminants are the lowest. In this scenario, the metric results are the lowest for datasets with lower variability, such as newspaper datasets. Both tests show that

using polynomial bases (Second-Order & Third-Order Polynomial) or colorimetric weighted bases (Weighted PCA & Weighted Pseudo Inverse) with least-squares fit produced estimated reflectances with low metameric mismatches under different illuminants. Test 2 also showed that for newsprint datasets, Third-Order Polynomial performed the best when a different newsprint dataset was used for training, while for textile datasets, Weighted Pseudo Inverse had the lowest mean RMSE when a different textile dataset was used for training. Furthermore, in the cases where W1 was used as a training data set to make spectral estimates for N2, the metameric mismatch under different illuminants was within acceptable limits with a mean ΔE_{ab}^* below 1 for the best cases and when F1 (paper containing OBA) was used as training data to make spectral estimates for T2 (textile containing OBA) the metameric mismatch under different illuminants was comparable to the performance of T1 that is when another textile dataset was used as a training data with a mean ΔE_{ab}^* below 2.4 for the best cases. The accuracy of the least-squares fit was reduced for textile datasets due to the presence of fluorescent whitening agents, which resulted in sharper peaks in the blue region. Test 3 evaluated spectral estimation methods on the radiance datasets of different displays. Results showed that spectral estimation performed well when training and test data were from the same dataset, but performed poorly when using data from a different display dataset with similar technology. Given that there are no practical spectral reproduction use cases that require the estimation of radiance spectra from tristimulus values of a display, the evaluation of spectral estimation workflows in colour management for display technologies is not further considered.

The results showed that even when training reflectances have some dissimilarity, the results still lead to acceptable metameric differences because their reflectances are smooth and have similar peak wavelengths. Therefore, depending on the degree of similarities in the material components, many spectral datasets or printing conditions can be grouped together, and a single reflectance dataset can represent a common training dataset for the reflectance estimation of that group. Although, Third-Order Polynomial and Weighted Pseudo Inverse spectral estimation methods performed the best in the tests, Second-Order Polynomial and Weighted PCA are not significantly different. These methods are also computationally not costly or complex to implement. Third-Order Polynomial spectral estimation method can be easily and efficiently encoded in an ICC profile as matrices using iccMAX calculator element programming, which is given in Listing B.2 in the attached Appendix C. The results of this study show that spectral datasets based on printing conditions can be standardised and help develop efficient and accurate colour management workflows with spectral PCS useful for various industries.

I carried out a literature review, picked the relevant spectral estimation methods, implemented the different methods, analysed the results with respect to different methods and training data, developed the colour management workflow for spectral estimation, compiled all the findings, drew important conclusions, and

wrote the article.

3.1.2 Article III: Spectral Estimation: As a Sensor Adjustment Transform

T. Habib, P. Green and P. Nussbaum, 'Spectral estimation: As a Sensor Adjustment Transform (Under Review),' *Optics Express*, 2023

In this article, we discuss the issue of illuminant metamerism, which occurs when two objects with different reflectance functions appear to be the same colour under one light but different under another due to differences in the spectral power distribution between the two lights. When the spectral reflectance of an object is not available, its colour appearance under different illuminants in the colorimetric domain is predicted by a sensor adjustment transform (SAT), which may be a chromatic adaptation transform (CAT) that tries to achieve colour constancy or a material adjustment transform (MAT) that tries to achieve material constancy under varying illuminants, as discussed in Section 2.3.1.

A CAT predicts the corresponding colours and is derived from experimental data where the observers match the colours under different illuminants. CATs include Linear Bradford CAT [120], CAT02 [62], and CAT16 [98], which use the corresponding colour data to optimise transformation matrices that are applied to convert tristimulus values to and from a sharpened cone space. In the case of MATs, a material match of the object (i.e., its surface spectral reflectance) is predicted rather than an appearance match. Logvinenko defined a metameric mismatch volume, which is for a given colour under one illuminant its corresponding volume that contains all the possible colours under another illuminant [121]. Zhang et al. evaluated this theory by choosing all metameric reflectances under one illuminant from a large collection of measured reflectances and creating its corresponding metameric mismatch volumes by rendering tristimulus values under different illuminants [122]. It was found that the centroid value of this volume can be used to predict colours with a minimum metameric mismatch compared to the well-known CATs. Derhak developed a MAT that uses a colour equivalency representation called Wpt (Waypoint) [94]. Oleari developed CATs by optimising the conversion of tristimulus values under different viewing conditions to an ABC colour space such that it preserves colour constancy [100] but Derhak states that these CATs relate to material constancy because they optimise cone excitations and refers to them as Oleari's MATs [94]. Burns developed a spectral estimation-based CAT, which ensures that tristimulus values rendered under a destination illuminant do not fall outside of the spectral locus and do not depend on the corresponding colour datasets for training or fine-tuning [123]. This method is a modification of the spectral estimation algorithm proposed by van Trigt that finds the unique reflectance curve with a minimum slope squared integrated over the wavelengths of the visible range without the need for training

reflectance data [85]. After spectral estimation is performed, the tristimulus value calculated under the destination illuminant is further adjusted to match the luminance Y of the source tristimulus value that completes this CAT.

In Article II, we established that a priori knowledge-based spectral estimation methods created estimated reflectances that are a close material match to the reference, and thus minimise metameric mismatches under different lighting conditions. In this article, we compare the results of the two best performing estimation methods Weighted Pseudo Inverse and Third-Order Polynomial from Article II along with different training datasets with the results of the CAT's and MATs discussed in the previous paragraph in predicting the colorimetry of a stimulus under different destination lights. That is, the comparisons are made against Linear Bradford CAT, CAT02, CAT16, Oleari's MAT, Waypoint MAT, Burns spectral estimation, and Burns CAT (Burns spectral estimation and luminance scaling together). Here, we aim to assess how well different methods perform to achieve material constancy or minimise metameric mismatch.

Mean, 95th percentile and maximum ΔE_{00}^* were reported for the stimulus adapted to and from CIE illuminants D50, D65, A, F11 and LED-VI. For the Munsell dataset [118], the a priori knowledge-based spectral estimation methods (training and test data belong to Munsell dataset) performed the best for all combinations of source and destination illuminants. In this case, the Waypoint MAT and Burns spectral estimation were comparable and performed significantly better than the rest of the CATs.

For the newspaper dataset N2 from Table 3.1, the two a priori knowledge-based spectral estimation methods performed the best compared to the rest of the methods when the training data and test data belonged to the same dataset or training data is another newspaper dataset N1. When web offset on lightweight coated paper (W1) is used as training data, the two spectral estimation methods still perform better than the other CATs and MATs. Although, in the case of textile dataset containing OBA, all three cases where the training data belonged to T2 itself, T3 (another textile data) or Fogra data F1 (offset litho on premium coated containing OBA) performed significantly better than the rest of the methods. Burns spectral estimation, Waypoint MAT and Oleari MAT performed similarly to each other and were better than the CATs, which is expected as CATs try to achieve colour constancy instead of material constancy.

This article also investigated the performance of the two spectral estimation methods (Weighted Pseudo Inverse and Third-Order Polynomial) in predicting colorimetry of the corresponding colours by estimating reflectances of the corresponding colour data using three different training datasets (M1, N2, and T2). The corresponding colour datasets used for this analysis and their source and destination illuminants are CSAJ (D65, A), Helson (C, A), Lam & Rigg (D65, A), and LUTCHI (D65, D50). Mean ΔE_{ab}^* were reported for the spectral estimation methods, CATs and MATs. In these cases, all the results from all the methods were comparable, although CAT s performed slightly better than spectral estimation

methods and the MATs. This may be due to the fact that all the reflectances used for training are from inks/pigments, which are smooth reflectances and tend to preserve colour constancy.

Therefore, this study finds that spectral estimation methods, such as Weighted Pseudo Inverse and Third-Order Polynomial, perform better in minimising metameric mismatches when good training data is used. However, when the training dataset is not a good material match or has high variability, the metameric mismatch increases. The results show that spectral estimation can be a good alternative to traditional CATs and MATs for predicting tristimulus values under different illuminants, especially when material constancy is the objective. To attain colour constancy, training data that contain smooth reflectances that tend to preserve colour constancy can be an option.

The spectral estimation methods used here were evaluated in previous work by me. I used the chosen spectral estimation methods to reproduce colour under different illuminants and to evaluate its role as a sensor adjustment transform (SAT). I also made comparisons of the results with other known SATs and made important conclusions about the performance of spectral estimation methods as a SAT. In addition, I compiled all the analyses and conclusions and wrote the article.

3.1.3 Article VII: Colour Management of Material Appearance

T. Habib, 'Colour Management of Material Appearance,' in *Colour Engineering: Fundamentals and Applications (Under Production)*, P. Green, Ed., John Wiley & Sons, 2023

This section provides a summary of several supplementary contributions that were important intermediate requirements leading to the core contributions and helped in answering the research objectives during the course of the Ph.D.

Article VII is a chapter written as part of a book in press [46]. This chapter introduces material appearance rendering, describes the support for material appearance in the iccMAX colour management system, and explains a custom workflow of material appearance rendering encoded inside an ICC profile. This chapter makes use of Article V and Article VI to develop the colour-managed workflow to render material appearance. A summary of this chapter is given below.

The ICC.1 [35] specification defines the architecture for communicating colour using a PCS based on D50 colorimetry and the CIE 1931 2° Standard Observer. Although this framework works well to manage the colour appearance under various viewing conditions of flat images or surfaces, it is highly constrained when it comes to providing support for PCS other than reference PCS, including spectral data in a transform and no support for 3D surface appearance.

The development of 2.5D and 3D printing, 3D imaging systems, augmented reality, and virtual reality imaging systems has made it necessary to understand and communicate the colour of a 3D environment, including material appearance and 3D appearance information in the ICC profiles. Therefore, instead of just managing the colour appearance, it is now essential to manage the material appearance information in ICC profiles. One way to describe the material appearance of an opaque object is by defining a bidirectional reflectance distribution function (BRDF). A BRDF defines how light falling on an object interacts with its surface. By including support for BRDF and texture information in the form of a height map or a normal map, the iccMAX architecture has made it possible to encode material appearance information in an ICC profile [31]. BRDF support present in iccMAX is used to generate parameters for variants of the Blinn-phong, Ward, Cook-Torrance and Lafortune BRDF models. There are two direct ways to provide BRDF information in an ICC profile. The first method involves using **BRDFStruct** type tags to provide BRDF parameters directly to a 3D rendering system. The second method of providing BRDF information in an ICC profile involves using **BRDFFunction** type tags that would require external fitting of the included information to a BRDF model to acquire BRDF parameters for 3D rendering [31]. Alternatively, a BRDF model can also be encoded in an ICC profile using Calculator Elements Programming. In this chapter, a novel custom workflow to encode a BRDF model inside an ICC profile is described.

To implement this workflow, a TIFF file containing the BRDF parameters related to a BRDF model is required. The BRDF parameters can be obtained by measuring the appearance of a colour target using an appearance measurement device or by fitting BRDF measurements to a model. A profile can be created that maps the device colours to the appropriate BRDF parameters using the interpolation-based optimised BRDF parameters algorithm based on interpolation described in Article V. This profile can convert the device colours to BRDF parameters and store them in a TIFF file or can be directly connected to the custom BRDF profile workflow described next. The custom workflow uses the iccMAX paradigm to BRDF rendering presented in Article VI with the modification that this workflow also processes a normal map to render a complete 3D surface appearance. Therefore, the input in this workflow can be BRDF parameters without texture information in the form of a normal map or BRDF parameters and a normal map. The Multiplex Connection Space (MCS) present in iccMAX is used to pass data between profiles using multiplex channels with identical multiplex channel type values. To create a connection space that identifies multiplex channels, Multiplex Identification (MID) profile is defined, that is, this profile identifies and converts device values to multiplex channel values. The profile class Multiplex Visualisation (MVIS) is defined to utilise the multiplex channels for visualisation. This MVIS profile needs to define the colour transform inside the **multiprocessing elements type** tag. Here, the BRDF model can be encoded using Calculator Element Programming to generate a surface appearance output. The light and viewing directions to these workflows are provided as run-time variables. A diagrammatic representation

of this 3D appearance rendering workflow for connecting an MID profile to an MVIS profile similar to Figure 3.2 is provided in the chapter attached as Article VII.

This opportunity to furnish a chapter[46] in a book was presented by my main supervisor, who is also the editor of the book. I designed the didactic flow of the chapter, tailored and streamlined all the knowledge gained so far through the research on the topic of colour management of material appearance, performed analysis, and generated results and diagrams for the chapter. I am the sole author of the chapter. This chapter was peer-reviewed by experts in the field.

3.1.4 Article VIII: 2.5D Printing: A Framework for Appearance Reproduction of Printed 3D Surfaces

T. Habib, P. Green and P. Nussbaum, ‘2.5D Printing: An Appearance Reproduction Framework for Printed 3D Surfaces (Under Review),’ *Journal of Imaging Science and Technology*, 2023

In this paper, a stepwise appearance reproduction framework for 2.5D printing is presented. The framework is designed to produce BRDF parameters for an image with XYZ values measured at 0°:45° geometry. A workflow was previously developed for 2D printing, where an interpolation method was used to predict BRDF parameters from the XYZ values and BRDF parameters of the primary and secondary printed colours of a particular printer and substrate. However, 2.5D printing has a spatially variable height, which causes the device colours printed on surfaces of different slopes to differ from the same device colours printed on a flat surface. To account for this change in colour due to the change in surface slope, we developed a colour adjustment algorithm that adjusts the colour of the tristimulus values of the flat target to predict the corresponding tristimulus value on a surface with some slope. These adjusted colours are then used by the BRDF interpolation algorithm to predict the BRDF parameters for each pixel with a particular slope. The output is an image with channels that have the BRDF parameters and the normals from the normal map.

For 23 colour patches printed on a flat substrate and the same set of colour patches printed on sloped surfaces at angles of 15°, 30°, 45°, and 60°, the diffuse colours were measured at 0°:45° geometry. It was observed that both the mean and maximum ΔE_{00}^* values between the flat colour patches with their corresponding colours on each sloped surface increase with increasing slope angle, with the 45° slope having the most colour inconsistency compared to the flat target. This highlights the need for a colour adjustment algorithm to predict the colours of sloped surfaces from the colours of the flat target. The mean and maximum ΔE_{00}^* values obtained after applying the colour adjustment algorithm minimise the colour between flat colours vs. sloped colours.

Two versions of the Cook-Torrance BRDF model with seven and nine parameters

Table 3.2: Colour difference between optimised BRDF (OB) results and interpolated BRDF parameters algorithm (IB) and adjusted interpolated BRDF parameters algorithm (AIB) for 15 test colour patches at different incidence and reflection angles for all slopes together

	Mean ΔE_{00}^*		Median ΔE_{00}^*		Max ΔE_{00}^*	
	IB	AIB	IB	AIB	IB	AIB
	Optimised BRDF1 (OB)	4.39	<u>3.95</u>	4.46	<u>3.84</u>	18.97

were used for the modelling. The colour difference between the measured BRDF and the optimised BRDF obtained for the primary and secondary colours of the flat target was calculated. The results show that the optimised BRDF had a mean ΔE_{00}^* of around 5 for all colour patches for both versions of the BRDF model. It was observed that there is no significant difference in using the model with nine parameters. Therefore, the framework was carried forward with the BRDF model with seven parameters due to efficiency.

The colour difference between the optimised BRDF of 15 test colours on each slope and the interpolated BRDF (IB) of the flat target and the colour difference between the optimised BRDF of 15 test colours on each slope and its corresponding slope colour-adjusted interpolated BRDF (AIB) of the flat target were calculated. The colour differences were calculated for three regions: diffuse reflection, specular reflection, and near-to-specular reflection. The AIB method minimises the mean ΔE_{00}^* for all cases except specular reflections. However, the number of specular reflections is a handful, and ΔE_{00}^* colour difference at high reflections might not relate to perceived colour difference the same way it relates to the perceived colour difference of diffuse reflections. The grand mean, median, and maximum ΔE_{00}^* values considering all test colour patches of all slopes together were also computed. It was observed that the AIB method yields the lowest ΔE_{00}^* values as shown in table 3.2.

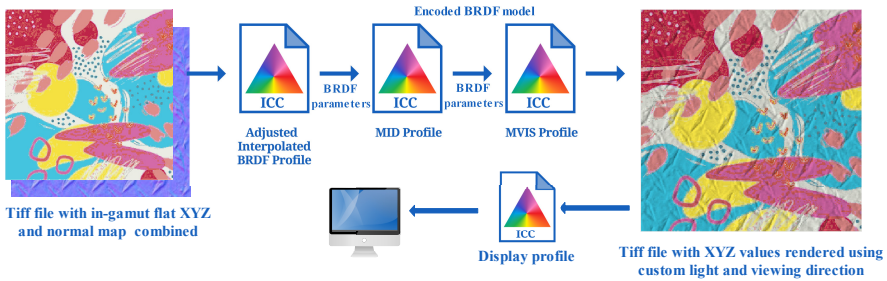


Figure 3.1: A practical appearance reproduction framework for 2.5D printing.

This AIB method can be used to predict the BRDF parameters for a TIFF file containing XYZ values and surface normals from a normal map that is used to retrieve the slope information for each pixel and apply the adjusted colour algorithm accordingly. The output will be a TIFF file containing the BRDF parameters along

with the surface normals, which can be used for BRDF rendering through iccMAX based MCS profiles to reproduce the material appearance for any global light and viewing direction passed at runtime to this colour management pipeline as shown in Figure 3.1.

3.2 Supplementary Contributions

In this section the supplementary contributions are discussed that helped in achieving the goals in the core contributions.

3.2.1 Article I: Spectral reproduction: drivers, use cases and workflow

T. Habib, P. Green and P. Nussbaum, ‘Spectral reproduction: drivers, use cases and workflow,’ *Electronic Imaging*, vol. 32, pp. 1–6, 2020

The vast majority of colour reproduction systems are based on trichromacy, which involves stimulating the three cones of the human visual system in ratios that match the desired appearance. This approach is efficient and flexible, but it has several limitations; the most significant being that matches may not hold when the viewing illumination varies due to metamerism. Therefore, as discussed in Section 2.2 spectral reproduction approach is preferred, whereby colour reproduction is carried out using spectral data, that is, more than three channels. In this paper, we discuss the advancement in technology that enables a spectral reproduction system today, present use cases to highlight the need for such a system, and give an overview of the components required to realise such a system.

There are many fields where precise spectral information or colour-accurate reproduction is very important, such as in the field of medical imaging, cultural heritage preservation, graphics and arts, cosmetics, packaging industry, etc. The increasing interest in the use of spectral data has led to the development of spectral acquisition systems (e.g. multispectral and hyperspectral devices), fast processors, and efficient storage devices to store and handle spectral and multichannel data. It can be considered a cycle where the need for spectral data boosts the development of technologies, and these advancements, in turn, provide the ground for it to be used to solve many new spectral reproduction goals. Some use cases where spectral reproduction is desired or can be used are discussed next.

In spot colour reproduction, spot colour printed on a particular substrate has to be matched to process inks printed on the same substrate. The reflectance data of spot colour are stored in the ICC profile and/or PDF file using the CxF/x4 file format. This spectral information is used to find the optimal combination of

process inks that would create spot colour reproduction of minimum metameric mismatch. This can be achieved by spectral matching, such as inverting a spectral printer model to find the optimal ink set [58]. There are other workflows in which a model is developed to predict the colour (either colorimetric or spectral) of the overprints, that is, when a spot colour is printed on a process colour or another spot colour [124, 125]. Similarly, in a printing pipeline, when ink is changed or the ink sequence is switched, then the printer needs to be characterised again to map the new state. This characterisation can also use a spectral printer model [55, 126, 127] and reflectance of the inks can be stored and accessed from the CxF/x4 file. Spectral matching is also required when two prints from two different printers or a print and a reference have to match or have the least metameric mismatch possible under different lighting conditions [128]. Substrate colour adjustment is another important step in printing when the characterisation data white point is different from the substrate whitepoint and a correction is required. This is usually done colorimetrically as defined in ISO 12647-2 [129] and a spectral variant this is shown by Gudzenchuk et al. [130]. A photorealistic rendering system is used to create an image that looks like a real scene, which is another use case where spectral reproduction is essential. This system requires a database of natural spectra that matches what an observer would see in real life with support for various physical effects such as fluorescence, diffraction, and polarisation [131, 132]. A multispectral approach is used to implement high-fidelity colour reproduction, which is crucial in medical imaging and the reproduction of artwork [133, 134]. In medical imaging, high-fidelity colour and spectral data can aid in disease quantification and treatment assessment. Observer metamerism, where colour matching functions differ between observers, can lead to difficulties in matching colour accurately on a display. Wide colour-gamut displays, with their spectrally narrow primaries, can exacerbate this problem. One solution is to apply individual colour matching functions to spectra to achieve personalised reproduction. Several studies argue for a personalised spectral softproofing to reduce observer metamerism [135–137]. Spectral data of an image can be used for embedding watermarks for copyright protection, temper detection, authentication, etc. Metameric pairs of a colourant can be used to implement watermarks where watermarks are invisible under normal lighting conditions, but can be deciphered by illuminating the printed image with infrared light, narrow-band illumination or UV light depending on the characteristics of the watermark [138]. These are some of the use cases that highlight the immediate need for spectral reproduction workflows and could be handled by colour management itself in the future.

All of the above use cases make it clear that the most important component is spectral data that are not easily available. Therefore, spectral processing techniques, such as spectral estimation, can be applied to multispectral or colorimetric data to convert them to spectral reflectance or radiance when needed. This approach can also be used when spectral data is compressed to lower-dimensional data for storage efficiency. The evaluation of different spectral estimation methods

and their performance in minimising metameric mismatch will be addressed in Articles Article II: Spectral Estimation: Evaluation and Application and Article III: Spectral Estimation: As a Sensor Adjustment Transform (Sections 3.1.1 & 3.1.2).

The various use cases of spectral reproduction have some common components in their workflows. The workflow involves taking an input image, performing some intermediate spectral processing, and creating an image that meets the reproduction goal. Therefore, the following units are identified as essential to a spectral reproduction system, an input unit and an output unit that can be colorimetric, spectral, or multispectral image, and the processing units pertaining to a reproduction goal as shown in the figure. The colour management architecture, iccMAX, allows support for spectral data, flexibility in using any illuminant or colour matching function, and programmable transforms using calculator elements [31], which can be used to develop a spectral reproduction system. The encoding of a spectral estimation method using iccMAX has been successfully implemented and a profile is created to produce the estimated reflectance of an XYZ image; the A2B and B2A tags of such a profile are given in the Listing B.1 in the attached Appendix C.

I reviewed existing use cases and workflows, established the importance of the topic, proposed how different workflows can be connected, put all the work together and authored this article.

3.2.2 Article IV: Estimation of BRDF Measurements for Printed Colour Samples

T. Habib, P. Green and P. Nussbaum, 'Estimation of BRDF Measurements for Printed Colour Samples,' vol. 29, pp. 123–128, 2021

To model the material appearance of a surface, the bidirectional reflectance distribution function (BRDF) is crucial. Measuring the BRDF necessitates information about the position of the surface, the direction of the incident light, the direction of reflection, and the amount of light reflected. The BRDF is evaluated over a hemisphere by altering the angles of the light source and the detector, making it possible to measure the reflected light over a variety of incident and reflection angles. There are several ways to measure BRDF, including using a gonio-reflectometer [103, 104], a dome-shaped system [105, 106], or an image-based system [107–109]. A gonio-reflectometer makes very precise BRDF measurements, but measuring BRDF for printed target colours requires measuring each colour patch, which is very time-consuming. To simplify the process, in this article, we propose a BRDF measurement estimation method that reduces the number of measurements needed to acquire the BRDF of any printed colour patch related to a particular printer and substrate. In addition, BRDF of primary and secondary colours can be used to render the appearance of any printed surface for a particular printer and substrate which will be discussed in the article V.

The BRDF of 17 flat printed samples on glossy paper was measured using a GON 360 goniometer equipped with a CAS 140CT array spectrophotometer. These reflectances were measured in the range of 380 to 780 nm in 5 nm steps, for five incidence angles (-60°, -45°, -30°, -15°, and 0°) and over a range of reflection angles (-30° to 65° in intervals of 5°). The training set for the estimation of the BRDF measurements of the printed colour patches included the measured BRDF of the substrate (white, cyan (100,0,0,0), magenta (0,100,0,0) and yellow (0,0,100,0) printed samples and the BRDF of 13 test samples were measured for evaluation. For this work, we consider test samples that are a mix of white, cyan, magenta, and yellow only, and (100,100,100, 0) is considered black.

The colour of a material is determined by measuring diffuse reflection usually at a 0°:45° geometry, while the specular reflection at mirror angles is primarily the colour of the light source. The remaining intermediate angles combine diffuse and specular reflections. Reflectances with dominating diffuse reflections have a spectral shape similar to the 0°:45° measurement, whereas the reflectances from adjacent reflection angles to the specular peak have dominating specular reflection. As measurements move away from the specular peak, the influence of specular reflection is reduced. This allows for the modelling of specular reflection at mirror angles separately from the rest. The reflectance at other reflection angles with dominating diffuse reflection and near-to-specular reflections (reflection angles that are within 10° from the mirror angle) are modelled using the same predictor reflectances in this article.

To estimate the BRDF measurement, a third-order polynomial regression model was used. A regression model was created for each combination of the incidence angle and the reflection angle, resulting in 91 total combinations. The predictor set included two base reflectances of substrate ($xw1$ & $xw2$), cyan ($xc1$ & $xc2$), magenta ($xm1$ & $xm2$), and yellow ($xy1$ & $xy2$) samples chosen at specific incidence and reflection angles (-45°,45°) and (-60°,65°) respectively. These reflectances were combined to form the predictor matrix X as shown in Equation 3.1. The response vector Y as shown in Equation 3.1 was a combination of the training reflectances of the substrate (yw), cyan (yc), magenta (ym) and yellow (yy) measured at the same set of incidence and reflection angles for which the estimation model was created. For example, if the estimation model is for incidence and reflection angles at (-30°,40°), respectively, then the training reflectances of the four primary colour patches measured at those angles formed the response vector Y .

$$X = \begin{pmatrix} xw1 & xw2 \\ xc1 & xc2 \\ xm1 & xm2 \\ xy1 & xy2 \end{pmatrix}, \quad Y = \begin{pmatrix} yw \\ yc \\ ym \\ yy \end{pmatrix} \quad (3.1)$$

As described above, the two defined base reflectances at angles (-45°,45°) and (-60°,65°) of a test sample were required to predict the reflectances at any other combination of incidence and reflection angles using its corresponding estima-

tion model. Similarly, we proposed the use of two base reflectances measured at $(-45^\circ, 45^\circ)$ midrange and $(-60^\circ, 60^\circ)$ highest specular reflection to model the reflectance of the specular reflection at any combination of incidence and reflection angle. Therefore, this article shows that, to estimate the BRDF measurements of a test sample, four measurements of the sample at $(-45^\circ, 45^\circ)$, $(-60^\circ, 60^\circ)$, $(-45^\circ, 0^\circ)$ and $(-60^\circ, 65^\circ)$ are required. This approach reduces the measurement requirement from 100 reflectances to just 4 for each test sample, which is a mix of the primary inks and the substrate.

BRDF measurements were estimated for 13 test samples at five incidence angles and 20 reflection angles, except for angles with shadowed reflections. The normalised root mean square difference (NRMSD) and the colour differences ΔE_{00}^* and ΔE_{IPT} were calculated relative to the reference measurements. The results were analysed on the basis of diffuse, near-to-specular, and specular reflections. The estimated spectra of diffuse reflections had low NRMSD and colour differences, while the estimated spectra of near-to-specular reflections had the highest NRMSD and colour differences. The estimated spectra of the specular reflections had moderate NRMSD and colour differences.

Article IV shows that polynomial regression with two predictors can estimate spectra at diffuse reflection angles well, although specular reflectances are overestimated. Spectra at near-to-specular reflections are difficult to estimate accurately. Large colour differences occur at near-to-specular peak areas, and because the spectral shape is not properly estimated, visible hue differences are seen in near-to-specular angles. Luminance values are well estimated for both diffuse and specular reflections. There is no definite best or worst estimate based on colour samples, indicating that combining primary colours to estimate the spectra of other ink mixes is effective. However, a new method is necessary to model near-to-specular and specular spectra in the future. Despite this limitation, using this model can reduce the necessary BRDF measurements at diffuse reflections to just two for each printed colour patch.

I looked into this research idea due to the lack of measured spectral BRDF data and therefore the need for estimated spectral BRDF data of printed colours. I developed the new methodology of estimating the measured BRDF using primary colours' BRDF data, analysed the results and found the accuracy, possibilities and limitations of the methodology. I wrote the article stating all the findings along with the methodology. The measured data set used here is the same as the data used in previous work by me with a different aim. This data set was measured by FOGRA as acknowledged in the article.

3.2.3 Article V: BRDF rendering by interpolation of optimised model parameters

T. Habib, P. Green and P. Nussbaum, 'BRDF rendering by interpolation of optimised model parameters,' in *Color and Imaging Conference*,

Society for Imaging Science and Technology, vol. 28, 2020, pp. 162–168

To achieve accurate material appearance reproduction, we need to understand the different components of appearance in relation to the human visual system. Colour management in printing uses diffuse colour measurement at a single light and detector geometry to map device values to the measured tristimulus values that form the PCS. When this workflow is used for softproofing of printed objects, it can reproduce colours well under a single geometry but does not have adequate information to reproduce a realistic appearance that includes colour and/or gloss reproduction under different light and viewing directions. To measure colour with gloss and surface geometry, bidirectional reflectance distribution function (BRDF) must be used. BRDF measurements fitted to a BRDF model can describe the appearance of a material surface accurately. In printing, it is then required to print a colour target and find the optimised BRDF parameters to a model for each target colour which can then be used to model the material appearance of printed colour for a particular printer and substrate. Therefore, a framework is needed which involves choosing a BRDF model, fitting BRDF parameters, and finding an efficient method to obtain from the PCS, i.e., the tristimulus values their corresponding BRDF parameters. In this article, an interpolation method is developed to map any $45^\circ:0^\circ$ geometry tristimulus value to their corresponding BRDF parameters. The interpolation method can be used to create a lookup table that can be encoded in an ICC version 4 profile ICC.1 or encode the interpolation method itself in an ICC version 5 profile (iccMAX) [31].

The BRDF measurements of the eight primary and secondary printed colours and nine test samples were measured by FOGRA. These measurements were also used in the previous Article IV. The BRDFs of the substrate (white), C, M, Y, CM, CY, MY, and CMY samples were fitted to the Ward and Cook Torrance BRDF models. The BRDF parameters have diffuse components $\mathbf{R}_x, \mathbf{R}_y, \mathbf{R}_z$ that define the colour of the material and specular components \mathbf{k} and \mathbf{m} that define the specular lobe. An interpolation method has been developed from the Shepard interpolation and Neugebauer model to find the BRDF parameters of a BRDF model for an input tristimulus value of $45^\circ:0^\circ$ geometry. The algorithm is a modification of the Shepard interpolation with inspiration from the Neugebauer model to mix eight secondaries and primaries in an irregular space.

Algorithm for Interpolation of BRDF Parameters from an Irregular Lattice:

Let the input tristimulus value be the vector \mathbf{I} , and the tristimulus values of the eight primary and secondary colours be the vectors \mathbf{I}_i and their corresponding BRDF parameters be the vectors \mathbf{B}_i where $i \in 1, 2, 3, \dots, 8$ and $\mathbf{B}_i \in \mathbb{R}^5$.

Calculate the chromaticity coordinates vector \mathbf{C} of \mathbf{I} and the chromaticity coordinates vectors \mathbf{C}_i of \mathbf{I}_i , respectively, where $i \in 1, 2, 3, \dots, 8$. For a given tristimulus value, the chromaticity coordinates x, y, z are given by: $x = X/(X + Y + Z)$, $y = Y/(X + Y + Z)$, $z = Z/(X + Y + Z)$.

Find the distance between the vectors \mathbf{C} and \mathbf{C}_i , based on L_p norm as follows: $d_i = |\mathbf{C} - \mathbf{C}_i|_p$, where p can be chosen accordingly. In this case, we have chosen $p = 2$, which reduces it to the Euclidean distance.

Create vectors \mathbf{S}_i that store the index i of \mathbf{d}_i in ascending order of distance values in vector \mathbf{d}_i , i changes from 1 to 8.

Set $n = 1$ and do the following:

1. Set the variable of colour difference $\mathbf{E} = 1000$.
2. Calculate the distance $\mathbf{D}_i = \|\mathbf{I} - \mathbf{I}_{S_i}\|$, where i changes from 1 to n .
3. Calculate the tristimulus value \mathbf{T}' as: $\mathbf{T}' = \frac{\sum_{i=1}^n \mathbf{I}_{S_i} \mathbf{D}_i^\mu}{\sum_{i=1}^n \mathbf{D}_i^\mu}$ where μ can be chosen accordingly. In this case, we have chosen $\mu = 1$.
4. Calculate the colour difference \mathbf{E}' using ΔE_{00}^* between \mathbf{T}' and \mathbf{I} .
5. If $\mathbf{E}' < \mathbf{E}$, then set $\mathbf{E} = \mathbf{E}'$, interpolated tristimulus vector $\mathbf{T} = \mathbf{T}'$, and calculate interpolated BRDF parameters vector \mathbf{B} as: $\mathbf{B} = \frac{\sum_{i=1}^n \mathbf{B}_{S_i} \mathbf{D}_i^\mu}{\sum_{i=1}^n \mathbf{D}_i^\mu}$
6. Increment n and continue step 2 to step 6 until $n = 8$.

Once we have the closest tristimulus value \mathbf{T} and its corresponding BRDF parameters \mathbf{B} , then we need to scale each tristimulus coordinate ($\mathbf{T}_x, \mathbf{T}_y, \mathbf{T}_z$) of \mathbf{T} to the tristimulus coordinates ($\mathbf{I}_x, \mathbf{I}_y, \mathbf{I}_z$) of \mathbf{I} and apply the same individual scaling to the diffuse components ($\mathbf{R}_x, \mathbf{R}_y, \mathbf{R}_z$) of \mathbf{B} , respectively:

$$a = \frac{\mathbf{I}_x}{\mathbf{T}_x}, \quad b = \frac{\mathbf{I}_y}{\mathbf{T}_y} \text{ and } c = \frac{\mathbf{I}_z}{\mathbf{T}_z}$$

By scaling with \mathbf{a} , \mathbf{b} and \mathbf{c} we get $\mathbf{T} = (\mathbf{I}_x, \mathbf{I}_y, \mathbf{I}_z)$ and the diffuse component of the BRDF is $\mathbf{B} = (a\mathbf{R}_x, b\mathbf{R}_y, c\mathbf{R}_z)$.

The above interpolation method was applied to obtain the interpolated BRDF parameters for the nine test samples. Reference BRDF measurements and optimised BRDF parameters for these nine samples were used to evaluate the performance of the interpolated BRDF parameters. The results showed that the interpolated BRDF parameters lie within the accuracy obtained by the optimised parameters. Therefore, the accuracy of the interpolated BRDF method depends on how well the optimised BRDF parameters and the model used for the primary and secondary inks describe their material appearance. This interpolation method can be integrated into colour management such that given a file with diffuse tristimulus values an ICC profile can generate the corresponding BRDF parameters and these parameters can be used by the iccMAX-based BRDF rendering paradigm described in Article VI to generate the material appearance of a printed surface.

I selected the essential data for the proposed workflow, performed BRDF optimisation, designed and developed 2D printing rendering workflow through the interpolation of BRDF parameters, generated and analysed the results, and authored the article. Measurement of selected data was carried out by FOGRA, which is acknowledged in the paper.

3.2.4 Article VI: Implementing directional reflectance in a colour managed workflow

T. Habib, P. Green and A. Sole, 'Implementing directional reflectance in a colour managed workflow,' in *London Imaging Meeting*, Society for Imaging Science and Technology, vol. 1, 2020, pp. 119–123

Article VI describes a colour management framework to render the material appearance of flat printed samples. BRDF models, such as the Cook-Torrance and Ward models, are commonly used to model material appearance properties. The article uses BRDF measured by Sole et al. to optimise the isotropic Ward BRDF model to obtain the BRDF parameters for different printed samples. These BRDF parameters along with the BRDF model can be used to compute the colorimetry of a sample in the incident and viewing directions. The objective of this article is to show that a BRDF workflow is possible using iccMAX and describes the implementation, performance, and limitations of this workflow.

Sole et al. [109] used wax-based inks printed on a matte-coated white paper as samples. Seven different colour samples, white, red, cyan, Pantone 10309C, magenta, Pantone 10213C and Pantone 10253C were printed using an OCE ColourWave 600 printer. Then they were pasted as strips on a circular structure with a marked angular ruler at the bottom and measured using an image-based setup for 10 different illumination angles. The illumination source was configured to approximate a point light source, and a Nikon D200 DSLR camera was used as the acquisition system. The captured RGB intensities were converted to XYZ using the camera spectral sensitivity and the CIE 1931 2° Standard Observer, and the light and viewing angles for each pixel were computed. These XYZ along with the light and viewing directions were then fitted to Ward BRDF model to obtain the BRDF parameters. This is how Sole et al. obtained BRDF parameters that can be used to render the material appearance of printed samples. They also measured the BRDF of the printed samples using a telespectoradiometer for a range of incidence angles and reflection angles. In this article, we used these BRDF measurements in the colorimetric domain (XYZ) to optimise the Ward BRDF model and obtain the respective BRDF parameters. Then a workflow is developed where the Ward BRDF model is encoded inside an ICC profile, the light and viewing directions are given at runtime as environment variables, the input is a file containing the optimised BRDF parameters and the output is a file containing the new XYZ values rendered under the given light and viewing directions.

The workflow described in the previous paragraph involves using the iccMAX colour management framework to transform input data into a simulation of the directional appearance on a display. Such a workflow is useful for softproofing. The core task is to transform from an XYZ space representing the diffuse reflectance (0°:45° geometry) to an adjusted XYZ representing the appearance

of the material once the given angles of illumination and viewing have been taken into account. This transformation cannot be handled by the ICC.1 colour management architecture [35] since it specifies a point-wise transform with a limited set of transform elements, and the aprofile connection space (PCS) is defined to represent a matte, diffusely reflecting planar surface measured with a $0^\circ:45^\circ$ geometry and under D50 illuminant colorimetry. To overcome this limitation, the ICC.2 architecture is used, i.e. iccMAX [31], which extends the ICC.1 architecture and provides much richer support for colour management of other types of material and other geometries of measurement. iccMAX supports a wider range of transform elements and fully directional illumination, measurement, and viewing geometries. It also includes an option to use Calculator Element Programming, a scripting language that makes transforms fully programmable.

In the proposed workflow, the BRDF model is encoded in a **calculatorElements** tag in the main function using a Multiplex Connection Space (MCS) framework as shown in Figure 3.2. The MCS comprises the Multiplex Identification (MID) and the Multiplex Visualisation (MVIS) profiles. The BRDF model-optimised parameters for each sample are passed through the input channels to the MID profile and then used by the BRDF model encoded in the MVIS profile. The light and viewing directions are passed as runtime variables to the MVIS profile. The MVIS profile processes the input and uses the encoded BRDF model to generate the XYZ in the appropriate light and viewing geometry. The output channels containing the rendered XYZ values are then passed through the MVIS profile, which connects them to the colorimetric PCS, performing any processing needed to convert them to this PCS. **MultiplexTypeArrayTags** are defined to assign channel names and are used to match channels in and out of the Multiplex Connection Space (MCS) and to verify channel compliance with any subset requirements between profiles. Optional **multiplexDefaultValuesTag** defines default values for channels. The MID profile uses an **AToM0** tag to provide the transform from device channel data to MCS channel data, while the MVIS class profile uses **MToB0** (colorimetric) tags to provide the transform from MCS channel data to PCS channel data.

The tristimulus values rendered from the BRDF parameters optimised using the BRDF measured by the telespectoradiometer and the tristimulus values rendered from the BRDF parameters optimised by Sole et al. in different light and viewing directions are used to analyse the colorimetric output of the ICC profile-based rendering workflow implemented in this work. The mean ΔE_{00}^* obtained for each case was less than 1 for all samples. The luminance Y obtained from the ICC profile and the reference (i.e. XYZ obtained from the BRDF measured by the telespectoradiometer) at one incidence angle and different reflection angles were plotted for evaluation. The findings indicate that the Ward BRDF model behaves as predicted, generating a Gaussian output with a seamless effect when incorporated into an ICC profile. Additionally, these results demonstrate that the BRDF rendering achieved through ICC profile encoding matches the efficiency of other computational workflows used for rendering.

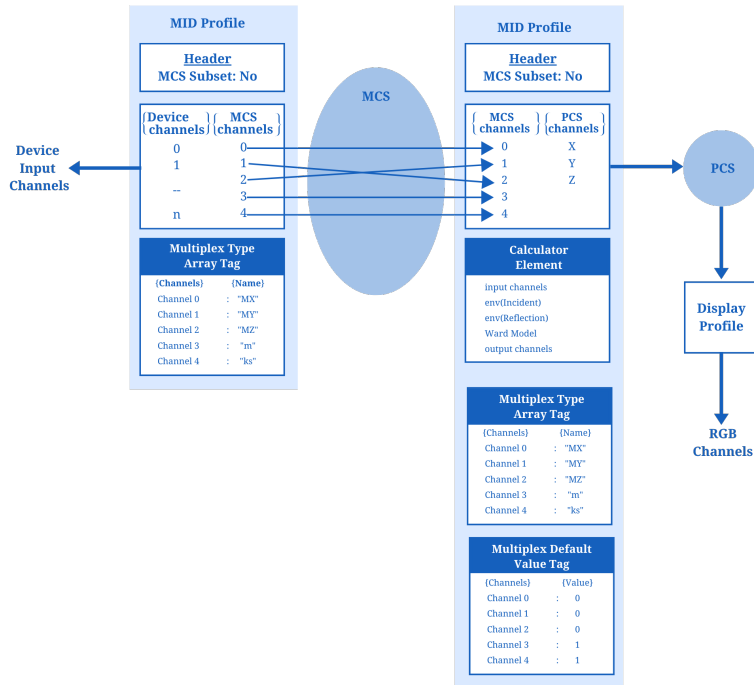


Figure 3.2: iccMAX-based appearance rendering workflow using MID and MVIS profiles for encoding a BRDF model.

I conceived the research idea, developed the colour management workflow, carried out the practical implementation of BRDF optimisation and profile creation, performed an analysis of the results, and authored the article. The experimental data used here were gathered by the third author in his previous work.

3.2.5 Article IX: A weighted goodness-of-fit metric for comparison of spectra

T. Habib, P. Green and P. Nussbaum, 'A weighted goodness-of-fit metric for comparison of spectra,' in *Sensing Colour, Proceedings of the International Colour Association (AIC) Conference 2022*, International Colour Association, 2022, pp. 397–404

Article IX discusses the challenge of evaluating the ability of spectral estimation procedures to predict the original spectra with existing metrics that fulfil only a specific criterion such as minimising the spectral difference or colorimetric difference [114]. This article describes various existing metrics used to evaluate

spectral data, such as RMSE, metameric difference (ΔM), Colour Inconstancy Index (CII), Smoothness Index (SI) and Spectral Comparison Index (SCI) discussed in Section 2.5. Then a new spectral estimation metric is proposed that considers both colorimetric and spectral differences and can be adjusted according to the target application goal. The article establishes criteria for spectral matches that relate to real-world colour reproduction objectives, such as minimising colour difference, spectral difference, hue difference, metameric mismatch, and non-smoothness. Then, the metrics corresponding to each of these criteria are defined and computed for a diverse set of original spectra and their estimated spectra or calculated from their tristimulus values. The resulting metric combines RMSE, ΔM , the difference in CII and the difference in SI into a single figure of merit that describes the fit between two spectra. The metric weights are adjusted to correlate well with SCI, which is another metric that considers both minimising the spectral difference and the colorimetric difference, but without the flexibility of adjustable weights. Since the new metric Combined Index (CI) has adjustable weights, it provides a useful means to compare spectra that can be adapted to particular criteria for a wide range of applications.

The new metric CI was used to evaluate the two best performing spectral estimation methods, Weighted Pseudo Inverse and Third-Order Polynomial described in Article II. The evaluation was carried out using three reflectance datasets cold-set offset on newsprint (D1), digital print on textile (D2) and web offset on light-weight coated paper (D3). Three cases were considered to determine the degree of metamerism between the estimated spectra and the reference spectra, case 1 where the test data and training data belonged to the same dataset D1, case 2 where the test dataset is D1 and the training dataset is D2 having similarly shaped spectral curves, and case 3 where the test dataset D2 and the training dataset D3 have quite different spectral curves between each other. This study analyses the correlation between CI and SCI with other metrics. The weights chosen for CI were found to correlate differently to different metrics. The results suggest that both CI and SCI can determine metamerism under different illuminants for the three cases of estimated spectra with varying degrees of metamerism in them. However, neither CI nor SCI showed any correlation with the difference in colour inconsistency (ΔCII) and difference in spectral smoothness (ΔSI).

The CI metric, with adjusted weights, performs similarly to SCI in evaluating estimated spectra with different degrees of metamerism when the given weights are used. Both metrics are effective in determining metamerism between two spectra under different illuminants. The weights of CI can be adjusted to optimise the outcome to a desired attribute, such as smoother spectra, low RMSE, metamerism, or colour inconstancy, depending on the target application.

I conceived the idea of the study, carried out the required literature review, implemented the workflow, and performed analysis to develop the metric. I also made comparisons with other metrics and wrote the article with the results obtained.

Chapter 4

Research Contributions

4.1 Fundamental Contributions to the Field of Research

To begin with, Article I highlighted the significance of spectral reproduction workflows and their components. It specifically emphasised the need to consider spectral estimation methods to implement these workflows in current colour management systems. **Articles II** provided insights into the effectiveness of various a priori knowledge-based spectral estimation methods to estimate reflectances. It also suggested grouping spectral datasets or printing conditions based on similarities in material components and offered practical guidance for integrating spectral estimation methods into a colour management workflow. **Article III** compared the effectiveness of spectral estimation with traditional CATs and MATs in predicting tristimulus values under different illuminants when material constancy is the objective. It concluded that simple spectral estimation methods can be used as a sensor adjustment transform to minimise metameric mismatches. Article V demonstrated the limitations and potential of using polynomial regression to estimate BRDF measurements for 2D printed samples with mixed inks. It also contributed to a significant reduction in the number of BRDF measurements required at diffuse reflections. Article IV introduced a novel method that uses interpolation to derive BRDF parameters from XYZ values of 2D printed surface colours with mixed inks. Additionally, the simplicity and efficiency of this interpolation method make it a suitable candidate for integration into colour management as a lookup table in ICC version 4, or the method can be encoded using ICC version 5. Article VI developed an efficient BRDF model workflow for appearance rendering using ICC profiles for any incident light angle and viewing angle pair. **Article VII** is a chapter in the book [46], *Fundamentals and Applications of Colour Engineering*, which is currently in press. The official cover of the book is shown in Figure 4.1. It explained in detail how material appearance can be rendered using normal maps in an iccMAX workflow, building upon the knowledge gained from Articles V & VI. This workflow has the potential to provide the necessary information

for softproofing of 2.5D or 3D printed surfaces. **Article VIII** provided a comprehensive framework to render the appearance of 2.5D printed objects that can be used for softproofing. It extended the knowledge gained in Articles V & VI and **Article VII** to 2.5D printing. Moreover, it also describes a file format required to hold appearance information in the framework. Lastly, Article IX contributed to the development of a new goodness-of-fit metric, CI with adjusted weights. The weights of CI can be adjusted to optimise the result for a desired attribute such as smoother spectra, low RMSE, metamerism, or colour inconstancy according to the target application.

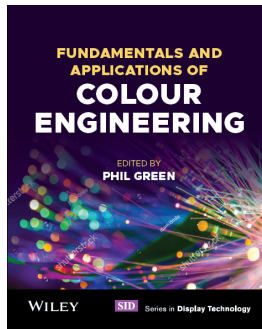


Figure 4.1: The official cover of the book, *Fundamentals and Applications of Colour Engineering*, which is currently in press [46].

4.2 Additional Contributions to the Field of Research

During my Ph.D. programme, I engaged in collaborative efforts with both academic and industrial institutions. As a part of the International Color Consortium (ICC), I made significant contributions to ISO/TC 130/JWG 7 which is a collaborative workgroup responsible for addressing standardisation in the field of colour management. These contributions were informed by my research in spectral estimation methods and the implementation of spectral profiles using iccMAX. The source codes that I developed as a part of these endeavours have been made accessible to a wider community on <https://www.color.org/index.xalter>.

During "ICC DevCon 2020: The Future of Color Management" event, I conducted three workshops on Spectral Reproduction, iccMAX BRDF Implementation, and Calculator Element Programming, which are included in Appendix A. The Spectral Reproduction workshop covered various use cases that require a spectral workflow, as well as the necessary processing requirements. This oral contribution incorporates work from Article I. In the iccMAX BRDF Implementation workshop, I provided an introduction to the theory of bidirectional reflectance distribution function (BRDF), BRDF modelling, and its support in the current colour management architecture. I also explained a framework for material appearance

rendering using iccMAX, which included work from Article VI. The Calculator Element Programming workshop consisted of a comprehensive programming lecture on the scripting language Calculator Element Programming, which is used within iccMAX profiles. This workshop also included two programming examples for implementing spectral estimation and BRDF modelling within a Version 5 ICC profile.

In addition to my previously mentioned contributions, I have actively engaged in other industrial collaborations and colour-related activities. I had the opportunity to pay industrial visits and training related to metrology at FOGRA, Munich, and another related to physically based rendering at Covision Lab, Brixen. I presented at "Colourlunch," a regular internal meeting at NTNU featuring experts discussing different colour topics every week. I also presented at the Colourlab workshop on material appearance, where I shared my insights on "Integrating Appearance in Colour Management." Furthermore, I have delivered didactic lectures on material appearance rendering and spectral reproduction to graduate students in colour science. I have also facilitated hands-on programming sessions and provided subject matter expertise to students working on their course projects, offering guidance and support.

Chapter 5

Discussion and Conclusion

5.1 Investigate the efficacy of various spectral estimation methods in handling metamerism and develop a framework for spectral estimation in a colour management workflow.

Spectral reproduction, as discussed in Section 2.2 is a framework that uses spectral information of an object or scene to improve the accuracy and consistency of colour reproduction, that is, especially to deal with the problem of metamerism. Article I describes use cases that employ or have the potential to employ a spectral workflow to achieve their colour reproduction goals. In printing, the spectral reflectance of a spot colour is used to find the best spectral match that can be obtained with process colours. Spectral printer characterisation is already an established pipeline and has widely known models such as the Kubelka-Munk model, the spectral Neugebauer model, and the cellular Yule–Nielsen spectral Neugebauer. Such models can be used to characterise a printer’s new state when ink is switched or the ink sequence is changed. Another use case is substrate colour adjustment, where the characterisation data have to be adjusted to the whitepoint of the substrate in use. ISO 12647-2 [129], defined how to apply this adjustment in the colorimetric domain, and recently this correction of the characterisation data due to the change in the whitepoint of the substrate has been solved in the spectral domain [130]. Scene-referred spectral reproduction requires a database of natural spectra that would match the visual impression of an observer to virtual scenes. Hi-fidelity colour reproduction is important in medical imaging and the reproduction of artworks that make use of multispectral or spectral data. These use cases underscore the importance of having procedures in place to accurately reproduce spectral characteristics through spectral reproduction workflows and indicate the need for colour management systems to switch from colorimetric workflows and communicate through a spectral PCS. Article I also shows that input and output components in a spectral reproduction workflow can be colorimetric or spectral

data. If the input data is colorimetric data, then additional processing is needed to estimate spectral data from the input, allowing for the implementation of a spectral workflow. Thus, the most important requirement in spectral reproduction is spectral data that can be measured or estimated.

Since measured spectral data are not easily available, spectral estimation methods have to be evaluated and standardised to use them in colour management. **Article II** investigated various spectral estimation methods and found their accuracy in predicting colour under different illuminants and proposed a suitable method that can also be encoded inside an ICC profile using iccMAX with ease. Using polynomial bases or colorimetric weighted bases with least-squares fit produced estimated reflectances with low metameric mismatches under different CIE illuminants (D50, D65, A, F11 and LED-VI). **Article II** also demonstrated that when training data are selected by matching material components with the test data, it is possible to obtain spectral estimates with satisfactory spectral and colorimetric outcomes. For example, when the test data was a newsprint dataset (cold-set offset on newsprint) and the spectral data for training were another newsprint dataset or a dataset like web offset on lightweight coated paper that has some dissimilarities in material components, it resulted in spectral estimates with an acceptable metameric mismatch. A similar trend was observed for the spectral estimates of textile data when spectral data from a different textile dataset or Fogra dataset (offset litho on premium coated paper) were used for training. Although in this case, both the textile and Fogra dataset had substrates containing OBA with reflectances having sharp peaks in the blue region, which made the Fogra dataset have spectral similarities with the textile dataset but the presence of sharp peaks reduced the accuracy of the least squares fit compared to the newsprint dataset. These findings also suggest that, on the basis of printing conditions, spectral data can be grouped together so that a single training dataset can be used for training spectral estimation models to predict spectral estimates of the colorimetric print dataset belonging to that group. The condition for combining such printing conditions is that spectral estimates should produce low metameric mismatches under several different illuminants. Finally, **Article II** proposed that Third-Order Polynomial spectral estimation can be used for spectral estimation from XYZ data as it produces low mean and max metameric differences and shows that it can be easily encoded within an iccMAX based ICC profile given in Listing B.2 in the attached Appendix C. Thus, this article provides an efficient solution to spectral PCS or spectral processing through current colour management architecture using a simple a priori knowledge-based spectral estimation method and carefully selected training data.

Article III evaluated the performance of the two best performing spectral estimation methods (Third-Order Polynomial and Weighted Pseudo Inverse methods) found in **Article II** along with the selection of training data to minimise metameric mismatch, that is, to preserve material constancy compared to existing CATs and MATs. In this work, we follow the distinction established by Derhak, a SAT that tries to achieve colour constancy is a CAT and that tries to achieve

material constancy is a MAT. Comparisons were made against Linear Bradford CAT, CAT02, CAT16, Oleari’s MAT, Waypoint MAT, Burns spectral estimation, and Burns spectral estimation based CAT given in Section 2.3.1 for a fifteen combination of source and destination illuminants using CIE illuminants (D50, D65, A, F11 and LED-VI). The colour difference ΔE_{00}^* between the predicted destination tristimulus values and the reference tristimulus values obtained using the measured reflectance under the destination illuminant was reported. The results proved that with good training data selection as discussed in the previous paragraph, the metameric mismatch under the 15 combination of illuminants was the lowest for the two a priori knowledge-based spectral estimation methods when used to predict colorimetry of the Munsell dataset, newsprint dataset and textile dataset using k-fold cross-validation. For datasets like Munsell where the variability is high, the Burns spectral estimation method and Waypoint methods performed similarly to each other and were better than the other CATs and MATs. Zhang et al. carried out the prediction of colorimetry under a destination illuminant by finding the centroid of a metameric mismatch volume obtained from a collection of metameric reflectances under the destination illuminant [122]. Table 5.1 shows the results obtained by Zhang et al. in their work for the prediction of Munsell data colour under two combinations of source and destination illuminants and the results obtained by the a priori knowledge-based methods assessed in **Article III**. The table shows that the two spectral estimation methods performed significantly better and these estimation methods are also simple to implement.

Table 5.1: Mean and 95th percentile of ΔE_{00}^* between reference destination tristimulus values and predicted tristimulus values obtained by Zhang et al. using the centroid method [122] and the results obtained using Weighted Pseudo Inverse and Third-Order Polynomial spectral estimation methods, going from the source illuminant A and F11 to the destination illuminant D65, respectively.

Method	Mean ΔE_{00}^*		95 th percentile of ΔE_{00}^*	
	A-D65	F11-D65	A-D65	F11-D65
Centroid method (Zhang et al.)	1.27	1.82	3.42	4.99
Weighted Pseudo Inverse	0.74	0.95	1.90	2.68
Third-Order Polynomial	0.79	1.05	2.39	2.75

Article III also shows that both a priori knowledge-based spectral estimation methods produce the lowest mean and maximum ΔE_{00}^* values when the training dataset is either from the same dataset or another dataset with similar reflectance characteristics. For example, when the training dataset is either from the same newsprint or another newsprint dataset, the grand mean ΔE_{00}^* across all combinations of illuminant pairs from source and destination is less than 0.5, and the average of the maximum ΔE_{00}^* values is less than 2. When the training dataset is different in material components from the test dataset, such as using web offset on lightweight coated as training data, the mean and maximum ΔE_{00}^* values of the two spectral estimation methods are still significantly better than other CATs and MATs. The grand mean ΔE_{00}^* , in this case, is less than 0.8, and the average

of the maximum ΔE_{00}^* values is less than 3. Similarly, for the textile dataset, both spectral estimation methods produce the smallest mean and maximum ΔE_{00}^* values when the training dataset is from the same dataset or another dataset with similar reflectance characteristics. When the training dataset has some difference in material components, such as using the Fogra dataset as training data, which has an optically brightened substrate that is premium coated paper rather than textile, the mean and maximum ΔE_{00}^* values are still significantly low and, interestingly, the results were comparable to the results obtained when the training data used was textile. These findings solidify the outcome of **Article II** that simple a priori knowledge-based spectral estimation methods with training data selected based on a material match to test data performed extremely well in minimising metamerism mismatch and also prove that such methods performed significantly better than existing SATs.

Article II also compared the performance of the two a priori knowledge-based spectral estimation methods using three different training datasets Munsell (M), newsprint (N), and textile (T) to predict the colorimetry of the corresponding colour data against the performance of other CATs and MATs. The corresponding colour datasets selected for this analysis and their source and destination illuminants are CSAJ (D65, A), Helson (C,A), Lam & Rigg (D65, A) and LUTCHI (D65, D50). The results shown in Table 5.2 suggest that the two a priori knowledge-based spectral estimation methods performed similarly to the MATs, although they did not perform significantly worse than the CATs. For the Helson dataset, the a priori knowledge-based spectral estimation methods performed similarly to CATs. The use of different training datasets did not show any significant differences in the results. This may be due to the smooth reflectances of the training datasets which tend to preserve colour constancy despite the slight inaccuracy that arises from the use of standard illuminants in the tristimulus values calculation of the estimated spectra, while the measured illuminants in the corresponding colour datasets are slightly different from these standard illuminants. Therefore, this provides enough evidence that such methods along with the training dataset can be a good alternative to a MAT and depending on the smoothness of the training reflectances and the variability of the dataset, such methods can also be used to achieve colour constancy.

The findings and analyses presented in Article I and **Articles II & III** address the research questions that were initially proposed. Specifically, Article I highlights the significance of spectral reproduction in colour workflows, emphasising the crucial role that spectral data and estimation procedures play in this process. **Article II** proposes a workflow for integrating spectral estimation into the current colour management system, outlining the training data requirements, and evaluating its performance. Lastly, **Article III** provides empirical evidence supporting the use of spectral estimation methods as a viable alternative to existing SATs, as they effectively reduce metamerism mismatches in a variety of illuminants.

Table 5.2: Overall ΔE_{94} between destination tristimulus values of corresponding colours and adapted/estimated tristimulus values under varying destination illuminants. Spectral estimation methods estimated reflectances of corresponding colours using Munsell (M), newsprint (N) and textile (T) as training data, respectively.

Method	CSAJ	Helson	Lam & Rigg	Lutchi	Average
Cat02	3.67	3.60	2.98	3.41	3.42
Cat16	3.94	4.13	3.47	3.30	3.71
Linear Bradford	3.71	3.47	2.84	3.43	3.36
Burns CAT	3.81	4.19	3.15	3.68	3.71
Oleari's MAT	4.63	4.72	3.89	4.27	4.38
Waypoint MAT	4.28	4.02	3.83	4.53	4.17
Weighted Pseudo Inverse(M)	4.14	3.76	3.48	4.51	3.97
Third-Order Polynomial (M)	4.22	3.77	3.51	4.46	3.99
Weighted Pseudo Inverse (N)	4.71	3.65	3.42	4.29	4.02
Third-Order Polynomial (N)	4.39	3.76	3.47	4.34	3.99
Weighted Pseudo Inverse (T)	4.69	3.65	3.46	4.36	4.04
Third-Order Polynomial (T)	4.35	3.57	3.31	4.37	3.90

5.2 Investigate rendering of material appearance in 2.5D printing.

In previous chapters, we have discussed that to render the material appearance of an object, BRDF measurements of the surface and its modelling are essential. To measure BRDF accurately a goniospectroradiometer is used and reflectance measurements are taken over a hemisphere for different light and viewing directions. However, such measurements are very time-consuming. Especially, if BRDF measurements for several surfaces are desired as in the case of printing, when the material appearance of printed objects depends on ink mixes and substrates used. Article IV tries to address the problem of acquisition of large numbers of BRDF measurements for different printed colours by suggesting a BRDF measurement estimation workflow for different surface colours that are a combination of halftoned primary inks and the substrate. This workflow uses the measured BRDF of the primary inks cyan, magenta, yellow, and the substrate. Evaluation of 13 test samples that were different colour patches with different surface reflectance properties was carried out. The workflow estimated BRDF measurements for five incidence angles and 20 reflection angles, except for the shadowed and missing reflections. The results were analysed for diffuse reflection, near-to-specular reflection, and specular reflection sections. The estimated BRDF measurements at diffuse reflection angles showed low overall NRMSD values, with a minimum of 0.005 and a maximum of 0.008. Similarly, the colour differences for these measurements were low, with a mean ΔE_{00}^* of 0.329 and a mean ΔE_{IPT} of 0.004. For specular reflection, the NRMSD values were higher than for diffuse reflection, with a mean NRMSD of 0.104. The colour differences for specular reflection measurements were also comparatively high, with a mean ΔE_{00}^* of 2.147 and a mean ΔE_{IPT} of 0.016. Near-to-specular reflection measurements showed the highest NRMSD and colour differences compared to the

estimated spectra of diffuse reflection and specular reflection. The mean NRMSD was 0.166, and the maximum was 0.947. The mean ΔE_{00}^* was 10.991, and the mean ΔE_{IPT} was 0.148. The results show that the BRDF measurement estimation workflow was accurate for diffuse reflection measurements, but less accurate for specular and near-to-specular reflection measurements. Article V calculated the optimised BRDF parameters for eight colour samples using the Ward and Cook Torrance BRDF models. Tristimulus values were calculated for five incidence angles and a range of reflection angles. The mean ΔE_{00}^* values for the Ward and Cook Torrance BRDF models compared to the reference were 6.79 and 6.5, respectively. The specular peaks of the measured data were observed to increase with increasing incidence angle. The results showed that the BRDF parameters obtained from the interpolation method lie within the accuracy obtained by the optimised parameters for both the Ward and Cook Torrance models. All these results were important to finally proceed towards creating a framework for 2.5D appearance reproduction. **Article VIII** demonstrates this framework in which printed samples of flat and sloped targets were printed and measured. Following the work in Article V, the interpolated BRDF method was used to find the BRDF parameter of an XYZ value of any slope using the interpolated BRDF method with the optimised BRDF of primary and secondary colours of the flat target. It was observed that the colour difference between a colour patch on the flat target and the corresponding colour patch on the sloped surface increased with an increase in slope angle. Therefore, a colour adjustment method was developed to adjust the flat XYZ values to an XYZ value on a slope where the slope values of the colours are extracted from the normal map.

5.3 Design an appearance reproduction framework for 2.5D printing using the current colour management architecture, iccMAX.

Article VI demonstrated that the Ward BRDF model can be encoded in an ICC profile. This custom workflow of implementing a BRDF model within an ICC profile is achieved through an MCS connection where the light and view direction are supplied at run-time. The BRDF parameters were passed pixelwise using a TIFF file as input. The colour-managed workflow produced identical results to the Ward model implementation in Matlab for the equivalent adapted colorimetry and agreed well with previous results. This was further extended in **Article VII** to include a normal map along with the BRDF parameters in the TIFF file. The generated images are useful for simulating the appearance of printed inks and for softproofing. A complete workflow from the XYZ tristimulus values to the BRDF parameters and then applying the BRDF model through multiplex connection space to obtain XYZ values in the light and viewing directions passed at run-time is shown in Figure 5.1. The normal map is passed along with XYZ values as input

which is read by the MVIS profile.

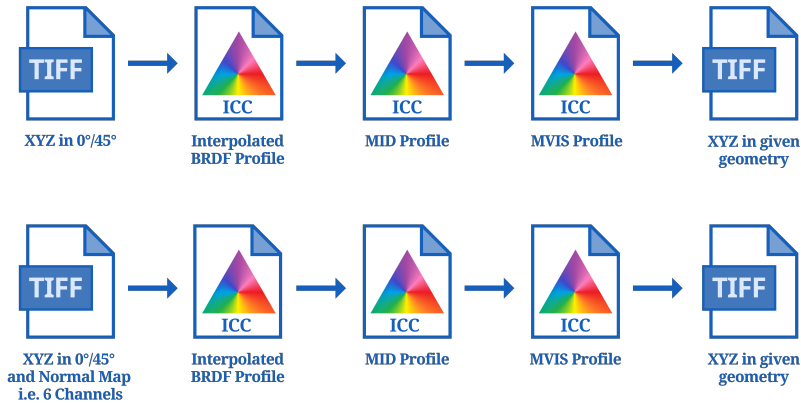


Figure 5.1: Appearance reproduction framework for 2D printing (upper row) and with surface normals (lower row)

Article VIII extends this framework to reproduce the material appearance of 2.5D printed surfaces where the slope information is used to adjust the colour for surfaces with slopes greater than 0° using the adjusted interpolated BRDF profile shown in figure 5.2. The framework also describes a file format required to store and communicate material appearance information. This file format channels have BRDF parameters and surface normals which are utilised by ICC profiles for appearance rendering.

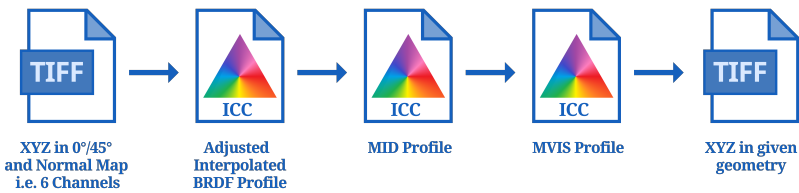


Figure 5.2: Appearance reproduction framework for 2.5D printing.

5.4 Conclusion

First, we showed from the findings in **Article II** that the estimated reflectances show reduced metameric mismatches under different illuminants when the training dataset contains similar material components as that of the test dataset. Additionally, the results indicate that even when the training reflectances are dissimilar, acceptable metameric differences are achieved, owing to the smoothness

of their reflectances and similar peak wavelengths, albeit varying in amplitudes. For instance, the training reflectances of offset-litho on premium-coated paper can be employed to estimate reflectances of textile datasets due to their resemblance in fluorescence and having reflectance curves with sharp peaks in the blue region. This implies that, based on material components, various spectral datasets or printing conditions can be combined, and a single reflectance dataset can represent a common training dataset for reflectance estimation of the entire group. In addition, in **Article III**, a comparison was made between two spectral estimation methods and several well-known CATs and MATs. The results showed that the two spectral estimation methods, namely Weighted Pseudo Inverse and Third Order Polynomial, were found to perform significantly better than other CATs and MATs in minimising metameric mismatch, provided that the training data used was carefully selected. Thus, we showed the importance of using good training datasets, as even simple spectral estimation methods can be used as a sensor adjustment transform to minimise metameric mismatches or achieve material constancy, and if colour constancy is desired, then a training dataset with smooth reflectance that tends to preserve colour under different lighting conditions can be used. These findings are important in colour management, where profiles often depend on chromatic adaptation transforms to predict colours when using a different colorimetry than the standard D50. **Articles II** and **III** provide evidence to adopt spectral estimation methods for spectral PCS.

Article VII explains how to render material appearance using colour management in a didactic manner. It introduces a workflow to extract BRDF parameters and perform appearance rendering through ICC profiles for any incident light angle and viewing angle pair. The results of this colour-managed workflow were consistent with the implementation of the Ward model in Matlab. Furthermore, this article also showed how to incorporate a normal map along with the BRDF parameters in colour management. A file format that includes the BRDF parameters and the normal map channels pixel-wise is required to realise this workflow and render spatially varying BRDF. This rendering workflow was based on 2D printing, i.e. flat, homogeneous surface colours. **Article VIII** showed how material appearance rendering can be achieved for a surface with spatially varying height, that is, for a 2.5D printed surface. This article also achieved an efficient rendering workflow to reproduce the appearance of any printed colour with varying surface normal and light and viewing direction by mixing the BRDF of primary and secondary colours of a flat target and adjusting the colours according to the angle of slope. This workflow also showed that only the BRDF of the primaries and secondaries inks printed on a flat surface and reflectance measurement at $0^\circ:45^\circ$ geometry of white and black samples printed for a number of sloped surfaces are enough for this rendering workflow. This can be a practical and effective way to softproof a 2.5D printed object. However, the accuracy of the workflow depends on the accuracy of the optimised BRDF obtained for the primary and secondary colours and the minimisation technique used in the BRDF interpolation method discussed in Article V. This workflow can be integrated into colour management

using the iccMAX encoding described in **Article VII** together with the normal map. This framework required a file format that carries BRDF parameters and surface normals in its channels.

Supplementary article IV, proposed the use of two predictors and polynomial regression to accurately estimate spectra for diffuse reflections of BRDF measurements. However, this model tends to overestimate specular reflectances, while preserving their relative distribution reasonably well. It does not accurately predict spectra for near-to-specular reflections at angles of 5° and 10° from the specular peaks, indicating the need for a different approach to model these reflectances. The luminance Y values are estimated precisely for both diffuse and specular reflections. However, this model reduced the requirements for measuring BRDF for diffuse reflections to just measuring for two light and viewing direction pairs, and then estimating for the rest of the directions. Article V provided a novel algorithm for obtaining BRDF parameters for any $0^\circ:45^\circ$ XYZ by interpolating the optimised BRDF parameters of the printed primary and secondary colours. We showed how this can be used to handle the appearance reproduction of a 2.5D printed surface in **Article VIII**. Similarly, Article VI showed an elegant way to render the material appearance of a 2D printed surface with an isotropic BRDF model encoded within a ICC profile.

Supplementary Article IX proposed a goodness-of-fit metric, which applies weights to different metrics based on selected criteria and combines them to assess the fit between two spectra. This metric is helpful because it allows the weights of the components of this metric to be adjusted according to their relative importance in a given application.

Figures 5.3, 5.4 and 5.5 summarise the tasks completed that were set out during the initial stage of the Ph. D. which was discussed at the end of Chapter 1. Every deliverable, course and training planned was completed except for one. Deliverable, *Evaluation of reproduction using psychophysical experiments and objective quality metrics* was not completed due to time constraints and left as future work.

5.5 Future Scope

Articles II & III suggested that training datasets can be grouped together based on their similarity in printing conditions, this can be further evaluated with reflectance datasets for industrial use cases and can be adopted by ICC recommend standard training datasets required for implementing spectral estimation through ICC profiles. In addition, spectral estimation can be adopted to connect colour profiles through a spectral PCS. Moreover, the same estimation procedure can be recommended as a sensor adjustment transform whenever a profile needs to connect to another profile having different colorimetry. This work opens the door to the realisation of different workflows for spectral reproduction through ICC

Work Plan No.	Goal	Deliverable	Completed
WP1	Spectral reproduction	• Documenting review on chromatic adaptation transforms and spectral reproduction workflows and use cases.	✓
		• "Spectral reproduction: Drivers, use cases, and workflow.", paper submission to Electronic Imaging 2020.	✓
WP2	Spectral estimation method and evaluation	• New method to evaluate the accuracy of a spectral estimation method.	✓
		• Paper submission about spectral estimation method for colour management in a conference.	✓
WP3	Appearance modelling using iccMAX and evaluation	• Reflectance models and other appearance attribute models implementation using iccMAX.	✓
		• Paper on implementing and visualising reflectance models using iccMAX and submission to London Imaging Meeting 2020.	✓
WP4	Appearance reproduction framework and colour management	• An appearance reproduction framework for 2.5D printing.	✓
		• Evaluation of reproduction using psychophysical experiments and objective quality metrics.	—
		• Paper submission on topic of 2.5D appearance reproduction framework to a journal.	✓
WP5	File format for 2.5D appearance reproduction framework	• Introduction of file format to store spectral data, and appearance attributes in the colour management system.	✓
WP6	Thesis writing	• Documentation of the prototypes created, and final PhD thesis compiled.	✓

Figure 5.3: Status of deliverables that were planned in the Ph. D. proposal at the initial stage

colour management, which will require a good testing paradigm that can assess both spectral and colorimetric quality.

Articles VII & VIII provide an appearance reproduction framework for 2.5D printing which can be encoded into an ICC profile using iccMAX. This workflow should be further tested by conducting a psychophysical experiment by printing a 2.5D object and comparing its appearance with its corresponding softproof created using the workflow. This can also be categorised according to texture information from normal maps such as surface with high textural detail and low textural detail, and evaluate the quality of the softproof based on such categories. There is also potential for this workflow to include BRDF measurements of a varnished surface and model gloss. This would require the black and white slope samples to be printed with the varnish allowed by the printer and then measured and modelled. The BRDF modelling can be improved by choosing models according to the material surface, improving the optimisation technique or changing to log space or Jacobian space for optimisation. This should be tested because the accuracy of the BRDF model will also improve the accuracy of the BRDF interpolation method. It is also interesting to see if the adjusted colour

Course Name	ECTS	Level	Semester	Location	Completed
Research Ethics	2.5	Ph. D.	S 2020	Gjøvik	✓
Colour Science	5	Ph. D.	S 2020	Gjøvik	✓
Colour Imaging	7.25	Ph. D.	S 2020	Trondheim	✓
Scientific Communication	5	Ph. D.	S 2022	Gjøvik	✓
Four training schools as part of ApPEARS	10	Ph. D.	S 2020 to A 2022	Gjøvik, Darmstadt, Paris, Bristol	✓

1. S 2020 = Spring semester 2020 2. A 2022 = Autumn semester 2022

Figure 5.4: Status of courses that were planned in the Ph. D. proposal at the initial stage

Code	Course Name	Partners	ECTS	Location	Completed
TE1	Imaging and quality – from colour to appearance	NTNU	4	Gjøvik	✓
TE2	Material appearance workflow	FHG	2	Darmstadt	✓
TE3	Metrology for appearance	CNAM	2	Paris	✓
TE5	Printing innovation and applications	UWE	2	Bristol	✓

1. FHG = Fraunhofer-Gesellschaft 2. CNAM = National Conservatory of Arts and Crafts
3. UWE = University of the West of England

Figure 5.5: Status of trainings that were planned in the Ph. D. proposal at the initial stage

algorithm for slopes can be modified to characterise a 2.5D printer based on colour varying with respect to slopes. The BRDF dataset obtained for 2.5D printed samples can be further used for printer characterisation purpose. In this work, 23 samples of the 72 printed samples were measured because the acquisition of BRDF measurements was time-consuming. The BRDF measurement estimation method developed in Article IV could be used to minimise the number of diffuse measurements, and only specular and near-to-specular reflection measurements should be taken at a denser light and viewing angles encompassing the specular lobe. This workflow should be tested for different printed materials along with varnished surfaces.

References

- [1] J. Yuan, G. Chen, H. Li, H. Prautzsch and K. Xiao, 'Accurate and Computational: A review of color reproduction in Full-color 3D printing,' *Materials & Design*, vol. 209, p. 109 943, 2021.
- [2] *Mimaki 3D Printer*, https://mimaki.com/special/3d_print/, Accessed: 04-04-2023.
- [3] *Stratasys 3D Printers and Softwares*, <https://www.stratasys.com/en/3d-printers/printer-catalog/>, Accessed: 04-04-2023.
- [4] *Canon Production Printing*, <https://cpp.canon/products/touchstone/>, Accessed: 04-04-2023.
- [5] *Casio 2.5D Printer, Mofrel*, <https://mofrel.casio.jp/ja/index.html>, Accessed: 04-04-2023.
- [6] *Casio Mofrel*, <https://hackaday.com/tag/mofrel/>, Accessed: 04-04-2023.
- [7] *Processing Optical Component with Inkjet Printing*, <https://blog.drupa.com/de/processing-optical-component-with-inkjet-printing/>, Accessed: 04-04-2023.
- [8] *Mimaki JFX200 series*, <https://mimaki.com/product/inkjet/i-flat/jfx200-2513/>, Accessed: 04-04-2023.
- [9] C. Parraman, P. O'Dowd and M. Harding, '2.5 D printing: The evolution of the Water Lily,' *Electronic Imaging*, vol. 28, pp. 1–8, 2016.
- [10] M. R. Pointer, 'Measuring visual appearance-a framework of the future. Project 2.3 measurement of appearance.,' 2003.
- [11] A. Standard, *E284, Standard Terminology of Appearance*, 2002.
- [12] C. 175:2006, *A framework for the measurement of visual appearance, International Commission on Illumination*.
- [13] F. H. Imai, D. R. Wyble, R. S. Berns and D.-Y. Tzeng, 'A feasibility study of spectral color reproduction,' *Journal of Imaging Science and Technology*, vol. 47, no. 6, pp. 543–553, 2003.
- [14] M. Yamaguchi, H. Haneishi and N. Ohyama, 'Beyond red–green–blue (RGB): spectrum-based color imaging technology,' *Journal of Imaging Science and Technology*, vol. 52, no. 1, pp. 10 201–1, 2008.

- [15] P. Urban, M. R. Rosen and R. S. Berns, 'Spectral image reconstruction using an edge preserving spatio-spectral Wiener estimation,' *JOSA A*, vol. 26, no. 8, pp. 1865–1875, 2009.
- [16] J. Gerhardt and J. Y. Hardeberg, 'Simple Comparison of Spectral Color Reproduction Workflows,' in *Image Analysis: 16th Scandinavian Conference, SCIA 2009, Oslo, Norway, June 15-18, 2009. Proceedings 16*, Springer, 2009, pp. 550–559.
- [17] M. R. Luo, 'Extreme Colour Reproduction: Spectral and Preferred,' in *Advanced Materials Research*, Trans Tech Publ, vol. 174, 2011, pp. 3–7.
- [18] C. Eugène, 'Measurement of "total visual appearance": a CIE challenge of soft metrology,' in *12th IMEKO TC1 & TC7 Joint Symposium on Man, Science & Measurement*, IMEKO Budapest, 2008, pp. 61–65.
- [19] M. Lindstrand, 'Instrumental gloss characterization–In the light of visual evaluation: A review,' *Journal of Imaging Science and Technology*, vol. 49, no. 1, pp. 61–70, 2005.
- [20] F. B. Leloup, G. Obein, M. R. Pointer and P. Hanselaer, 'Toward the soft metrology of surface gloss: A review,' *Color Research & Application*, vol. 39, no. 6, pp. 559–570, 2014.
- [21] G. Ged, A.-M. Rabal-Almazor, M. E. Himbert and G. Obein, 'Assessing gloss under diffuse and specular lighting,' *Color Research & Application*, vol. 45, no. 4, pp. 591–602, 2020.
- [22] D. Gigilashvili, J.-B. Thomas, J. Y. Hardeberg and M. Pedersen, 'Translucency perception: A review,' *Journal of Vision*, vol. 21, no. 8, pp. 4–4, 2021.
- [23] F. Bianconi, A. Fernández, F. Smeraldi and G. Pascoletti, 'Colour and texture descriptors for visual recognition: A historical overview,' *Journal of Imaging*, vol. 7, no. 11, p. 245, 2021.
- [24] M. Haindl and J. Filip, *Visual texture: Accurate material appearance measurement, representation and modeling*. Springer Science & Business Media, 2013.
- [25] C. Schwartz, R. Sarlette, M. Weinmann, M. Rump and R. Klein, 'Design and implementation of practical bidirectional texture function measurement devices focusing on the developments at the university of bonn,' *Sensors*, vol. 14, no. 5, pp. 7753–7819, 2014.
- [26] J. Filip, R. Vávra and M. Krupička, 'Rapid material appearance acquisition using consumer hardware,' *Sensors*, vol. 14, no. 10, pp. 19 785–19 805, 2014.
- [27] C. Parraman and M. V. O. Segovia, *2.5 D Printing: Bridging the gap between 2D and 3D applications*. John Wiley & Sons, 2018.
- [28] ISO 3664:2009, 'Graphic technology and photography — Viewing conditions,' *ISO, Geneva*, 2009.

- [29] ISO 12646:2015, 'Graphic technology and photography — Displays for colour proofing — Characteristics,' *ISO, Geneva*, 2015.
- [30] ISO 14861:2015, 'Graphic technology and photography — Requirements for colour soft proofing systems,' *ISO, Geneva*, 2015.
- [31] ICC, 'Specification ICC.2:2019 Image technology colour management — extensions to architecture, profile format and data structure,' *International Color Consortium*, 2019.
- [32] M. Rosen, 'Navigating the roadblocks to spectral color reproduction: Data-efficient multi-channel imaging and spectral color management,' Ph.D. dissertation, Rochester Institute of Technology, 2003.
- [33] B. Wang, H. Xu, M. R. Luo and J. Guo, 'Spectral-based color separation method for a multi-ink printer,' *Chinese Optics Letters*, vol. 9, no. 6, p. 063 301, 2011.
- [34] P. Urban and R. S. Berns, 'Parameter mismatch-based spectral gamut mapping,' *IEEE transactions on image processing*, vol. 20, no. 6, pp. 1599–1610, 2010.
- [35] ICC, 'Specification ICC.1:2022 Image technology colour management — architecture, profile format, and data structure,' *International Color Consortium*, 2022.
- [36] M. Page, G. Obein, C. Boust and A. Razet, 'Adapted modulation transfer function method for characterization and improvement of 3D printed surfaces,' *Electronic Imaging*, vol. 29, pp. 92–100, 2017.
- [37] T. P. Van Song, C. Andraud and M. V. Ortiz-Segovia, 'Towards spectral prediction of 2.5 d prints for soft-proofing applications,' in *2016 Sixth International Conference on Image Processing Theory, Tools and Applications (IPTA)*, IEEE, 2016, pp. 1–6.
- [38] S. H. Westin, H. Li and K. E. Torrance, 'A field guide to brdf models,' in *SIGGRAPH*, 2004.
- [39] R. Montes and C. Ureña, 'An overview of BRDF models,' *University of Grenada, Technical Report LSI-2012-001*, 2012.
- [40] T. Habib, P. Green and P. Nussbaum, 'Spectral reproduction: drivers, use cases and workflow,' *Electronic Imaging*, vol. 32, pp. 1–6, 2020.
- [41] T. Habib, P. Green and P. Nussbaum, 'Spectral estimation: Evaluation and Application (Under Review),' *Optics Express*, 2023.
- [42] T. Habib, P. Green and P. Nussbaum, 'Spectral estimation: As a Sensor Adjustment Transform (Under Review),' *Optics Express*, 2023.
- [43] T. Habib, P. Green and P. Nussbaum, 'Estimation of BRDF Measurements for Printed Colour Samples,' vol. 29, pp. 123–128, 2021.

- [44] T. Habib, P. Green and P. Nussbaum, 'BRDF rendering by interpolation of optimised model parameters,' in *Color and Imaging Conference*, Society for Imaging Science and Technology, vol. 28, 2020, pp. 162–168.
- [45] T. Habib, P. Green and A. Sole, 'Implementing directional reflectance in a colour managed workflow,' in *London Imaging Meeting*, Society for Imaging Science and Technology, vol. 1, 2020, pp. 119–123.
- [46] T. Habib, 'Colour Management of Material Appearance,' in *Colour Engineering: Fundamentals and Applications (Under Production)*, P. Green, Ed., John Wiley & Sons, 2023.
- [47] T. Habib, P. Green and P. Nussbaum, '2.5D Printing: An Appearance Reproduction Framework for Printed 3D Surfaces (Under Review),' *Journal of Imaging Science and Technology*, 2023.
- [48] T. Habib, P. Green and P. Nussbaum, 'A weighted goodness-of-fit metric for comparison of spectra,' in *Sensing Colour, Proceedings of the International Colour Association (AIC) Conference 2022*, International Colour Association, 2022, pp. 397–404.
- [49] A. Sharma, *Understanding color management*. John Wiley & Sons, 2018.
- [50] S. Westland, C. Ripamonti and V. Cheung, *Computational colour science using MATLAB*. John Wiley & Sons, 2012.
- [51] 'Common Color Management Workflows & Rendering Intent Usage,' ICC, Tech. Rep., 2005.
- [52] 'The value of iccMAX,' ICC, Tech. Rep., 2018.
- [53] 'iccMAX MultiProcessingElement Calculator Programming,' ICC, Tech. Rep., 2018.
- [54] S. Zuffi and R. Schettini, 'Innovative method for spectral-based printer characterization,' in *Color Imaging: Device-Independent Color, Color Hardcopy, and Applications VII*, SPIE, vol. 4663, 2001, pp. 1–7.
- [55] S. Zuffi, R. Schettini and G. Mauri, 'Spectral-based printer modeling and characterization,' *Journal of Electronic Imaging*, vol. 14, no. 2, pp. 023 008–023 008, 2005.
- [56] B. Bastani and B. Funt, 'Spectral gamut mapping and gamut concavity,' 2007.
- [57] D.-Y. Tzeng, 'Spectral-based color Separation algorithm development for multiple-ink color reproduction,' Ph.D. dissertation, Rochester Institute of Technology Rochester, 1999.
- [58] J. Gerhardt and J. Y. Hardeberg, 'Spectral color reproduction minimizing spectral and perceptual color differences,' *Color Research & Application*, vol. 33, no. 6, pp. 494–504, 2008.

- [59] B. Sun, H. Liu and S. Zhou, 'Spectral separation for multispectral image reproduction based on constrained optimization method,' *Journal of Spectroscopy*, vol. 2014, 2014.
- [60] D. Eliav, S. Roth and M. Ben Chorin, 'Multi-primary spectral display for soft proofing,' *Journal of Imaging Science and Technology*, vol. 51, no. 6, pp. 492–501, 2007.
- [61] CIE 15:1986, 'Colorimetry,' *CIE Central Bureau, Vienna*, 1986.
- [62] CIE 15:2004, 'Colorimetry,' *CIE Central Bureau, Vienna*, 2004.
- [63] ISO 13655:2017, 'Graphic technology — Spectral measurement and colorimetric computation for graphic arts images,' *ISO, Geneva*, 7.
- [64] CIE 15:2018, 'Colorimetry,' *CIE Central Bureau, Vienna*, 2018.
- [65] 'Recommended practice for tabulating spectral data for use in colour computations,' CIE, Tech. Rep., 2005.
- [66] C. Li, M. R. Luo and B. Rigg, 'A new method for computing optimum weights for calculating CIE tristimulus values,' *Color Research & Application*, vol. 29, no. 2, pp. 91–103, 2004.
- [67] C. Li, 'CIETC1-71 Perspective: An Overview on Accurately Computing Tristimulus Values,' in *Color and Imaging Conference*, Society of Imaging Science and Technology, vol. 16, 2008, pp. 22–27.
- [68] V. Babaei, S. H. Amirshahi and F. Agahian, 'Using weighted pseudo-inverse method for reconstruction of reflectance spectra and analyzing the dataset in terms of normality,' *Color Research & Application*, vol. 36, no. 4, pp. 295–305, 2011.
- [69] G. Wu, X. Shen, Z. Liu, S. Yang and M. Zhu, 'Reflectance spectra recovery from tristimulus values by extraction of color feature match,' *Optical and Quantum Electronics*, vol. 48, no. 1, pp. 1–13, 2016.
- [70] R. Schettini and B. Barolo, 'Estimating reflectance functions from tristimulus values,' *Applied Signal Processing*, vol. 3, no. 2, pp. 104–115, 1996.
- [71] H. S. Fairman and M. H. Brill, 'The principal components of reflectances,' *Color Research & Application*, vol. 29, no. 2, pp. 104–110, 2004.
- [72] F. Ayala, J. F. Echávarri, P. Renet and A. I. Negueruela, 'Use of three tristimulus values from surface reflectance spectra to calculate the principal components for reconstructing these spectra by using only three eigenvectors,' *JOSA A*, vol. 23, no. 8, pp. 2020–2026, 2006.
- [73] F. Agahian, S. A. Amirshahi and S. H. Amirshahi, 'Reconstruction of reflectance spectra using weighted principal component analysis,' *Color Research & Application*, vol. 33, no. 5, pp. 360–371, 2008.

- [74] Y. Zhao and R. S. Berns, 'Image-based spectral reflectance reconstruction using the matrix R method,' *Color Research & Application*, vol. 32, no. 5, pp. 343–351, 2007.
- [75] P. Stigell, K. Miyata and M. Hauta-Kasari, 'Wiener estimation method in estimating of spectral reflectance from RGB images,' *Pattern Recognition and Image Analysis*, vol. 17, no. 2, pp. 233–242, 2007.
- [76] S. H. Amirshahi and S. A. Amirshahi, 'Adaptive non-negative bases for reconstruction of spectral data from colorimetric information,' *Optical review*, vol. 17, no. 6, pp. 562–569, 2010.
- [77] S. Zuffi, S. Santini and R. Schettini, 'Correcting for not feasible values in reflectance function estimation using linear models,' *AIC Colour*, vol. 5, 2005.
- [78] D. Dupont, 'Study of the reconstruction of reflectance curves based on tristimulus values: comparison of methods of optimization,' *Color Research & Application*, vol. 27, no. 2, pp. 88–99, 2002.
- [79] S. Bianco, 'Reflectance spectra recovery from tristimulus values by adaptive estimation with metameric shape correction,' *JOSA A*, vol. 27, no. 8, pp. 1868–1877, 2010.
- [80] A. Hajipour and A. Shams-Nateri, 'Effect of classification by competitive neural network on reconstruction of reflectance spectra using principal component analysis,' *Color Research & Application*, vol. 42, no. 2, pp. 182–188, 2017.
- [81] F. M. Abed, S. H. Amirshahi and M. R. M. Abed, 'Reconstruction of reflectance data using an interpolation technique,' *JOSA A*, vol. 26, no. 3, pp. 613–624, 2009.
- [82] E. Chen and T.-R. Chou, 'Spectral reflectance recovery of various materials based on linear interpolation with nonparametric metameric spectra of extreme points,' in *Proceedings of the 3rd International Conference on Cryptography, Security and Privacy*, 2019, pp. 247–255.
- [83] B. G. Kim, J.-w. Han and S.-b. Park, 'Spectral reflectivity recovery from the tristimulus values using a hybrid method,' *JOSA A*, vol. 29, no. 12, pp. 2612–2621, 2012.
- [84] R. S. Berns, F. W. Billmeyer Jr and R. S. Sacher, 'Methods for generating spectral reflectance functions leading to color-constant properties,' *Color Research & Application*, vol. 10, no. 2, pp. 73–83, 1985.
- [85] C. Van Trigt, 'Smoothest reflectance functions. I. Definition and main results,' *JOSA A*, vol. 7, no. 10, pp. 1891–1904, 1990.
- [86] C. Van Trigt, 'Smoothest reflectance functions. II. Complete results,' *JOSA A*, vol. 7, no. 12, pp. 2208–2222, 1990.

- [87] L. El Ghaoui and H. Le Bret, 'Robust solutions to least-squares problems with uncertain data,' *SIAM Journal on matrix analysis and applications*, vol. 18, no. 4, pp. 1035–1064, 1997.
- [88] H. R. Kang, *Computational color technology*. Spie Press Bellingham, 2006.
- [89] M. W. Derhak, E. L. Luo and P. J. Green, 'Fast chromatic adaptation transform utilizing Wpt (Waypoint) based spectral reconstruction,' in *London Imaging Meeting*, Society for Imaging Science and Technology, vol. 2020, 2020, pp. 49–53.
- [90] M. W. Derhak, *Spectrally Based Material Color Equivalency: Modeling and Manipulation*. Rochester Institute of Technology, 2015.
- [91] A. Werner, 'Spatial and temporal aspects of chromatic adaptation and their functional significance for colour constancy,' *Vision research*, vol. 104, pp. 80–89, 2014.
- [92] M. D. Fairchild, *Colour Engineering: Fundamentals and Applications*. John Wiley & Sons, 2013.
- [93] C. Gao, Z. Wang, Y. Xu, M. Melgosa, K. Xiao, M. H. Brill and C. Li, 'The von Kries chromatic adaptation transform and its generalization,' *Chinese Optics Letters*, vol. 18, no. 3, p. 033 301, 2020.
- [94] M. W. Derhak and R. S. Berns, 'Introducing Wpt (Waypoint): A color equivalency representation for defining a material adjustment transform,' *Color Research & Application*, vol. 40, no. 6, pp. 535–549, 2015.
- [95] S. E. Susstrunk, J. M. Holm and G. D. Finlayson, 'Chromatic adaptation performance of different RGB sensors,' in *Color Imaging: Device-Independent Color, Color Hardcopy, and Graphic Arts VI*, SPIE, vol. 4300, 2000, pp. 172–183.
- [96] G. D. Finlayson and S. Süssstrunk, 'Performance of a chromatic adaptation transform based on spectral sharpening,' in *Proc. IS&T;/SID 8th Color Imaging Conference*, vol. 8, 2000, pp. 49–55.
- [97] 'A Colour Appearance Model for Color Management Systems: CIECAM02,' Commission Internationale de l'Éclairage, Tech. Rep., 2004.
- [98] C. Li, Z. Li, Z. Wang, Y. Xu, M. R. Luo, G. Cui, M. Melgosa, M. H. Brill and M. Pointer, 'Comprehensive color solutions: CAM16, CAT16, and CAM16-UCS,' *Color Research & Application*, vol. 42, no. 6, pp. 703–718, 2017.
- [99] C. Li, Y. Xu, Z. Wang, M. R. Luo, G. Cui, M. Melgosa, M. H. Brill and M. Pointer, 'Comparing two-step and one-step chromatic adaptation transforms using the CAT16 model,' *Color Research & Application*, vol. 43, no. 5, pp. 633–642, 2018.

- [100] C. Oleari, M. Melgosa and R. Huertas, 'Generalization of color-difference formulas for any illuminant and any observer by assuming perfect color constancy in a color-vision model based on the OSA-UCS system,' *JOSA A*, vol. 28, no. 11, pp. 2226–2234, 2011.
- [101] I. Tastl, M. A. Lopez-Alvarez, A. Ju, M. Schramm, J. Roca and M. Shepherd, 'A Soft-proofing Workflow for Color 3D Printing-Addressing Needs for the Future,' *Electronic Imaging*, vol. 2019, no. 6, pp. 479–1, 2019.
- [102] T. Weyrich, J. Lawrence, H. P. Lensch, S. Rusinkiewicz, T. Zickler *et al.*, 'Principles of appearance acquisition and representation,' *Foundations and Trends® in Computer Graphics and Vision*, vol. 4, no. 2, pp. 75–191, 2009.
- [103] J. Murray-Coleman and A. Smith, 'The automated measurement of BRDFs and their application to luminaire modeling,' *Journal of the Illuminating Engineering Society*, vol. 19, no. 1, pp. 87–99, 1990.
- [104] J. E. Proctor and P. Y. Barnes, 'NIST high accuracy reference reflectometer-spectrophotometer,' *Journal of research of the National Institute of Standards and Technology*, vol. 101, no. 5, p. 619, 1996.
- [105] J. Gu, C.-I. Tu, R. Ramamoorthi, P. Belhumeur, W. Matusik and S. Nayar, 'Time-varying surface appearance: acquisition, modeling and rendering,' *ACM Transactions on Graphics (TOG)*, vol. 25, no. 3, pp. 762–771, 2006.
- [106] M. Ben-Ezra, J. Wang, B. Wilburn, X. Li and L. Ma, 'An LED-only BRDF measurement device,' in *2008 IEEE Conference on Computer Vision and Pattern Recognition*, IEEE, 2008, pp. 1–8.
- [107] S. R. Marschner, S. H. Westin, E. P. Lafortune and K. E. Torrance, 'Image-based bidirectional reflectance distribution function measurement,' *Applied optics*, vol. 39, no. 16, pp. 2592–2600, 2000.
- [108] J. Günther, T. Chen, M. Goesele, I. Wald and H.-P. Seidel, 'Efficient acquisition and realistic rendering of car paint,' in *Vision, Modeling, and Visualization*, Citeseer, vol. 5, 2005, pp. 487–494.
- [109] A. S. Sole, I. Farup and S. Tominaga, 'An image-based multi-directional reflectance measurement setup for flexible objects,' in *Measuring, Modeling, and Reproducing Material Appearance 2015*, SPIE, vol. 9398, 2015, pp. 162–172.
- [110] J. F. Blinn, 'Models of light reflection for computer synthesized pictures,' in *Proceedings of the 4th annual conference on Computer graphics and interactive techniques*, 1977, pp. 192–198.
- [111] B. Walter, 'Notes on the Ward BRDF,' *Program of Computer Graphics, Cornell University, Technical report PCG-05*, vol. 6, 2005.
- [112] R. L. Cook and K. E. Torrance, 'A reflectance model for computer graphics,' *ACM Transactions on Graphics (ToG)*, vol. 1, no. 1, pp. 7–24, 1982.

- [113] M. Luo, B. Rigg and K. Smith, 'Cmc 2002 colour inconstancy index; cmccon02,' *Coloration Technology*, vol. 119, no. 5, pp. 280–285, 2003.
- [114] F. H. Imai, M. R. Rosen and R. S. Berns, 'Comparative study of metrics for spectral match quality,' in *Conference on colour in graphics, imaging, and vision*, Society for Imaging Science and Technology, vol. 2002, 2002, pp. 492–496.
- [115] I. Nimeroff and J. Yurow, 'Degree of metamerism,' *JOSA*, vol. 55, no. 2, pp. 185–190, 1965.
- [116] J. S. Viggiano, 'The comparison of radiance ratio spectra: Assessing a model's "goodness of fit",'" in *Advanced Printing of Conference Summaries: SPSE's 43rd Annual Conference*, 1990, pp. 222–225.
- [117] P. J. Green, 'A smoothness metric for colour transforms,' in *Color Imaging XIII: Processing, Hardcopy, and Applications*, SPIE, vol. 6807, 2008, pp. 155–159.
- [118] U. Eastern Finland, *Munsell colors glossy (all) (Spectrofotometer measured)*, <https://sites.uef.fi/spectral/munsell-colors-glossy-all-spectrofotometer-measured/>, Accessed: 2023-01-20.
- [119] *FOGRA51 spectral dataset*, <https://www.color.org/chardata/fogra51.xalter>, Accessed: 2023-01-20.
- [120] ISO 15076-1:2010, 'Image technology colour management - Architecture, profile format, and data structure,' *ISO, Geneva*, 2010.
- [121] A. D. Logvinenko, B. Funt and C. Godau, 'Metamer mismatching,' *IEEE Transactions on Image Processing*, vol. 23, no. 1, pp. 34–43, 2013.
- [122] X. Zhang, B. Funt and H. Mirzaei, 'Metamer mismatching in practice versus theory,' *JOSA A*, vol. 33, no. 3, A238–A247, 2016.
- [123] S. A. Burns, 'Chromatic adaptation transform by spectral reconstruction,' *Color Research & Application*, vol. 44, no. 5, pp. 682–693, 2019.
- [124] K. Deshpande and P. Green, 'A simplified method of predicting the colorimetry of spot color overprints,' in *Color and Imaging Conference*, Society for Imaging Science and Technology, vol. 2010, 2010, pp. 213–216.
- [125] C. R. Lin, J. F. Xu and J. L. Xu, 'Prediction Algorithm of Spectral Reflectance of Spot Color Ink Based on Color Parallel and Superposition Model,' in *Advanced Materials Research*, Trans Tech Publ, vol. 430, 2012, pp. 1176–1182.
- [126] Y. Chen, R. S. Berns and L. A. Taplin, 'Six color printer characterization using an optimized cellular Yule-Nielsen spectral Neugebauer model,' *Journal of Imaging Science and Technology*, vol. 48, no. 6, pp. 519–528, 2004.
- [127] J. Guo, H. Xu, M. R. Luo and B. Wang, 'Spectral characterisation of colour printer based on a novel grey component replacement method,' *Chinese Optics Letters*, vol. 9, no. 7, pp. 073 301–073 301, 2011.

- [128] L. G. Coppel, S. Le Moan, P. Z. Elias, R. Slavuj and J. Harderberg, 'Next generation printing-Towards spectral proofing,' *Advanced in Printing and Media Technology*, vol. 41, pp. 19–24, 2014.
- [129] ISO 12647-2:2013, 'Process control for the production of half-tone colour separations, proof and production prints — Part 2: Offset lithographic processes,' *ISO, Geneva*, 2013.
- [130] A. Gudzenchuk, P. Green and H. Don, 'Printer spectral color characterization adjustment for change in substrates,' *Electronic Imaging*, vol. 34, pp. 1–5, 2022.
- [131] J. Meng, F. Simon, J. Hanika and C. Dachsbacher, 'Physically meaningful rendering using tristimulus colours,' in *Computer Graphics Forum*, Wiley Online Library, vol. 34, 2015, pp. 31–40.
- [132] K. D. A. C. A. Wilkie and W. Purgathofer, 'Tone reproduction and physically based spectral rendering,' in *Eurographics*, 2002.
- [133] M. Yamaguchi, H. Haneishi, H. Fukuda, J. Kishimoto, H. Kanazawa, M. Tsuchida, R. Iwama and N. Ohyama, 'High-fidelity video and still-image communication based on spectral information: Natural vision system and its applications,' in *Spectral imaging: eighth international symposium on multispectral color science*, SPIE, vol. 6062, 2006, pp. 129–140.
- [134] M. Yamaguchi, Y. Murakami, H. Hashizume, H. Haneishi, Y. Kanno and Y. Komiya, 'High-fidelity color video reproduction of open surgery by six-band camera,' in *Medical Imaging 2010: Image Perception, Observer Performance, and Technology Assessment*, SPIE, vol. 7627, 2010, pp. 61–69.
- [135] B. Oicherman, M. R. Luo, B. Rigg and A. R. Robertson, 'Effect of observer metamerism on colour matching of display and surface colours,' *Color Research & Application*, vol. 33, no. 5, pp. 346–359, 2008.
- [136] D. Long and M. D. Fairchild, 'Reducing observer metamerism in wide-gamut multiprimary displays,' in *Human Vision and Electronic Imaging XX*, SPIE, vol. 9394, 2015, pp. 265–277.
- [137] Y. Asano, *Individual colorimetric observers for personalized color imaging*. Rochester Institute of Technology, 2015.
- [138] R. Bala, K. M. Braun and R. P. Loce, 'Watermark encoding and detection using narrowband illumination.,' in *Color Imaging Conference*, 2009, pp. 139–142.

Included Articles

Article I

T. Habib, P. Green and P. Nussbaum, 'Spectral reproduction: drivers, use cases and workflow,' *Electronic Imaging*, vol. 32, pp. 1–6, 2020

Spectral reproduction: drivers, use cases and workflow

Tanzima Habib, Phil Green and Peter Nussbaum, Norwegian University of Science and Technology, Gjøvik, Norway

Abstract

This paper identifies the drivers that enable spectral reproduction today and have the ability to increase its usage in the future. Different use cases of spectral reproduction in the field of colour imaging are discussed along with some of the possible workflows. Some workflows are further divided into input, spectral processing and output units as an example, such that the individual spectral processing units that can be encoded in an ICC profile can be identified. It also gives a map of how some common processing elements can be connected in order to constitute a spectral reproduction system.

Introduction

The majority of today's colour reproduction systems are based on trichromacy, whereby the three cones of the human visual system are stimulated in ratios that match those of the desired appearance. Trichromatic reproduction is efficient, requiring only three primaries, and there can be considerable flexibility in the choice of primaries for particular reproduction goals. Nevertheless, trichromatic reproduction has a number of limitations, the most obvious being that matches are metameric and may not hold when the spectral power distribution of the viewing illumination varies.

Spectral data are being increasingly used at all stages of the colour reproduction workflow. This demand has also led to the evolution of spectral acquisition systems that can capture narrow band spectral data with precision, processors that can compute and handle data faster, storage devices that are portable and can store large amount data and output devices that has wider/bigger gamut to reproduce a close match to the original colour. With the availability of multispectral and hyperspectral cameras and other spectral imaging devices, spectral and multi-channel data is now more abundant. This has enabled the acquisition of surface reflectance that holds accurate colour information of a scene. For example, using reflectance samples, spectral characterisation of printers is achieved where the device dependent space is described by a reflectance function. In the colorant industries, spectral reflectance data of inks and paints help minimise metameric effects. In cultural heritage conservation, spectral data is used to characterise materials and used for restoration.

It may also be necessary to transform from a colorimetric domain to a higher dimension spectral domain for intermediate processing. For example, watermarking images in the spectral domain can make the watermark imperceptible [1]. It also enables the use of metameric samples to hide data for a range of illuminants. Spectral reproduction can also be used to perform chromatic adaptation [2]. An intermediate spectral reproduction step can help create an image that looks like a real scene using a photorealistic rendering system.

Because spectral data provides more information about material properties and enables increase accuracy for colour matching, spectrally-defined colour reproduction is in demand in

fields like medical imaging, cultural heritage, (artwork reproduction, textiles etc. Graphic communication industries are especially interested in the use of spectral data to create accurate reproduction of spot colours. Spectral data can be used to reduce metameric effects, which is important for colour critical work and for accurate characterisation of devices [3] [4].

Many spectral reconstruction methods have been developed to enable conversion between three-component data and spectral data. Simple methods like principal component analysis [5] [6] or pseudo inverse methods [7] are frequently used, while more complex methods use neural network, support vector regression and constrained linear programming [8]. Below we review an example of such methods within a spectral reproduction workflow and the current colour management architecture.

A complete spectrally based colour management framework is now possible where the input, the output and all intermediate processing can be spectral, by making use of the iccMAX colour management architecture. It is also anticipated that a colour appearance framework can be better defined using spectral information where BRDF data can be used to model gloss and texture in addition to colour.

Although technology today provides a strong basis for the implementation of spectral reproduction workflows, there are still certain physical limitations [9]:

- original scene spectra cannot have a complete match with the spectra reproduced by the output device or there cannot be a complete match between reproductions by different media devices (example a display and a print)
- there is usually a difference in the dynamic range of the original scene and the output device

We address these issues by mapping the original scene to the reproduction gamut that best represents the appearance of the original. (The evaluation of the quality of reproduction is outside the scope of this paper.) In this paper, we review spectral acquisition and processing, discuss the different use cases of spectral reproduction that are being used today and identify some of the spectral reproduction workflows and methods of connecting their different components.

Spectral acquisition and processing

Spectral acquisition is the capturing of image data over wavelength intervals smaller than be found in broadband trichromatic capture. Multispectral and hyperspectral imaging can also be based on wavelength intervals outside the visible spectrum (although here we consider only the visible spectrum). Measurement instruments can capture surface reflectance or transmittance of an object, or the spectral radiance or irradiance of a luminous source. Multispectral and hyperspectral imaging devices are increasingly used in applications such as medical imaging and cultural heritage, where precise spectral data of a scene is critical for image capture

and possibly reproduction [9]. Spectral processing methods such as spectral estimation can be applied to multispectral or colorimetric data with a priori knowledge to convert them to spectral reflectance or radiance when required instead of using hyperspectral data that requires larger storage or bandwidth to transmit over the internet [10].

Various spectral processing steps are required to achieve a reproduction aim. Noise removal, dimensionality increase or decrease, transformations from spectral to colorimetry, spectral separation, spectral matching, gamut mapping etc. can be performed. These processes can be computationally expensive and hence the encoding of spectral reproduction workflows within colour management should be carefully designed for computational efficiency. We will discuss a few examples in the following sections.

Spectral Reproduction

Some of the use cases of spectral reproduction are discussed below:

Use case 1: Spot colour reproduction

In printing, it is often required to match a spot colour using process colours for example to reproduce a brand colour on a document. In such a case, the spectral reflectance of the spot colour is used to find the best spectral match that can be obtained with the process colours. The reflectance of the spot colour is stored in the ICC profile and/or PDF file using the CxF/x4 file format [11], and a spectral matching algorithm can then be used to find the best combination of process colours. Similar spectral characterisation can be done for the reflectances of spot colour tints and overprints. Another example for spectral reproduction is the prediction of the colorimetry of spot colour overprints of two inks for the purpose of previewing using a linear combination of the reflectances of the two inks [12, 13].

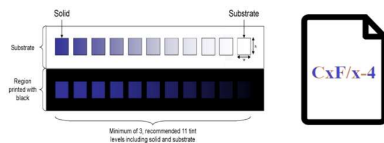


Figure 1. Spot colour reproduction

Use case 2: Ink switching

When an ink is switched or an ink sequence is changed as shown in figure 2., a printer needs to be characterised to map the new state. This can be done using spectral characterisation and CxF-4 files to access the reflectance data. Many different spectral characterisation algorithms exist [3] [14] [15].



Figure 2. Ink switching

Use case 3: Substrate colour adjustment

Substrate correction adjusts colorimetry to compensate for substrate colour in order to obtain a visual match. A degree of adaptation is applied, depending on how close the substrate white point is to the reference white point. data method for achieving this colorimetrically is defined in ISO 12647-2. If this adjustment is computed in the spectral domain, a new way to apply partial adaptation to the spectral reproduction can be developed instead of only performing media relative adjustment. This use case is for future consideration.

Use case 4: Data hiding

Watermarking objects for copyright protection, temper detection, authentication etc. is another use case where spectral data of an image can be used for such embedding. Metameric pairs of a colorant can be used to implement the watermarks. A few methods were suggested by Bala et. al [1]. Metameric colours can be used to create an image and to embed corresponding watermarks that can be easily deciphered by an infrared light/or narrow band illumination/ or using UV light (figure 3) depending on the characteristics of the watermark [1]. Spectral estimation of colorimetry before the watermarking stage is essential in this workflow.

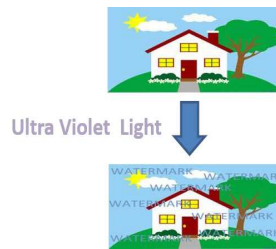


Figure 3. Watermarking using metameric colours [1]

Use case 5: Scene referred spectral reproduction

In order to create an image that is similar to that perceived by an observer looking at a real scene, a photorealistic rendering system is used [16] [17]. In this case a database of natural spectra is required that would match the visual impression of an observer to virtual scenes. Apart from that, different physical effects such as fluorescence, diffraction, polarization etc. must be supported by the rendering system which is not possible using a tristimulus transport which is dependent on the colour space. It has been pointed out [18], that spectral space has to be used in a physically meaningful rendering system where the output is to be used for predictive purposes. With the advent of High Dynamic Range and Wide Colour Gamut devices, the photorealistic rendered images can be accurately handled. Also, the new colour management architecture can be used to create profiles for such realistic and spectral based rendering.

Use case 6: Hi-fidelity colour reproduction

Hi-fidelity colour reproduction is important in medical imaging and reproduction of art works. In the case of medical imaging, hi-fidelity colour as well as spectral data can help quantify diseases and assess treatments [19] [10]. Spectral data of a scene can be used to reproduce a scene that is colorimetrically accurate. When spectral

images are compressed then one has to ensure that the reconstruction process enables both colorimetric accuracy and spectral accuracy. This ensures that the hi-fidelity of colour reproduction will be preserved under different illumination.

Use case 7: Spectral BRDF

Bi-directional reflectance distribution function (BRDF) is used to render synthetic images at different orientations of the viewing angle and the illumination angles. This is important for reproducing the colour of an object in images as the direction of light or viewing changes. This can be achieved by computing the new reflectance per pixel based on parameters obtained from a BRDF model such as Ward and Cook-Torrance. There are many ways to implement BRDF using iccMAX. BRDF tags can be used to obtain BRDF parameters using an ICC profile or a BRDF model can be encoded with its optimized parameters in an ICC profile to render reflectances directly per pixel by applying the profile. For optimization of parameters, a database of BRDF measurements are required. Many image-based BRDF measurement set ups have been proposed over the years for faster acquisition [20] [21] [22] [23] [24]. Once such set up has been proposed by Sole et. al [25] where the sample on a circular frame is fixed and shot by RGB/multispectral camera for different camera(viewing) and light source angles. A BRDF rendering workflow is given in figure 4.

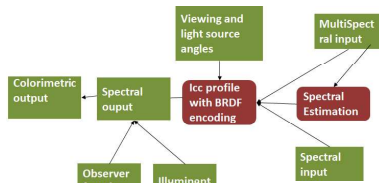


Figure 4. A spectral BRDF Workflow

Use case 8: Reducing metamerism mismatch

In colour reproduction, it is desirable that the prints from two different printing devices matched under different illuminants. For this the two prints have to be matched spectrally. While an exact spectral match is difficult, the best scenario is to minimize the degree of metamerism mismatch for prints or printed objects for a set of illuminants [26] [27]. This is especially important for packaging industries, fine arts, catalogues etc. One such workflow is proposed by Coppel et. al. [27] where spectral separation is carried out by choosing the ink combinations that has spectral match to the target spectra such that that they are within a chosen colour difference threshold under D50 illuminant, from these chosen set again the final ink combination is chosen such that it produces the least colour difference under different set of illuminants. This particular method was inspired by a spectral gamut mapping method described by Urban and Roy [28]. A generic spectral reproduction workflow is given in figure 5.

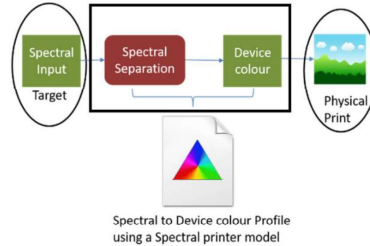


Figure 5. A spectral proofing workflow

Use case 9: Display matching with custom observers

Differences in colour matching functions between observers leads to problems in matching colorimetry on a display. This is called observer metamerism [29]. Wide Colour Gamut displays have spectrally narrow primaries which increases the degree of observer metamerism. One approach is to apply individual colour matching functions to spectra to obtain a personalized reproduction. There are many studies that discuss observer metamerism and the need for personalized softproofing [30] [31] [32] [33]. One such workflow can be when we wish to match Observer 1's print to Observer 2's colour perception, where we can use the colour matching function of Observer 1 to characterise a printer and apply this profile to reproduce a print that matches the colour perception of observer 2.

Connecting spectral reproduction workflows

All the above spectral reproduction use cases have some common components in their workflows. The generic workflow is, given an input image (colorimetric, spectral or multispectral) we perform some intermediate spectral processing and output an image that satisfies a reproduction goal. Processing units such as BRDF processing, process colour matching, spectral characterisation, and custom observer colour matching represent the reproduction goals while processing modules such as spectral estimation, spectral gamut mapping etc. are the common intermediate processing units that can be used by any workflow. The input to such a spectral reproduction system can be colorimetric, spectral or multi-spectral data with the flexibility to pass more parameters (e.g. viewing angle, illumination angle) as input while the output can be obtained in colorimetric, spectral or multispectral domain. Figure 6 gives an overview of such a spectral reproduction system whose individual components can be envisioned to be encoded and connected using the new colour management architecture. This new colour management architecture is called iccMAX and it is an extension of ICC V4, developed to cater to requirements such as support for spectral data, flexibility in using any illuminant or colour matching function, programmable transforms using calculator element etc [34] [35].

Encoding a spectral estimation method using iccMAX has been successfully implemented in which a profile is created to produce

the estimated reflectance of an XYZ image. An intermediate transformation step is included in the profile to convert images from other colour spaces to XYZ before the spectral estimation process. This image can then be used for further processing to achieve a reproduction aim. A good example of BRDF implementation using iccMAX is described by Vogh [36].

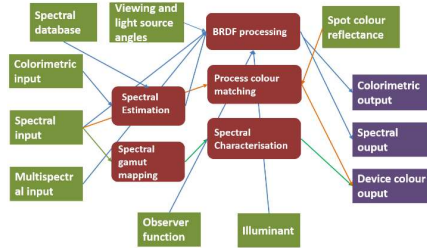


Figure 6. Connecting different spectral reproduction units

Conclusion

This paper reviews spectral reproduction use cases and workflows to establish the necessity of moving towards a spectral colour management. Spectral estimation, BRDF rendering etc. using spectral ICC profile is now possible. These researches can open new doors towards achieving other spectral reproduction goals. But certain needs have yet to be addressed to create an efficient and consistent spectral reproduction system. Some of these requirements are - standardization of intermediate spectral processing units such as spectral estimation, more object specific spectral database has to be created, new metrics to assess the quality of spectral reproduction are required and there should be support for multichannel profiles in existing graphic editors.

Author Biography

Tanzima Habib is a PhD scholar at NTNU, Norway. She has a diverse background in software engineering and geoinformatics, and her interest lies primarily in the domain of colour management and image processing.

Phil Green is Professor of Colour Imaging at the Colour and Visual Computing Laboratory, NTNU, Norway. He is also Technical Secretary of the International Colour Consortium.

Peter Nussbaum is Associate Professor at NTNU, Gjøvik within the Faculty of Computer Science and Media Technology and Department of Computer Science.

References

- [1] R. Bala, K. M. Braun and R. P. Loece, "Watermark encoding and detection using narrowband illumination," in *Color and Imaging Conference*, 2009.
- [2] S. A. Burns, "Chromatic adaptation transform by spectral reconstruction," *Color Research & Application*, 2019.
- [3] Y. Chen, R. S. Berns and L. A. Taplin, "Six color printer characterization using an optimized cellular Yule-Nielsen spectral Neugebauer model," *Journal of Imaging Science and Technology*, vol. 48, no. 6, pp. 519-528, 2004.
- [4] M.-C. Lo and C.-L. J. H. T.-H. Chen, "Characterization of High-Fidelity Color Printing Devices Using Illuminant-Independent Approaches for Color Imaging Application.," *NIP & Digital Fabrication Conference*, vol. 2, pp. 597-602, 2008.
- [5] H. S. Fairman and M. H. Brill, "The principal components of reflectances," *Color Research & Application: Endorsed by Inter-Society Color Council, The Colour Group (Great Britain), Canadian Society for Color, Color Science Association of Japan, Dutch Society for the Study of Color, The Swedish Colour Centre Foundation, Colour Soc*, vol. 29, no. 2, pp. 104-110, 2004.
- [6] F. Agahian, S. A. Amirshahi and S. H. Amirshahi, "Reconstruction of reflectance spectra using weighted principal component analysis," *Color Research & Application: Endorsed by Inter-Society Color Council, The Colour Group (Great Britain), Canadian Society for Color, Color Science Association of Japan, Dutch Society for the Study of Color, The Swedish Colour Centre Foundation, Colour Soc*, vol. 33, no. 5, pp. 360-371, 2008.
- [7] V. Babaci, S. H. Amirshahi and F. Agahian, "Using weighted pseudo-inverse method for reconstruction of reflectance spectra and analyzing the dataset in terms of normality," *Color Research & Application*, vol. 36, no. 4, pp. 295-305, 2011.
- [8] W. F. Zhang and D. Q. Dai, "Spectral reflectance estimation from camera responses by support vector regression and a composite model," *I. JOSA A*, vol. 25, no. 9, pp. 2286-2296, 2008.
- [9] F. H. Imai, "Spectral-based Imaging Techniques and the Image Quality Challenge," in *Ninth International Symposium on Multispectral Colour Science and Application, IS&T*, 2007.
- [10] M. Yamaguchi, Y. Murakami, H. Hashizume, H. Haneishi, Y. Kanno and Y. Komiya, "High-fidelity color video reproduction of open surgery by six-band camera," *Medical Imaging 2010: Image Perception, Observer Performance, and Technology Assessment*, vol. 7627, p. 762707, 2010.
- [11] ICC, "Proofing and printing documents that include spot inks," 20 02 2018. [Online]. Available: http://www.color.org/CxF_test.xalter.
- [12] K. Deshpande and P. Green, "A simplified method of predicting the colorimetry of spot color overprints," in *Color and Imaging Conference*, vol. 1, pp. 213-216, 2010.
- [13] C. Lin, J. Xu and J. Xu, "Prediction Algorithm of Spectral Reflectance of Spot Color Ink Based on Color Parallel and Superposition Model," in *Advanced Materials Research*, 2012.
- [14] S. Zuffi, R. Schettini and G. Mauri, "Spectral-based printer modeling and characterization," *Journal of Electronic Imaging*, vol. 14, no. 2, p. 023008, 2005.
- [15] J. Guo, H. Xu, M. R. Luo and B. Wang, "Spectral characterisation of colour printer based on a novel grey component replacement method.," *Chinese Optics Letters* 9, no. 9, pp. 073301-073301, 2011.
- [16] K. D. A. C. A. Wilkie and W. Purgathofer, "Tone reproduction and physically based spectral rendering," in *Eurographics*, 2002.

- [17] J. Meng, F. Simon, J. Hanika and C. Dachsbacher, "Physically meaningful rendering using tristimulus colors," vol. 34, no. 4, pp. 31-40., 2015.
- [18] R. A. Hall and D. P. Greenberg, "A testbed for realistic image synthesis," *IEEE Computer Graphics and Applications*, vol. 3, no. 8, pp. 10-20, 1983.
- [19] M. Yamaguchi, H. Haneishi, H. Fukuda, J. Kishimoto, H. Kanazawa, M. Tsuchida, R. Iwama and N. Ohyama, "High-fidelity video and still-image communication based on spectral information: Natural vision system and its applications," *Spectral Imaging: Eighth International Symposium on Multispectral Color Science*, vol. 6062, p. 60620G, 2006.
- [20] J. R. Bintz, M. J. Mendenhall, M. A. Marciniak, S. D. Butler and J. T. Lloyd, "A novel image-based BRDF measurement system and its application to human skin," *Reflection, Scattering, and Diffraction from Surfaces V*, vol. 9961, p. 996108, 2016.
- [21] A. S. Sole, I. Farup and T. S., "An image-based multi-directional reflectance measurement setup for flexible objects," *Measuring, Modeling, and Reproducing Material Appearance. International Society for Optics and Photonics*, vol. 9398, p. 93980J, 2015.
- [22] A. Sole, I. Farup and S. Tominaga, "Image based reflectance measurement based on camera spectral sensitivities," in *Electronic Imaging*, 2016.
- [23] S. R. Marschner, S. H. Westin, E. P. Lafortune and K. E. Torrance, "Image-based bidirectional reflectance distribution function measurement," *Applied optics*, vol. 39, no. 16, pp. 2592-2600, 2000.
- [24] K. F. Karner, H. Mayer and M. Gervautz, "An image based measurement system for anisotropic reflection," *Computer Graphics Forum*, vol. 15, no. 3, pp. 119-128, 1996.
- [25] A. Sole, I. Farup and P. B. Nussbaum, "Evaluating an image based multi-angle measurement setup using different reflection models," 2017.
- [26] M. E. L. Leow, W. K. M. Ng, B. P. Pereira, A. K. Kour and R. W. H. Pro, "Metamerism in aesthetic prostheses under three standard illuminants—TL84, D65 and F," *Prosthetics and orthotics international* 23, no. 2, pp. 174-180, 1999.
- [27] L. G. Coppel, S. Le Moan, P. Z. S. R. Elias and J. Y. Harderberg, "Next generation printing—Towards spectral proofing," *Advanced in Printing and Media Technology*, vol. 41, pp. 19-24, 2014.
- [28] P. Urban and R. S. Berns, "Paramer mismatch-based spectral gamut mapping," *IEEE transactions on image processing*, vol. 20, pp. 1599-1610, 2010.
- [29] M. D. Fairchild and R. L. Heckaman, "Measuring observer metamerism: The Nimeroff approach," *Color Research & Application*, vol. 41, no. 2, pp. 115-24, 2015.
- [30] A. Sarkar, "Identification and assignment of colorimetric observer categories and their applications in color and vision sciences," PhD diss, 2011.
- [31] Y. Asano, "Individual colorimetric observers for personalized color imaging," 2015.
- [32] B. Oicherman, M. R. Luo, B. Rigg and A. R. Robertson, "Effect of observer metamerism on colour matching of display and surface colours," *Color Research & Application: Endorsed by Inter-Society Color Council, The Colour Group (Great Britain), Canadian Society for Color, Color Science Association of Japan, Dutch Society for the Study of Color, The Swedish Colour Centre Foundation, Colour Soc*, vol. 33, no. 5, pp. 346-359, 2008.
- [33] D. Long and M. D. Fairchild, "Reducing observer metamerism in wide-gamut multiprimary displays," *Human Vision and Electronic Imaging XX*, vol. 9394, p. 93940T, 2015.
- [34] I. C. Consortium, "Icc.2:2018 Image technology colour management extensions xtensions to architecture, profile format, and data structure," [Online]. Available: <http://www.color.org/specification/ICC.2-2019.pdf>.
- [35] 2. International Color Consortium, "iccMAX multiprocessinglelement calculator programming," 2018. [Online]. Available: http://www.color.org/whitepapers/ICC_White_Paper45_Calculator_Programming-v3.pdf.
- [36] J. Vogh, "3D Appearance Management using iccMax," in *ICC Meeting on Display and 3D Printing*, Taipei, 2016, http://www.color.org/events/taipei/7-3D_Appearance_Management_using_iccMAX.pdf.

Article II

T. Habib, P. Green and P. Nussbaum, 'Spectral estimation: Evaluation and Application (Under Review)', *Optics Express*, 2023

This article is awaiting publication and is not included in NTNU
Open

Article III

T. Habib, P. Green and P. Nussbaum, 'Spectral estimation: As a Sensor Adjustment Transform (Under Review),' *Optics Express*, 2023

This article is awaiting publication and is not included in NTNU
Open

Article IV

T. Habib, P. Green and P. Nussbaum, 'Estimation of BRDF Measurements for Printed Colour Samples,' vol. 29, pp. 123–128, 2021

Estimation of BRDF Measurements for Printed Colour Samples

Tanzima Habib, Phil Green and Peter Nussbaum, Norwegian University of Science and Technology, Gjøvik, Norway

Abstract

In this paper, we describe a method to estimate BRDF measurements for different printed colours, using just the BRDF measurements of the substrate and the primary inks. A model is trained using the BRDF measurements of the unprinted substrate and the cyan, magenta, and yellow inks, where four different diffuse and specular measurements of each are used as predictors to find the reflectance factor at a different lighting and viewing angle. In this approach only four spectral measurements of each test colour are required to estimate BRDF. This reduces the number of measurements required to estimate BRDF of a printed surface and to estimate the spectral reflectances that describe its material surface characteristics.

Introduction

Obtaining the bidirectional reflectance distribution function (BRDF) for a material surface is essential in modelling surface appearance. To measure BRDF we need to know the position on the surface, the direction of the incident light, the direction of the reflection and the amount of light that is reflected. BRDF is measured over a hemisphere where the incident light angle and reflection angle changes direction parameterized by the azimuth angle and the zenith angle, making it a somewhat tedious and time-consuming process.

There are many ways to measure BRDF, including, a gonio-reflectometer, a dome-shaped system and image based BRDF measurements. A gonio-reflectometer illuminates the flat target and detects the reflectance using a sensor over a hemisphere around the target. This method of measuring BRDF is very precise with high angular resolution but also very time consuming [1-2]. The second type uses multiple detectors and light sources that are installed on a dome shaped frame and the full BRDF can be captured at once without moving any component [3-4]. A drawback of this system is that its installation requires many detectors and light sources which is expensive, and this also makes the system bulky as the size increases with the increase in resolution [3]. However, Ben-Ezra et al. has demonstrated that a smaller dome shaped system can be created by using light emitting diodes that both act as emitters and detectors. To avoid time consuming processes and high cost, much research has been done to acquire BRDF measurements using an image-based system where a digital camera, a light source and a spherical sample are used [5-8]. But an image-based system does not give us spectral data, which provides more information about the material characteristics.

Now if we need to measure BRDF for printed samples we will have to measure each colour patch. We make use of the ink mixing model for a print dataset such that using the BRDF measurements of the substrate and the primaries we can estimate the BRDF of other ink combinations.

In this paper, we present a BRDF measurement estimation method that addresses the requirement to reduce the number of measurements in order to model BRDF for a particular printer and substrate. These measurements then can be used to optimize a

BRDF model and obtain BRDF parameters to reproduce surface appearance of a particular printed surface.

In earlier work [9-10], we showed how a BRDF workflow is possible within an ICC profile using iccMAX and, given a tristimulus value obtained using 45°:0° measurement geometry, how we can estimate the BRDF parameters for that ink combination and substrate. For this work BRDF parameters are estimated by optimizing a BRDF model based on BRDF measurements. Estimating the BRDF measurements will simplify the process of implementing the BRDF workflow described.

Method

In this section, we discuss the method used to estimate BRDF measurements.

BRDF Measurements

The BRDF of seventeen printed samples on glossy paper were measured. The range of these reflectances is 380nm to 780nm, in steps of 5nm. A GON 360 goniometer equipped with CAS 140CT array spectrophotometer was used, and the BRDF at reflection angles from -30° to 65° in intervals of 5° were measured for five incidence angles 0°, -15°, -30°, -45° and -60°. Figure 1 shows the training set for BRDF measurement estimation. Samples chosen were the substrate, cyan, magenta, and yellow. Figure 2 shows the thirteen test samples whose BRDF were measured for evaluation.

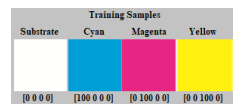


Figure 1. Visual representation of the substrate and the primaries cyan, magenta, and yellow that forms the training set.

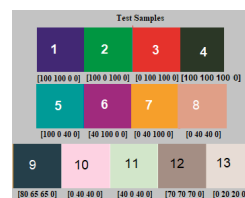


Figure 2. Visual representation of the thirteen test samples whose BRDF were measured.

Observations

Figure 3 and 4 shows the plots of reflectance factors obtained for incidence angle -60° and incidence angle -45° respectively with reflection angles -30° to 65° in steps of 5°, excluding the specular peak of the substrate and cyan sample respectively. The specular

reflections are primarily the illumination of the source spectral power distribution. Diffuse reflection at 0°:45° measurement geometry is the color of material. The intermediate angles combine both diffuse and specular reflections. The dominating diffuse reflections have spectral shape similar to the spectral shape of 0°:45° measurement. While the two reflectances at the adjacent reflection angles to the specular peak i.e., reflection angles 5° away from the specular peaks have dominating specular reflection, which can be seen in figure 3 and 4, and have reflectance factors relative to a perfect diffuser that are greater than 1. This is also seen for measurements at other incidence angles. It is also observed that among the dominating diffuse reflection spectra, the spectrum with the highest reflectance factors has a small degree of influence of specular reflection and thus changes its spectral shape slightly from the diffuse spectra. These spectra are with reflection angles 10° away from the specular peak. Thus, as the measurements move away from the specular peak the influence of specular reflection reduces. This helps us to separate the modelling of specular reflection from the rest and to select the predictor reflectances from the training set accordingly. Therefore, we decided to model spectra with dominating diffuse reflection and the near-to-specular reflection using the same predictor reflectances.

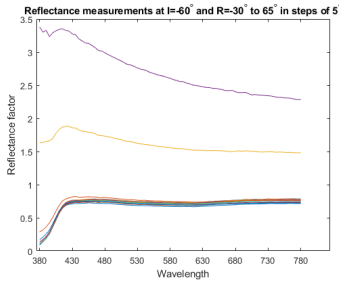


Figure 3. BRDF measurement plot of the substrate for incidence angle -60° and reflection angles -30° to 65° in steps of 5° excluding the specular peak.

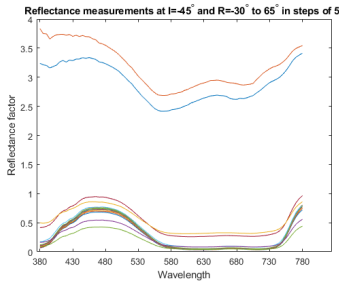


Figure 4. BRDF measurement plot of cyan for incidence angle -45° and reflection angles -30° to 65° in steps of 5° excluding the specular peak.

Estimation Method

A third-order polynomial regression was used to estimate the BRDF measurement. A regression model was created for each

combination of incidence angle and reflection angle. In this case, we have 5 incidence angles and 20 reflection angles forming a total of 100 combinations. When the reflection angle is close to the incidence angle of light, the detector occludes some light and the reflectance cannot be measured. In figure 5, the grey patches and the patches enclosed by black squares are the shadowed areas. These sets of incidence and reflection angles combination were not modeled because of this shadowing. Also, those combinations of angles for which measurement data were missing were not used for modelling. This finally gives us 91 combinations of incidence and reflection angles for which we can create the estimation models.

The predictor set comprises of two base reflectances of the substrate ($xw1, xw2$), cyan ($xc1, xc2$), magenta ($xm1, xm2$) and yellow ($xy1, xy2$) samples chosen at a particular set of (incidence angle, reflection angle) e.g.: (-45°, 0°) and (-60°, 65°). These reflectances are each of size 1x81 and are combined as shown in equation 1, to form the predictor matrix X .

$$X = \begin{pmatrix} xw1' & xw2' \\ xc1' & xc2' \\ xm1' & xm2' \\ xy1' & xy2' \end{pmatrix} \quad (1)$$

The response vector Y in equation 2 is the combination of training reflectances of yw, yc, ym and yy measured at (incidence angle, reflection angle) for which we are creating the estimation model. Once the model is created, for prediction we require the two defined base reflectances of the test samples. Using the same two base reflectances of a test sample we can predict the reflectances at any other combination of incidence and reflection angles using its corresponding estimation model.

$$Y = \begin{pmatrix} yw' \\ yc' \\ ym' \\ yy' \end{pmatrix} \quad (2)$$

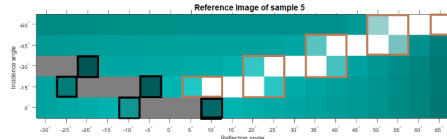


Figure 5. sRGB representation of the BRDF measurements of test sample 5 with incidence angles on the y-axis and reflection angles on the x-axis.

In figure 5, the white patches outside the brown squares are the specular peaks where incidence angle = -reflection angle. At these specular angles the reflectance spectra are predominantly the illumination spectra. The patches marked by the brown squares have a mix of specular reflection and diffuse reflection. As the area nears to the specular peak the specular reflection dominates diffuse reflection. We call these mixes near-to-specular reflections. The rest have dominating diffuse reflection.

Thus, while modelling, the two bases chosen for specular reflection, are (-45°, 45°) midrange specular reflection and (-60°, 60°) highest specular reflection for the training and test data. For patches with diffuse reflection and near-to-specular reflection are modelled with the same two bases, one at (-45°, 0°) and another at (-60°, 65°) the lightest patch of the training and test data that is not a specular peak. Therefore, to estimate BRDF measurements of a test sample, we will need in total of four measurements of that samples at (-45°, 45°), (-60°, 60°), (-45°, 0°) and (-60°, 65°). This reduces the requirement of measuring 100 reflectances per test sample to just 4.

Results and Discussion

For all the 13 test samples, the BRDF measurements have been estimated for five incidence angles and 20 reflection angles except for the shadowed and missing reflections. For all the estimated measurements, the normalized root mean square difference (NRMSD) was calculated relative to the reference measurements as shown in table 1. CIELAB based colour difference ΔE_{00} and colour difference ΔE_{IPT} in IPT colour space were calculated as shown in table 2 and 3 respectively. These colour difference models correspond to colour spaces that are designed for luminance levels from slightly above zero to that of a perfect diffuse white [11]. As the reflectance factors relative to the perfect diffuse reflector at near-to-specular peak go beyond 1 (i.e., they are brighter than a perfect diffuser), these colour difference models have a less defined relationship with perceived difference for these brighter colours. Colour difference in IPT colour space are said to be more perceptually uniform [12]. We show results for both ΔE_{00} and ΔE_{IPT} to illustrate the quality of prediction for these specular highlights. Figures 9-13 show how estimated luminance Y varies at every incidence angle and reflection angle combination compared to its reference. The results are discussed according to diffuse reflection, near-to-specular reflection and specular reflection sections next.

Diffuse reflection

Figure 6 shows the estimated BRDF measurement (blue solid line) and reference (red solid line), for all the test samples at incidence angle -30° and reflection angle -10° . The mean NRMSD of these estimated spectra is 0.008. The BRDF estimation at diffuse reflection angles have low overall NRMSD, with minimum at 0.005 corresponding to sample 1 while the maximum is for sample 4 (Black, [100,100,100,0]). Similarly, ΔE_{00} and ΔE_{IPT} differences are low for these set of estimated spectra. ΔE_{IPT} of 0.01 is considered as a just noticeable difference (JND). The mean ΔE_{00} is lowest at 0.329 corresponding to sample 5 and mean ΔE_{00} is highest at 2.147 corresponding to sample 4. The mean ΔE_{IPT} is lowest at 0.004 corresponding to sample 5 and mean ΔE_{IPT} is highest at 0.016 corresponding to sample 4. The maximum ΔE_{IPT} is 0.072 corresponding to sample 11.

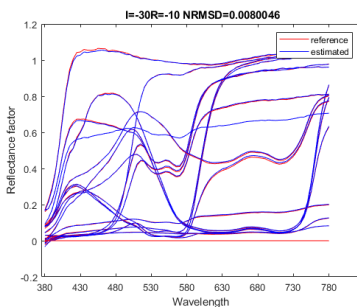


Figure 6. Estimated BRDF measurements plot of all the test samples at incidence angle -30° and reflection angle -10° with mean NRMSD of 0.008. Red solid line depicts reference measurement, and blue solid line depicts estimated measurement.

Specular reflection

Figure 7 shows the estimated BRDF measurement (blue solid line) and reference (red solid line), for all the test samples at incidence angle -30° and reflection angles 30° . The mean NRMSD of these estimated spectra is 0.104. There are only four specular reflections at angles $(-60^\circ, 60^\circ)$, $(-45^\circ, 45^\circ)$, $(-30^\circ, 30^\circ)$ and $(-15^\circ, 15^\circ)$ per sample. Two of these were used as predictors, and therefore only $(-30^\circ, 30^\circ)$ and $(-15^\circ, 15^\circ)$ specular reflectances have been estimated. The NRMSD is higher than NRMSD for diffuse reflections. Mean NRMSD is minimum at 0.029 corresponding to samples 3 and 13. The maximum is for sample 5 at 0.181. Similarly, ΔE_{00} and ΔE_{IPT} are comparatively high for these set of estimated spectra. The mean ΔE_{00} is lowest at 0.456 and mean ΔE_{IPT} is lowest at 0.012 corresponding to sample 13 and the mean ΔE_{00} is highest at 5.677 and mean ΔE_{IPT} is highest at 0.227 corresponding to sample 5. Maximum ΔE_{IPT} is 0.381 for sample 5.

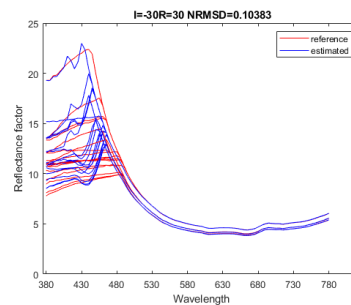


Figure 7. Estimated BRDF measurements plot of all the test samples at incidence angle -30° and reflection angle 30° with mean NRMSD of 0.104. Red solid line depicts reference measurement, and blue solid line depicts estimated measurement.

Near-to-specular reflection

Figure 8(a) shows an example of estimated BRDF measurement (blue solid line) and reference (red solid line), for test sample 5 at incidence angle -45° and reflection angle 50° and figure 8(b) shows the estimated BRDF measurement (blue solid line) and reference (red solid line), for test sample 5 at incidence angle -45° and reflection angle 55° . These spectra are reflectance factors of near-to-specular reflection i.e. reflection angle that is at most 10° away from specular reflection. This is specific to this BRDF dataset. The highest NRMSD and colour differences occur at these estimated spectra compared to the estimated spectra of diffuse reflection and specular reflection. Since, these are mixed reflections, the model is not able to fit properly using the base predictors. The mean NRMSD is lowest at 0.166 corresponding to sample 2. The maximum is for sample 7 at 0.947. The mean ΔE_{00} is lowest at 5.553 corresponding to sample 13 while mean ΔE_{IPT} is lowest at 0.062 corresponding to sample 8. The mean ΔE_{00} is highest at 10.991 corresponding to sample 6 and mean ΔE_{IPT} is highest at 0.148 corresponding to sample 7. Maximum ΔE_{IPT} is 0.484 corresponding to sample 7.

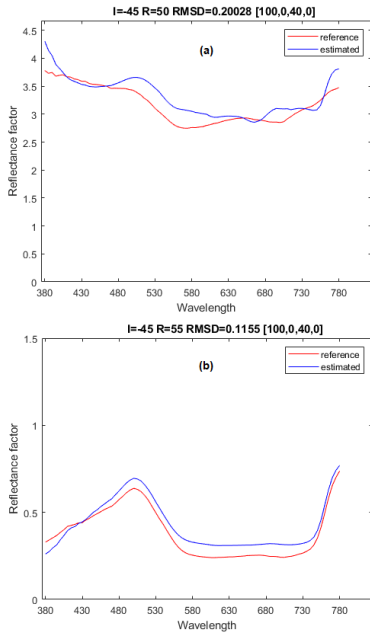


Figure 8. Estimated BRDF measurements plot of sample 5 at (a) incidence angle -45° and reflection angle 50° and (b) incidence angle -45° and reflection angle 55° . Red solid line depicts reference measurement, and blue solid line depicts estimated measurement.

Table1: Mean and max NRMSD of 13 test samples calculated category wise diffuse, specular, and near-to-specular.

Sr. No	Mean NRMSD Diffuse	Max NRMSD Diffuse	Mean NRMSD Specular	Max NRMSD Specular	Mean NRMSD Near Specular	Max NRMSD Near Specular
1	0.005	0.028	0.024	0.056	0.198	0.560
2	0.010	0.065	0.033	0.080	0.166	0.336
3	0.007	0.048	0.023	0.052	0.493	2.038
4	0.134	0.924	0.033	0.079	0.637	1.345
5	0.008	0.042	0.117	0.198	0.218	0.737
6	0.009	0.048	0.027	0.062	0.200	0.589
7	0.006	0.026	0.028	0.065	0.617	3.003
8	0.012	0.100	0.036	0.087	0.257	0.932
9	0.043	0.383	0.032	0.074	0.412	0.831
10	0.018	0.155	0.042	0.098	0.365	0.996
11	0.022	0.192	0.046	0.111	0.356	0.773
12	0.031	0.110	0.041	0.097	0.241	0.809
13	0.026	0.180	0.023	0.055	0.790	2.205

Table2: Mean and max ΔE_{00} of 13 test samples calculated category wise diffuse, specular, and near-to-specular.

Sr. No	Mean ΔE_{00} Diffuse	Max ΔE_{00} Diffuse	Mean ΔE_{00} Specular	Max ΔE_{00} Specular	Mean ΔE_{00} Near Specular	Max ΔE_{00} Near Specular
1	0.530	3.165	1.707	4.254	8.655	19.044
2	1.162	4.244	0.955	2.552	9.418	17.636
3	0.543	3.628	1.592	3.955	7.865	15.316
4	2.147	3.794	1.449	3.775	7.231	13.508
5	0.329	2.366	5.677	9.974	5.745	10.825
6	0.729	3.755	1.124	2.689	10.991	23.576
7	0.347	1.116	1.601	4.038	8.529	24.996
8	0.518	3.316	1.720	4.570	5.786	13.945
9	1.465	5.675	1.367	3.410	8.682	16.368
10	0.623	3.797	1.575	4.220	5.594	14.639
11	0.769	5.251	2.274	6.193	5.870	12.430
12	1.611	3.259	1.563	4.317	5.928	13.005
13	0.827	4.021	0.456	1.001	5.553	10.819

Table3: Mean and max ΔE_{IPT} of 13 test samples calculated category wise diffuse, specular, and near-to-specular.

Sr. No	Mean DEIPT Diffuse	Max DEIPT Diffuse	Mean DEIPT Specular	Max DEIPT Specular	Mean DEIPT Near Specular	Max DEIPT Near Specular
1	0.007	0.033	0.044	0.109	0.088	0.151
2	0.012	0.045	0.041	0.100	0.075	0.113
3	0.007	0.037	0.038	0.094	0.131	0.313
4	0.016	0.040	0.054	0.128	0.073	0.128
5	0.004	0.025	0.227	0.381	0.063	0.129
6	0.010	0.037	0.051	0.121	0.088	0.157
7	0.005	0.015	0.056	0.142	0.148	0.484
8	0.007	0.041	0.075	0.183	0.062	0.198
9	0.011	0.046	0.063	0.151	0.080	0.134
10	0.008	0.053	0.063	0.151	0.073	0.131
11	0.010	0.072	0.080	0.194	0.084	0.158
12	0.011	0.024	0.065	0.158	0.064	0.210
13	0.010	0.049	0.012	0.025	0.103	0.227

Luminance Comparison

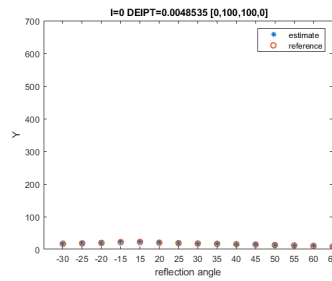


Figure 9. Luminance Y plot of test sample 3 at incidence angle 0° and reflection angles in x-axis, with mean ΔE_{IPT} of 0.0048. Red circle depicts reference Y, and blue asterisk depicts Y.

Figures 9-10 show luminance Y for sample 3 at incidence angles 0° , -15° , -30° , -45° and -60° respectively. Y value rises close to 700 at specular peaks. Y values are the worst predicted for reflection angles 5° and 10° away from specular peaks. For diffuse reflections the Y values are well predicted.

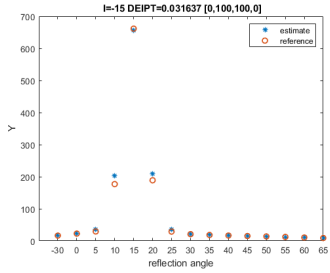


Figure 10. Luminance Y plot of test sample 3 at incidence angle -15° and reflection angles in x-axis, with mean ΔE_{IPT} of 0.0316. Red circle depicts reference Y, and blue asterisk depicts Y.

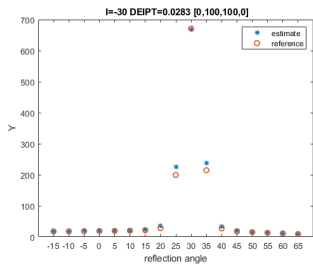


Figure 11. Luminance Y plot of test sample 3 at incidence angle -30° and reflection angles in x-axis, with mean ΔE_{IPT} of 0.0283. Red circle depicts reference Y, and blue asterisk depicts Y.

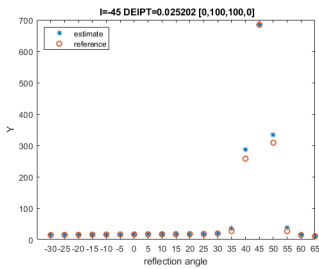


Figure 12. Luminance Y of test sample 3 at incidence angle -45° and reflection angles in x-axis, with mean ΔE_{IPT} of 0.0252. Red circle depicts reference Y, and blue asterisk depicts Y.

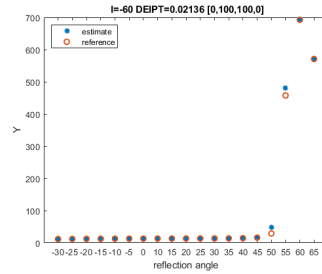


Figure 13. Luminance Y plot of test sample 3 at incidence angle -60° and reflection angles in x-axis, with mean ΔE_{IPT} of 0.0213. Red circle depicts reference Y, and blue asterisk depicts Y.

Visual representation

The reference and estimated BRDF measurements are converted to sRGB values, using which the reference sRGB and estimated sRGB images are created for visualisation purpose. Figure 14 shows that the diffuse part is quite accurately represented, when we compare the reference sRGB images to the estimated sRGB images. Large colour differences occur near-to-specular peak areas, and since the spectral shape is not properly estimated, visible hue differences are seen in near-to-specular angles. The luminance of the specular peak and at reflection angle of 5° around it is greater than that of the perfect diffuser, and therefore no colour difference can be represented as it is clipped to white in sRGB.

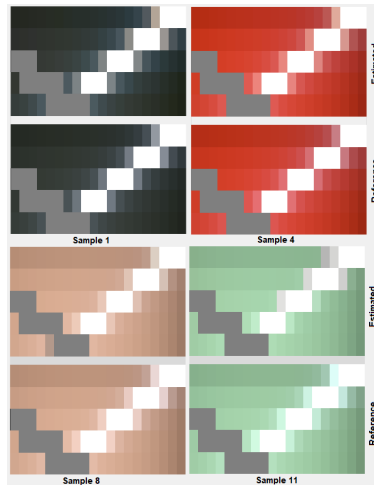


Figure 14. Visual representation of the BRDF measurements for samples 1, 4, 8 and 11. Reference and Estimated sRGB images are created using the measured BRDF and estimated BRDF respectively and representing them as patches in sRGB colour space for different incidence and reflection angles.

Conclusions

The results suggest that using polynomial regression and two predictors, spectra at diffuse reflection can be estimated well. Specular reflectances are overestimated but the relative distribution is reasonably well preserved. This model fails to estimate spectra at near-to-specular reflections, with reflection angles 5° and 10° from the specular peaks shows biggest error in this dataset. A different approach is needed to model these reflectances. The luminance Y values are well estimated for both diffuse and specular reflections. No colour sample has the overall best predicted results or the worst predicted, which suggests that mixing primaries to estimate spectra for other ink mixes works in this case. However, the worst prediction for diffuse spectra is for sample 1 i.e., black [100,100,100 0].

In the future, the specular and near-to-specular spectra should be modelled with a different approach such as a physically based BRDF model. Since printed substrates normally contain optical brightening agents, the fluorescent component of reflectance will need to be addressed. It will also be interesting to test BRDF datasets with different inks and substrates.

Acknowledgement

This project has received funding from the European Union's Horizon 2020 research and innovation programme under the Marie Skłodowska-Curie grant agreement No. 814158. Also, thanks to ApPEARS ESR 10 Donatela Saric from FOGRA for carrying out the reference measurements of all the samples.

References

- [1] J. F. Murray-Coleman, and A.M. Smith. "The automated measurement of BRDFs and their application to luminaire modeling." *Journal of the Illuminating Engineering Society*, 19(1), pp.87-99 (1990).
- [2] J.E. Proctor and P.Y. Barnes. "NIST high accuracy reference reflectometer-spectrophotometer." *Journal of research of the National Institute of Standards and Technology*, 101(5), p.619 (1990).
- [3] J. Gu, C.I. Tu, R. Ramamoorthi, P. Belhumeur, W. Matusik and S. Nayar. "Time-varying surface appearance: acquisition, modeling and rendering". *ACM Transactions on Graphics (TOG)*, 25(3), pp.762-771 (2006).
- [4] M. Ben-Ezra, J. Wang, B. Wilburn, X. Li and L. Ma. An LED-only BRDF measurement device. In 2008 IEEE Conference on Computer Vision and Pattern Recognition (pp. 1-8). IEEE (2008).
- [5] R. S. Marschner et al. "Image-based bidirectional reflectance distribution function measurement." *Applied optics* 39.16: 2592-2600 (2000).
- [6] J. Günther, T. Chen, M. Goesele, I. Wald and H. P. Seidel. "Efficient acquisition and realistic rendering of car paint." In *Vision, Modeling, and Visualization* (Vol. 5, pp. 487-494). Akademische Verlagsgesellschaft Aka (2005).
- [7] A. S. Sole, I. Farup and S. Tominaga. "An image-based multi-directional reflectance measurement setup for flexible objects." In *Measuring, Modeling, and Reproducing Material Appearance 2015* (Vol. 9398, p. 93980J). International Society for Optics and Photonics (2015).
- [8] A. S. Sole, I. Farup and P. Nussbaum. Evaluating an image based multi-angle measurement setup using different reflection models. *Electronic Imaging*, 2017(8), pp.101-107 (2017).
- [9] T. Habib, P. Green and A. Sole. Implementing directional reflectance in a colour managed workflow. In *London Imaging Meeting* (Vol. 2020, No. 1, pp. 119-123). Society for Imaging Science and Technology (2020).
- [10] T. Habib, P. Green and P. Nussbaum. BRDF rendering by interpolation of optimised model parameters. In *Color and Imaging Conference* (Vol. 2020, No. 28, pp. 162-168). Society for Imaging Science and Technology (2020).
- [11] M.D. Fairchild, and P.H. Chen. Brightness, lightness, and specifying color in high-dynamic-range scenes and images. In *Image Quality and System Performance VIII* (Vol. 7867, p. 78670O). International Society for Optics and Photonics.
- [12] T. Lu, F. Pu, P. Yin, T. Chen, W. Husak, J. Pytlarz, R. Atkins, J. Frhlich and G.M. Su, 2019. ITP colour space and its compression performance for high dynamic range and wide colour gamut video distribution. *ZTE Communications*, 14(1), pp.32-38.

Article V

T. Habib, P. Green and P. Nussbaum, 'BRDF rendering by interpolation of optimised model parameters,' in *Color and Imaging Conference*, Society for Imaging Science and Technology, vol. 28, 2020, pp. 162–168

BRDF rendering by interpolation of optimised model parameters

Tanzima Habib, Phil Green and Peter Nussbaum, Norwegian University of Science and Technology, Gjøvik, Norway.

Abstract

In this paper, we discuss an interpolation method which can be used to create a look up table to map tristimulus values to BRDF parameters. For a given tristimulus value, we interpolate the XYZ lattice formed by eight primaries and secondaries that were printed and measured, and their corresponding optimised BRDF parameters. The BRDF parameters are obtained by careful optimisation of the Ward model and Cook Torrance model with the BRDF measurements of these primaries. The interpolated BRDF parameters of nine test samples from the same printed samples were then evaluated against the optimised BRDF parameters and their reference BRDF measurements. The results show that, this simple and efficient interpolation method produces consistent BRDF parameters that preserves the diffuse colour of the input sample.

Introduction

Accurate reproduction of the appearance of a scene has always been a goal of colour imaging and it remains a challenge. This requires understanding different components of appearance w.r.t. the human visual system. Colour has been successfully described and measured using defined colour spaces and metrics like colour difference for various viewing conditions and material properties [1]. But to measure colour with gloss and surface geometry, the bidirectional reflectance distribution function (BRDF) must be used.

Adding surface appearance information to colour management will help describe the appearance for different lighting and viewing conditions and give the possibility of connecting different geometries between profiles. Although, there are rendering software applications that can model appearance, there is still the need to include appearance reproduction in colour management in order to implement it during acquisition, production and process control. To do that we need to have a good framework. The first important decision is to choose a BRDF model, use it to fit BRDF parameters, and then find an efficient method that can map tristimulus values to corresponding BRDF parameters.

Previously, we have used optimised BRDF parameters data from Sole et al. [2] and provided a framework using the iccMAX colour management framework that can produce XYZ data at given incidence angle and reflection angle using multiplex connection space [3]. Prior to iccMAX, ICC.1 architecture has been in use for profile creation which is well defined but highly constrained. iccMAX architecture addressed these constraints by making it possible to use connection space other than D50, providing support for spectral data both as an input or as a PCS, making profiles programmable by including calculator element programming, allowing the passing in of environment variables at run time, and allowing the use of directional appearance by providing support for BRDF models and Multiple Connection Space [4]. Given, this flexibility, we implemented a framework where a TIFF file storing the optimised BRDF of the individual samples as input is used to obtain a TIFF file of corresponding tristimulus values with the geometry of any incidence angle/reflection angle provided during runtime while applying the ICC profiles. The Multiplex

Connection Space (MCS) was used to implement the framework. Two components of the architecture which provide source data to the MCS are the Multiplex Identification (MID) profile and the Multiplex Visualisation (MVIS) profile [5]. First the MID profile was applied to the TIFF file that identifies the BRDF parameters pixelwise and passes them to the MVIS profile. The BRDF model (in our case the Ward model) was encoded in this MVIS profile that uses the BRDF parameters from the input channels, and the incidence and reflection angles that were provided as variables at runtime. The output is a TIFF file containing tristimulus values at that geometry. This paper is an extension of that preliminary work [3] which is limited to use only the known BRDF parameters and outputs tristimulus for a limited set of samples. In this paper, we explore the possibility of obtaining BRDF parameters from any given 45°:0° XYZ (which corresponds to the standard ICC profile connection space, PCS) such that the material connection space profiles can then be applied to create a TIFF file of XYZ at any geometry (incidence angle and reflection angle provided at runtime).

Therefore, the idea is to measure the BRDF of eight possible combinations of CMY inks. The eight samples are the substrate or white(0,0,0), C(100,0,0), M(0,100,0), Y(0,0,100), CM(100,100,0), CY(100,0,100), MY(0,100,100), and CMY(100,100,100) from the FOGRA Media Wedge CMYK V3.0 [6]. These BRDF measurements are used to find the optimised BRDF parameters of each sample using a BRDF model. We then developed an interpolation method that can map 45°:0° geometry tristimulus values to BRDF parameters using the 45°:0° geometry tristimulus values of the eight primaries and secondaries and their corresponding BRDF parameters. Thus, the objectives of this paper are: (a) to develop a simple and efficient interpolation method to map any 45°:0° geometry tristimulus value to BRDF parameters and (b) to use this interpolation method to either create a lookup table that can be encoded in a version 4 ICC profile or to encode the interpolation method in a version 5 (iccMAX) ICC profile.

Method

The BRDF measurements of the eight primaries and secondaries and the nine test samples shown in figure 1 chosen from the FOGRA Media Wedge CMYK V3.0 used in this paper were measured by FOGRA [6]. We then calculated the tristimulus values of eight primaries and secondaries and the test samples at 45°:0° geometry using the D65 illuminant and CIE 1964 colour matching functions. (We are considering 0°:45° geometry analogous to 45°:0° geometry and thus will be using only 45°:0° geometry hereafter.) We used the BRDF measurements and Ward BRDF model and Cook Torrance model to fit the BRDF parameters. This gives us the irregular lattice formed by the tristimulus values of the primaries and the secondaries and their corresponding BRDF parameters irregular lattice. We developed an interpolation method that will find the BRDF parameters for any given tristimulus value of 45°:0° geometry by interpolating the irregular lattices. For the interpolation method, we have modified the Shepard interpolation method [7] for irregular lattice/space combined with the Neugebauer equations [8] for mixing eight primaries and secondaries. We discuss the method used in detail next.

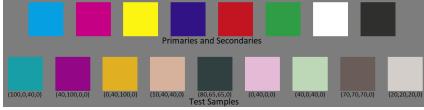


Figure 1. Eight primaries and secondaries and the nine test samples chosen from the FOGRA Media Wedge CMYK V3.0.

BRDF Measurements

All the samples were printed on a glossy white paper at FOGRA. The reflectance factor of the eight primaries and secondaries and the nine test samples were measured using GON 360 goniometer equipped with a CAS 140CT array spectrophotometer. The measurements were performed at incidence angles (θ_i) 0° , 15° , 30° , 45° and 60° and viewing angles (θ_r) that varies from 30° to -65° in intervals of 5° w.r.t. incidence angle space.

Ward BRDF

The isotropic and planar Ward BRDF model, in equation 1, gives the relationship between the colorimetric output at a point p , the intensity of the light source at that point p , the illuminant angle, reflection (detector) angle and the BRDF parameters. The specular lobe in this model is assumed to have a Gaussian distribution [9]. For the purpose of this analysis we consider the light source to be a point source and therefore, the incident light intensity will be the same in all direction.

$$I_p(\theta_i; \theta_r) = \begin{bmatrix} I_{pX} \\ I_{pY} \\ I_{pZ} \end{bmatrix} = I_i \cos \theta_i \begin{bmatrix} R_{dX} \\ R_{dY} \\ R_{dZ} \end{bmatrix} \frac{1}{\pi} + \frac{k_s}{\sqrt{\cos \theta_i \cos \theta_r}} \frac{e^{[-\tan^2 \delta / m^2]}}{4\pi m^2} \quad (1)$$

I_p is the tristimulus value at point P with incident angle θ_i and reflection angle θ_r , I_i is the incident light intensity, R_{dX} , R_{dY} and R_{dZ} are the spectral diffuse reflectance components, k_s is the specular coefficient of the sample and $\delta = (\theta_i - \theta_r)/2$ at point P .

Cook Torrance BRDF

The Cook Torrance BRDF is a physically based BRDF model based on the idea that only those microfacets oriented towards the H vector contribute to the final reflection at angle θ_r as show in figure 2 [10].

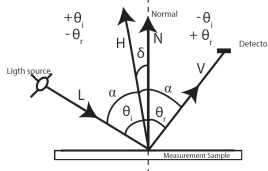


Figure 2. Angles and vectors used in the BRDF equations [10].

The specular term R_s in this case is the compound of the functions D , F and G as shown in equation 2, where D is the microfacets distribution, F is the Fresnel factor that is reflected from the entire surface with angle α between the H vector and the reflected light direction as shown in figure 2, and G is the geometric attenuation factor (i.e. light that is not accounted for due to shadowing and masking) as shown in equation 3. D is typically a Gaussian distribution and, in this case, we use the

Beckmann distribution as shown equation 4 [11] and F is considered to be 1.

$$R_s = \frac{FDG}{\pi(\mathbf{n} \cdot \mathbf{l})(\mathbf{n} \cdot \mathbf{v})} \quad (2)$$

$$G = \min \left\{ 1, \frac{2(\mathbf{n} \cdot \mathbf{h})(\mathbf{n} \cdot \mathbf{v})}{(\mathbf{v} \cdot \mathbf{h})}, \frac{2(\mathbf{n} \cdot \mathbf{h})(\mathbf{n} \cdot \mathbf{l})}{(\mathbf{v} \cdot \mathbf{h})} \right\} \quad (3)$$

$$D = \frac{1}{m^2 \cos^4 \delta} e^{-[(\tan \delta)/m]^2} \quad (4)$$

The simplified isotropic Cook Torrance BRDF model used in this paper is given in equation 5. For each primary and secondary sample, the tristimulus values calculated using the measured reflectance data, D65 illuminant and CIE 1964 colour matching functions are then used to fit and optimise the BRDF parameters k_s , R_{dX} , R_{dY} , R_{dZ} and m using the Nelder-Mead downhill simplex algorithm [12] and ΔE_{00} colour difference as the objective function [2] i.e. the ΔE_{00} between the measured and estimated tristimulus values was minimized.

$$I_p = \begin{bmatrix} I_{pX} \\ I_{pY} \\ I_{pZ} \end{bmatrix} = I_{ia} R_a + I_i \cos \theta_i \left(k_s R_s + (1 - k_s) \begin{bmatrix} R_{dX} \\ R_{dY} \\ R_{dZ} \end{bmatrix} \right) \quad (5)$$

I_p is the tristimulus value at point P with incident angle θ_i and reflection angle θ_r , I_i is the incident light intensity, R_{dX} , R_{dY} and R_{dZ} are the spectral diffuse reflectance components, k_s is the specular coefficient of the sample and $\delta = (\theta_i - \theta_r)/2$ at point P . The term $I_{ia} R_a$ is the ambient light which is assumed to be zero as the experiment was performed in dark conditions. The specular component R_s is already given in equation 2.

Neugebauer model

The Neugebauer model is used to predict spectra or colorimetry of half-toned colour prints. This model states that using the probability of area coverage by cyan, magenta and yellow inks, we can predict any colour formed in between. The probability of area coverage of these ink can be interpreted from the fractional area covered by cyan, magenta and yellow inks [8]. Let these probabilities be c , m and y then the probability of absence of these inks will be $(1-c)$, $(1-m)$ and $(1-y)$ respectively. Therefore, the probability of white i.e. the substrate will be $(1-c)(1-m)(1-y)$. The probability of pure cyan will be $c(1-m)(1-y)$, or a mix of cyan and magenta but no yellow will be $cm(1-y)$ and so on. Therefore, the spectrum or colorimetry can be obtained by mixing respective spectra/colorimetry of the eight primaries and secondaries according to the ink probabilities. This mixing can be obtained using interpolation methods like trilinear interpolation where the CMY primaries and secondaries form a regular lattice mapping to an irregular lattice. The Neugebauer equations can be summarised as below, where given, X_c, Y_c, Z_c , the tristimulus values of the eight primaries and secondaries and the probabilities c , m and y then the corresponding tristimulus value ($X_{cmY}, Y_{cmY}, Z_{cmY}$) is given by:

$$X_{cmY} = \sum_{i=1}^n (w_i X_i), \quad Y_{cmY} = \sum_{i=1}^n (w_i Y_i), \quad Z_{cmY} = \sum_{i=1}^n (w_i Z_i)$$

where,

$$w_i = [(1-c)(1-m)(1-y), c(1-m)(1-y), (1-c)m(1-y), (1-c)(1-m)y, cm(1-y), c(1-m)y, (1-c)my, cmy]$$

Shepard Interpolation

The Shepard interpolation is useful in interpolating data forming irregular lattice or scattered points [7]. It is a simple form of inverse distance weighted interpolation. Let there be a set of n scattered data points x_i and y_i where $i \in \{1, 2, \dots, n\}$, $x_i \in R^n$ and $y_i \in R^m$. For any point x the corresponding y value can be interpolated by weighting y_i with the inverse distance of x with x_i . Let distance $D_i = \|x - x_i\|_p$ where p is the Lp norm and can be chosen accordingly [13]. Then,

$$y = \frac{\sum_i^n y_i D_i^{-\mu}}{\sum_i^n D_i^{-\mu}}$$

Interpolation Method

An interpolation method has been developed from the Shepard interpolation and Neugebauer model to find the BRDF parameters of a BRDF model for an input tristimulus value of $45^\circ:0^\circ$ geometry. This is done by mixing the $45^\circ:0^\circ$ geometry tristimulus values of the eight primaries and secondaries and their corresponding BRDF parameters obtained using the BRDF model. This algorithm is a modification to the Shepard interpolation with inspiration from the Neugebauer model to mix eight secondaries and primaries but in an irregular space. The modification is done to preserve the chromaticity of the input first, by sorting the primaries and secondaries according to the closest chromaticity to the input. The top closest group of primaries and secondaries in chromaticity is chosen such that the inverse distance interpolation of the tristimulus values of this group of primaries and secondaries produces the least colour difference with the input. This helps in choosing the optimal number of primaries and secondaries required to mix. Once the closest interpolated tristimulus value and its corresponding BRDF parameters are obtained then the diffuse components of the interpolated BRDF parameters are scaled with individual factors such that these factors scale the interpolated tristimulus value to the input tristimulus value. The specular coefficient and the standard deviation obtained by the distance weighted interpolation then describes the specular lobe. The algorithm is described below.

Let the input tristimulus value be the vector I , and the tristimulus values of the eight primaries and secondaries be the vectors I_i and their corresponding BRDF parameters be the vectors B_i where $i \in \{1, 2, 3, \dots, 8\}$ and $B_i \in R^5$.

Calculate the chromaticity co-ordinates vector C of I and the chromaticity co-ordinates vectors C_i of I_i , respectively, where $i \in \{1, 2, 3, \dots, 8\}$.

For a given tristimulus value the chromaticity co-ordinates x, y, z are given by:

$$x = X/(X+Y+Z); y = Y/(X+Y+Z); z = Z/(X+Y+Z);$$

Find the distance between vectors C and C_i based on L_p norm as follows:

$$d_i = \|C - C_i\|_p$$

where p can be chosen accordingly, in this case we have chosen $p = 2$ which reduces it to Euclidean distance.

Create vectors S_i that store the index i of d_i in ascending order of distance values in vector d_i changes from 1 to 8.

Set $n = 1$ and do the following:

- Set colour difference variable $E = 1000$.
- Calculate distance $D_i = \|I - I_{S_i}\|$, where i changes from 1 to n .
- Calculate tristimulus value T' as:

$$T' = \frac{\sum_i^n I_{S_i} D_i^{-\mu}}{\sum_i^n D_i^{-\mu}},$$

where, μ can be chosen accordingly. In this case, we have chosen $\mu = 1$.

c.d Calculate the colour difference E' using ΔE_{00} between T' and I .

c.e If $E' < E$, then set $E = E'$, interpolated tristimulus vector $T = T'$, and calculate interpolated BRDF parameters vector B as:

$$B = \frac{\sum_i^n B_{S_i} D_i^{-\mu}}{\sum_i^n D_i^{-\mu}},$$

c.f Increment n and continue step b. to step f. until $n = 8$.

Once we have the closest tristimulus value T and its corresponding BRDF parameters B , then we need to scale each tristimulus co-ordinates (T_x, T_y, T_z) of T to the tristimulus co-ordinates (I_x, I_y, I_z) of I and apply the same individual scaling to the diffuse components (R_x, R_y, R_z) of B respectively:

$$a = I_x/T_x, \quad b = I_y/T_y, \quad \text{and} \quad c = I_z/T_z,$$

By scaling with a, b and c we get $T = (I_x, I_y, I_z)$ and the diffuse components of $B = (aR_x, bR_y, cR_z)$. This ensures that the input colour is preserved. It is possible because the diffuse components and the input tristimulus value share a relationship, and multiplying, both T and the diffuse components of B by the same ratios we still maintain the same relationship between the two.

Results and Discussion

The tristimulus values and the optimised BRDF parameters were calculated for white, C, M, Y, CM, CY, MY and CMY samples for the Ward and Cook Torrance BRDF models. Using these optimised BRDF parameters and their corresponding BRDF equation i.e. equation 1 or equation 5, the tristimulus values were calculated for the five incidence angles $0^\circ, 15^\circ, 30^\circ, 45^\circ$ and 60° (θ , space) and reflection angles -30° to 65° (θ , space) in intervals of 5° . ΔE_{00} is calculated between these values and the corresponding tristimulus values obtained using the measured reflectance data. The overall mean ΔE_{00} was 6.79 (Ward BRDF), 6.5 (Cook Torrance BRDF) for the eight primary and secondary samples. The specular peaks of the measured data in terms of Y (relative luminance) cd/m^2 increases with increasing angle of incidence. It should be noted that the tristimulus values of diffuse reflection obtained using the two models are scaled by $\cos(\theta)$ which decreases the overall brightness value as the incidence angle increases. The BRDF parameters obtained from the Ward model create specular peaks such that the scaling reverses the relationship of relative luminance with respect to the increase in incidence angle i.e. peak Y values decrease accordingly. This overall decrease in brightness as the incidence angles increases also occur in the case of the Cook Torrance model while the specular peaks still hold the same relationship after scaling as in the case of the reference BRDF measurements. The root mean square differences (RMSD) between the Y values of the reference specular highlights and the specular highlights obtained from the optimised BRDF parameters of the primaries and secondaries were also calculated. Figure 3a shows the relative luminance plot of the primary sample (yellow) with the highest RMSD i.e. $1.20 \times 10^2 \text{ cd/m}^2$ in the case of Cook Torrance model. Figure 3b shows the relative luminance plot of the sample (cyan) with the highest RMSD i.e. $1.40 \times 10^2 \text{ cd/m}^2$ in the case of Ward model, respectively.

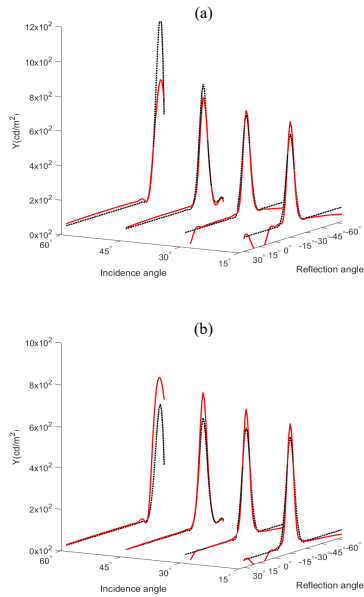


Figure 3. The Y values obtained from measured BRDF (red line) and optimised BRDF (black dotted line) parameters are plotted against the reflection angles for each incidence angle. Plot (a) is of primary Yellow which has the highest RMSD in Y for Cook Torrance model. Plot (b) is of secondary Cyan which has the highest RMSD in Y for Ward model.

The plot in figure 3a, shows that the specular peaks obtained from the Cook Torrance model at incidence angle 30° , 15° and 45° are close to the measured specular peaks, while for 60° incidence angle the specular peak is overestimated. In the case of the Ward Model, figure 3b shows that the specular peaks obtained are underestimated for all the incidence angles; however, as the incidence angles decrease the difference between the measured and the estimated specular peaks decreases. We will use these optimised BRDF parameters for our interpolation method.

The main objective in this paper is to derive an interpolation method and evaluate it by comparing the BRDF parameters output to the optimised BRDF parameters and the reference BRDF measurements. Given the results shown above, the BRDF parameters obtained from our interpolation method can be seen to lie within the accuracy obtained by the optimised parameters. (We limited our evaluation to the incidence and reflection angles used in the optimisation model in order to maintain reliability.)

Another observation is that, for tristimulus values around the specular peak, the Y (relative luminance) value goes above 100 cd/m^2 . The $J_{a,b}$, colour difference [14] was considered as the objective function but as it is designed for high dynamic range data, the colour differences obtained were very low which required the optimisation tolerance value to be reduced substantially. The optimised BRDF parameters thus obtained were not significantly better than the parameters obtained using

ΔE_{00} as the objective function. For this reason, we chose to use ΔE_{00} as the objective function.

The interpolation method was applied to nine test samples that have black value $K = 0$ from the FOGRA media wedge shown in figure 1 and evaluated for both Ward and Cook Torrance models. The reference BRDF measurements and the optimised BRDF parameters were obtained for these nine samples to evaluate the performance of the interpolated BRDF parameters. The root mean square differences (RMSD) between the interpolated BRDF and the optimised BRDF parameters were calculated. For illustration purposes, the samples with 50^{th} percentile and maximum of RMSD obtained using the Cook Torrance model are shown in figures 5 and 6, respectively, as sRGB representations. Figure 7 and 8 are sRGB representations of samples for which the RMSD between the interpolated BRDF and the optimised BRDF parameters using the Ward model is 50^{th} percentile and the highest, respectively. The black patches depict reflection angles at which the measurements were not possible when measuring the BRDF.

Figures 4a and 4b show the relative luminance obtained from the measured BRDF, optimised BRDF and interpolated BRDF parameters, plotted against reflection angles of samples with 50^{th} percentile and maximum of RMSD obtained using the Cook Torrance model. Figure 9a and 9b show the relative luminance against reflection angles plotted for the four incidence angles of samples with 50^{th} percentile and maximum of RMSD using the Ward model. The red solid line, dotted line and dashed line correspond to relative luminance values obtained from reference BRDF measurements, optimised BRDF parameters and the interpolated BRDF parameters respectively. The specular peaks obtained using interpolated method as seen in these plots follow the same characteristics found in the case of optimised BRDF of the primaries and secondaries discussed earlier.

We also calculated the average RMSD between the Y values obtained using interpolated BRDF parameters and reference Y values at specular highlights, and between Y values obtained from optimised BRDF parameters and reference Y values at specular highlights for each incidence angle for all the nine test samples as shown in table 1.

Table 1: Average RMSD of the nine test samples between the Y values obtained using interpolated BRDF parameters & reference Y values and RMSD between the Y values obtained using optimised BRDF parameters & reference Y values at specular highlights.

		15°	30°	45°	60°
Interpolated BRDF parameters & reference BRDF measurements	CT	0.48	0.37	0.66	2.24
	Ward	0.72	0.57	0.62	2.03
Optimised BRDF parameters & reference BRDF measurements	CT	0.82	0.66	0.54	1.61
	Ward	0.70	0.58	0.68	2.07

From the table we can see, that in the case of Cook Torrance model the predicted Y values are close to the reference Y values at incidence angles 30° , 45° and 15° . For incidence angle 60° the Y values are overestimated at the specular peak with an RMSD of above 2 i.e. around 200 cd/m^2 . The Y values of the specular peak obtained from interpolated BRDF parameters overestimates specular peaks more than the specular peaks from optimised BRDF parameters at 60° incidence angle.

In the case of Ward model, the Y values of specular highlights obtained using interpolated BRDF parameters are close to the Y values obtained using reference BRDF at incidence angles 30° , 45° and 15° . The RMSD of Y value is 2.03

i.e. around 203 cd/m^2 at incidence angle 60° . Results from the interpolated BRDF parameters and optimised BRDF parameters are similar in this case.

Estimation of specular peaks using interpolated BRDF remain consistent for all the samples. The Y values obtained using optimised BRDF parameters are not as consistent and close to the reference for all the samples. Specular peaks predicted using optimised BRDF parameters might suffer due to local minima.

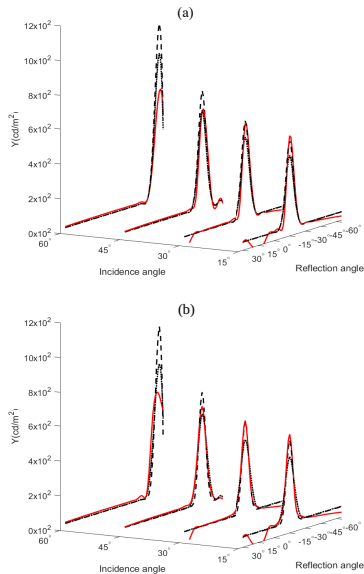


Figure 4. (a) is the plot for relative luminance Y that corresponds to test sample with 50th percentile of RMSD, (b) is the plot for relative luminance Y that corresponds to test sample with the maximum of RMSD obtained between interpolated BRDF parameters and optimised BRDF parameters for Cook Torrance model. Red solid line depicts BRDF measurements, dotted line depicts optimised BRDF parameters and dashed line depicts interpolated BRDF parameters.

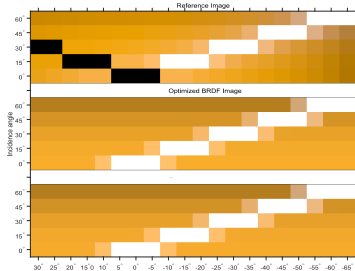


Figure 5. This figure corresponds to colorimetric representation of the reference BRDF measurements (top), optimised BRDF parameters (middle) and the interpolated BRDF parameters (bottom) of the sample that is 50th percentile of

RMSD between interpolated BRDF parameters and optimised BRDF parameters for Cook Torrance model.

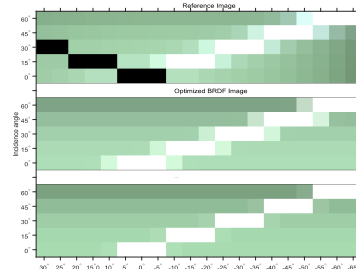


Figure 6. This figure corresponds to colorimetric representation of the reference BRDF measurements (top), optimised BRDF parameters (middle) and the interpolated BRDF parameters (bottom) of the sample that had maximum of RMSD between interpolated BRDF parameters and optimised BRDF parameters for Cook Torrance model.

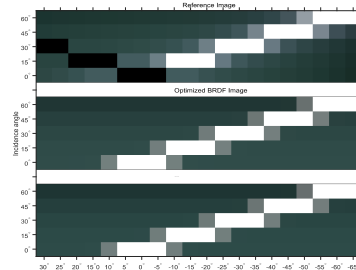


Figure 7. This figure corresponds to colorimetric representation of the reference BRDF measurements (top), optimised BRDF parameters (middle) and the interpolated BRDF parameters (bottom) of the sample that is 50th percentile of RMSD between interpolated BRDF parameters and optimised BRDF parameters for Ward model.

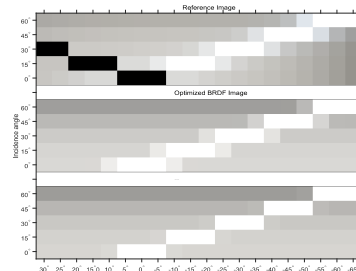


Figure 8. This figure corresponds to colorimetric representation of the reference BRDF measurements (top), optimised BRDF parameters (middle) and the interpolated BRDF parameters (bottom) of the sample that is maximum of RMSD between interpolated BRDF parameters and optimised BRDF parameters for Ward model.

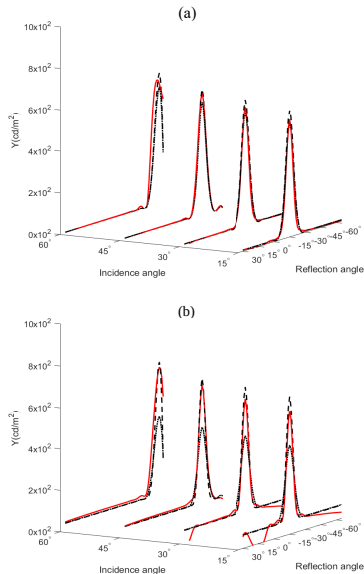


Figure 9. (a) is the plot for relative luminance Y that corresponds to test sample with 50th percentile of RMSD, (b) is the plot for relative luminance Y that corresponds to test sample with the maximum of RMSD obtained between interpolated BRDF parameters and optimised BRDF parameters for Ward model. Red solid line depicts BRDF measurements, dotted line depicts optimised BRDF parameters and dashed line depicts interpolated BRDF parameters.

Table 2 shows the average ΔE_{00} of diffuse reflections calculated between tristimulus values obtained using interpolated BRDF parameters, reference BRDF measurements and optimised BRDF for all the test samples. The average ΔE_{00} between the interpolated and optimised BRDF is close to 1. The overall colour difference obtained between the two BRDF models is similar. This shows that once BRDF parameters of the primaries and secondaries are carefully obtained then mixing these vertices using the interpolation method can retain the BRDF characteristics contributed by the optimised BRDF parameters of the primaries and secondaries and the input sample's diffuse colour. Since to obtain optimised BRDF parameters, the tolerance value, training data, initial parameters, optimisation method etc. must be properly chosen and tested for each sample every time, this interpolation method is a more reliable and efficient method to predict BRDF for a large number of samples.

Figure 10a shows, that for all nine test samples the chromaticity of diffuse reflection is preserved by interpolated BRDF parameters (white asterisks) and optimised BRDF (red dots) parameters and are as close to the chromaticity obtained from the reference BRDF measurements (black circles). Figure 10b shows that for all the nine test samples the chromaticity at specular reflection is close to D65 (black circle) for interpolated BRDF parameters (white asterisks) and optimised BRDF (red dots) parameters while the average chromaticity obtained from reference BRDF measurements (black dots) is (0.2789, 0.2908).

Table 2: Average colour difference of diffuse reflection of all test samples calculated between tristimulus values obtained from interpolated BRDF parameters, reference BRDF measurements and optimised BRDF parameters for Cook Torrance and Ward Model.

	CT $\Delta E(\text{diffuse})$	Ward $\Delta E(\text{diffuse})$
Interpolated BRDF parameters/ reference BRDF measurements	5.02	5.09
Optimised BRDF parameters/ reference BRDF measurements	4.74	4.85
Optimised BRDF parameters/ Interpolated BRDF measurements	1.17	1.11

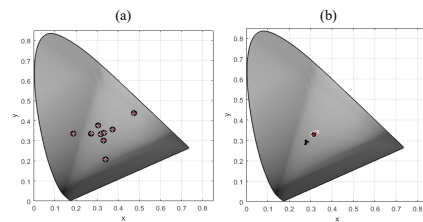


Figure 10. Mean chromaticity obtained from the optimised BRDF parameters, interpolated BRDF parameters and reference BRDF measurements for all the nine-test sample. (a) Chromaticity of diffuse reflections (b) Chromaticity of specular reflections plotted for measured BRDF (black circles), optimised BRDF (red dots) and interpolated BRDF (white asterisks).

Conclusions

From the results it is seen that the interpolated BRDF parameters remain consistent when used to derive the tristimulus values and the specular lobe w.r.t incidence angles. The interpolation method is able to predict the specular co-efficient k_s and standard deviation m reasonably well. When using the reference BRDF measurements, the fitted k_s and m values were quite similar among the primaries and secondaries. While the prediction has preserved the diffuse colour and obtained an acceptable specular peak for 45°, 30° and 15° incidence angle, the relative luminance difference increases for the 60° incidence angle, which is a limitation of the BRDF optimisation. The Cook Torrance model was able to predict the specular peaks' relationship to incidence angle seen in the reference BRDF measurements for all the samples, better than the Ward model. The interpolated BRDF parameters were also able to preserve these relationships. The chromaticity at diffuse reflection is preserved for all the samples while there is a shift in chromaticity at the specular highlights and as expected is closer to the chromaticity of the illumination used.

Other BRDF models such as Lafortune BRDF and Strauss BRDF should also be tested to see the performance of the interpolation method for different types of BRDF models. With an improved model and well optimised BRDF parameters for the primaries and secondaries, the interpolation method is expected to be able to predict parameters accurately for different incidence angles. Further, it is important to evaluate the interpolation method for samples with more complex surface properties. Due to its simplicity and efficiency this interpolation can be integrated into colour management as a lookup table in ICC version 4 or the method can be encoded using ICC version 5. These profiles that map XYZ to BRDF parameters along with

the previous work [3] done to obtain XYZ for a given geometry by applying ICC profile to the BRDF parameters in a TIFF file defines a complete framework to map tristimulus values from 45°:0° geometry (PCS) to tristimulus values at another geometry.

Acknowledgement

This project has received funding from the European Union's Horizon 2020 research and innovation programme under the Marie Skłodowska-Curie grant agreement No. 814158. Also, thanks to ApPEARS ESR 10 Donatela Saric from FOGRA for carrying out the reference measurements of all the samples.

References

- [1] J. Schanda, ed., "Colorimetry: understanding the CIE system." John Wiley & Sons, 2007.
- [2] Sole, A., Farup, I. and Nussbaum, P., 2017. Evaluating an image based multi-angle measurement setup using different reflection models. *Electronic Imaging*, 2017(8), pp.101-107.
- [3] Habib, T., Green, P. and Sole, A., 2017. Implementing directional reflectance in a colour managed workflow. *London Imaging Meeting*, 2020.
- [4] Derhak, M. and Graphics, O., 2018. Color appearance processing using iccMAX. *Electronic Imaging*, 2018(16), pp.323-1.
- [5] ICC.2:2018 Image technology colour management – Extensions to architecture, profile format, and data structure, iccMAX(2018).
- [6] FOGRA, https://www.colourmanagement.net/PDF/ugra_fogra-media-wedge-v3-0b.pdf, last accessed 2020/5/1
- [7] D. Shepard, "A two-dimensional interpolation function for irregularly-spaced data." In *Proceedings of the 1968 23rd ACM national conference* (pp. 517-524), 1968.
- [8] G. Sharma and R. Bala eds. "Digital color imaging handbook." CRC press, 2017.
- [9] G. J. Ward, Measuring and modeling anisotropic reflection. In *Proceedings of the 19th annual conference on Computer graphics and interactive techniques* (pp. 265-272), 1992.
- [10] A. Sole, "Image-Based Bidirectional Reflectance Measurement of Non-Diffuse and Gonio-Chromatic Materials." ISBN 9788232642847. Doctoral thesis at Norwegian University of Science and Technology (2019:344), 2019.
- [11] Cook, R.L. and Torrance, K.E., 1982. A reflectance model for computer graphics. *ACM Transactions on Graphics (TOG)*, 1(1), pp.7-24.
- [12] M. Smith, "A simplex method for function minimization." *The Computer Journal.*, 7(4):308-13 (1965).
- [13] L.K. Mestha, and S.A. Dianat, "Control of color imaging systems: analysis and design." CRC Press., 2018.
- [14] M. Safdar, M.R. Luo, G. Cui and Y.J. Kim, "A Uniform and Hue Linear Color Space for Perceptual Image Processing Including HDR and Wide Gamut Image Signals". In *Color and Imaging Conference* (Vol. 2017, No. 25, pp. 264-268). Society for Imaging Science and Technology, 2017.

Article VI

T. Habib, P. Green and A. Sole, 'Implementing directional reflectance in a colour managed workflow,' in *London Imaging Meeting*, Society for Imaging Science and Technology, vol. 1, 2020, pp. 119–123

<https://doi.org/10.2352/issn.2694-118X.2020.IIM-33>
 This work is licensed under the Creative Commons Attribution 4.0 International license.
 To view a copy of this license, visit <http://creativecommons.org/licenses/by/4.0/>.

Implementing directional reflectance in a colour managed workflow

Tanzima Habib, Phil Green and Aditya Sole, Norwegian University of Science and Technology, Gjøvik, Norway.

Abstract

This paper implements an appearance rendering workflow using the iccMAX architecture with the aim of reproducing the directional appearance of surface colours on a display. In previous work, the prints were measured bidirectionally using an image-based measurement setup, and the bidirectional reflectance distribution function of the materials was estimated using the well-established Ward reflectance model. This function was applied in a colour managed workflow using the ICC.2 architecture to render the appearance of the prints on a display. The seven used as samples to the renderings.

Introduction

Colour management is increasingly concerned with the rendering of appearance rather than solely colorimetry. While 3D rendering softwares like Mitsuba renderer is able to apply sophisticated models to generate realistic simulations, there is a need to integrate appearance reproduction into existing colour management frameworks that can be implemented in production and process control.

Modeling the appearance of a material/object surface should take into account the directions of incident light and viewing, together with the optical properties of the material. A reflectance model such as Cook-Torrance or an empirical Ward model is commonly used in computer graphic to model material reflectance properties and estimate the bidirectional reflectance distribution function (BRDF) [1]. Reflectance models can be classified into physical or phenomenological models. Physical models use optics and physics to define the function using the micro facet theory, while phenomenological models use analytical models to fit measured data and estimate reflectance [1].

A series of directional measurements can be used to optimize reflectance model coefficients which can then be used to estimate material BRDF at a given incident and viewing direction. Bi-directional reflectance can be measured with a goniospectrophotometer but this can be relatively time consuming [2]. To overcome this limitation, image-based measurement setups have been proposed and used [2-4]. Marschner et. al. [3] demonstrates such a measurement setup to measure a variety of different samples like paints, and human skin. A similar setup was used by Sole et. al. [5,6] to measure packaging print materials and estimate material BRDF by optimizing the coefficients of the Cook-Torrance [7] and the isotropic Ward [8] models. In [5], a printed sample that is wrapped around a cylinder of known radius is illuminated using a point light source and the resulting radiance from the curved sample is measured using an RGB camera as detector. Figure 1 shows the schematic of the measurement setup used by Sole et. al [5, 6].

The measurements thus obtained were used to optimize reflectance model coefficients to estimate the full BRDF of the measured samples [2, 6]. These optimized reflectance model coefficients can be used to obtain a rendering of the materials at different illumination and viewing directions.

A software renderer such as Mitsuba [10] can apply different reflectance models to generate realistic simulations

either spectrally or in the sRGB domain. Integrating the renderer into existing colour management frameworks however can be a challenge. The ICC.2 (iccMAX) architecture [16] recently introduced by the International Color Consortium (ICC) incorporates a stack-based scripting language that makes it possible to encode a functional transform such as BRDF [11] within the profile.

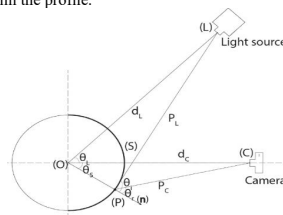


Figure 1. Image-based measurement setup [9].

In this paper, we use the BRDF coefficients calculated by Sole et. al. to optimize the isotropic Ward reflectance model. The coefficients were used as input data to the Ward model encoded in an iccMAX profile, which was then used to compute the colorimetry of a sample at different incident and viewing directions.

The objectives of the work presented in paper are:

1. to show a BRDF workflow is possible using iccMAX
2. to describe the implementation, performance and limitations of this workflow.

Image-based measurement

The samples used by Sole et al [5] were wax based inks printed on a matte coated white paper. They were pasted as strips on a circular structure with a marked angular ruler at the bottom as shown in Figure 1. Seven different colour samples namely, white, red, cyan, Pantone 10309C, magenta, Pantone 10213C and Pantone 10253C were printed using an OCE ColourWave 600 printer. These samples were measured using the image-based setup for 10 different illumination angles.

A tungsten illumination source was configured to approximate a point light source and the acquisition system was a Nikon D200 DSLR camera. The setup is shown in Figure 1 where the semi-circle S is the sample with radius R and center O . C is the position of the sensor (camera) placed normally from the mid-point of S at a distance d_C from O . L is the position of the light source at a distance d_L from O . The RGB intensities were taken from the raw images of the samples and the incident and reflected angles at each pixel (P) were calculated from the illumination angles (θ_i). (Full details can be found in Sole et. al. [5, 6]). The captured RGB intensities were converted to XYZ using the matrix M derived using the camera spectral sensitivity and the CIE 2° observer colour matching function [12].

The cyan and magenta samples were measured by Sole et. al. in [5] using a telespectroradiometer. These measurements provide a reference for analysis of the colorimetric output from the ICC profiles implemented in the present study.

Ward Model

As the samples are isotropic and planar, the isotropic Ward model was used to fit the measured reflectance data [5]. The equation for the isotropic and planar Ward model in this case is given by equation 1.

$$I_p(\theta_i; \theta_r) = \begin{bmatrix} I_{dx} \\ I_{dy} \\ I_{dz} \end{bmatrix} = I_i \cos \theta_i \left(\begin{bmatrix} R_{dx} \\ R_{dy} \\ R_{dz} \end{bmatrix} \frac{1}{\pi} + \frac{k_s}{\sqrt{\cos \theta_i \cos \theta_r}} \frac{e^{-\tan^2 \theta_r / m^2}}{4\pi m^2} \right) \quad (1)$$

where I_p is the camera colorimetric output (XYZ) at pixel P with incident angle θ_i and reflection angle θ_r . I_i is the incident light intensity, R_{dx} , R_{dy} and R_{dz} are the spectral diffuse reflectance components, k_s is the specular coefficient of the sample and $\cos \theta = \cos((\theta_i - \theta_r)/2)$ at pixel P [5].

Obtaining Ward Model coefficients

Reflection coefficients K_s , R_{dx} , R_{dy} and R_{dz} and m were fitted and optimized using the Nelder-Mead downhill simplex algorithm [13], with ΔE_{00} colour difference as the objective function [5].

Method

Workflow using iccMAX

A colour management framework applies a series of transforms in order to connect the source values to a destination colour space. In our case we wish to connect input data to a simulation of the directional appearance on a display. The connection from source device to XYZ, and from XYZ to display device, can be handled by device profiles, and so the core task addressed in this paper is to transform from XYZ representing the diffuse reflectance to an adjusted XYZ representing the appearance of the material once the angles of illumination and viewing have been taken into account.

Implementing the Ward model as described above is not possible within the colour management architecture defined by ICC.1 [14, 15] since this specifies a point-wise transform with a limited set of transform elements (curve, matrix and look-up table), and the Profile Connection Space (PCS) is defined to represent a matt, diffusely reflecting planar surface measured with a 0:45 geometry, and with a D50 illuminant.

ICC.2 [16], however, extends the ICC.1 architecture and provides a much richer support for colour management of other types of material and other geometries of measurement and viewing. Of relevance to our application, ICC.2 supports a wider range of transform elements, and fully directional illumination, measurement and viewing geometries.

ICC.2 incorporates the curve, matrix and LUT elements of ICC.1, but with fewer restrictions - unlike the fixed element sequence in ICC.1 transforms, they are defined more flexibly and can be applied in any number and order. ICC.2 also includes an option to use the 'calc' element, a script language which makes transforms fully programmable.

There are two basic modes in which BRDF data can be incorporated in an ICC.2 profile. Where it is expected that an external application, such as 3D rendering software, will perform the processing, *BRDFStruct* tags allow parameters for a BRDF model to be provided with the image data. Such an example was outlined by Vogh [17]. Where it is desired that the colour management module (CMM) uses the device data and BRDF parameters to compute PCS values representing the appearance of a material at a given illumination and viewing angle, the required processing can be performed by the ICC.2 CMM. In this

case the transform must be defined by the profile creator, since while ICC.2 includes tags which allow angular geometry to be input with the image data, a conforming CMM is not required to have the ability to apply a BRDF model.

Although other ICC.2 transform elements could in principle be used to specify a BRDF transform, the most direct way to encode such a model is to use a calc element. A calc element is incorporated in a *multiProcessingElement*, which can be included in many of the ICC.2 transform types. BRDF Function tags, for example, provide four channels for specification of illumination and viewing angles in terms of both azimuth and elevation, in addition to the channels representing the source colour space. However, in our application we wish to define five optimized parameters for each colour for the Ward BRDF model, as described above, and rather than specify illumination and viewing angles for each pixel we only define a single set of angles for the image.

The *brdfToA1Tag* provides additional channels for specification of illumination and viewing angles, but not for parameters as defined by the Ward model.

Other options for defining these parameters include:

- using an xCLR colour space, where x would be the number of source colour space channels plus four, in conjunction with an AToB1 tag.
- using a multiplex connection space (MCS) that supports the additional channels.

Since the model parameters identify the material rather than the colour, in this initial implementation we have chosen to use an MCS to connect input XYZ data and optimized coefficients with the visualization.

Multiplex Connection Space

Data representing multiple channels is passed into an MCS by a Multiplex Identification (MID) profile. Once in the MCS, the channels can be routed through different pathways depending on the requirements. A Multiplex Visualization (MVIS) profile can be used to connect the channels to a colorimetric or spectral PCS, performing any processing needed to convert to this PCS [18]. The *multiplexTypeArrayTags* is defined to assign channel names and is used to match channels in and out of the MCS, and check channel compliance to any subset requirements between profiles. The optional *multiplexDefaultValuesTag* defines default values for channels. A MID class profile uses an *AToM0* tag to provide the transform from device channel data to MCS channel data while MVIS class profile can use *MToS0* (spectral) or *MToB0* (colorimetric) tags to provide transform from MCS channel data to PCS channel data. Once the source and destination profiles are connected, the source MCS channels connect to the destination MCS channels with matching names [16]. The workflow of MID - MVIS connection with no subset requirements is used to encode the Ward model as shown in Figure 3. The Ward model is encoded in a *calculatorElements* tag as a main function [19].

In this workflow, the BRDF model optimized coefficients (R_{dx} , R_{dy} , R_{dz} , k_s and m) for each sample are passed through 'nc0005' input channels to the MID profile. These 5 input channels are passed to the MVIS profile through MCS connection. The desired viewing angles θ_i and θ_r are passed in at run-time as environment variables (*incident* and *reflection* respectively) to the MVIS profile, where the Ward model is encoded as in Eqn. 1 inside the calculator element tag of *MToA0* tag. The MVIS profile takes the 5 input channels, together with the environment variables for incident and viewing angles, and

applies the encoded Ward model to output PCS XYZ [19]. This workflow was implemented as follows:

1. A TIFF file is used to store per pixel the five BRDF coefficients R_{ds} , R_{dv} , R_{dz} , k_s and m .
2. A MID profile reads these channels from the TIFF file and passes them to the MCS.
3. An MVIS profile then takes the channels from the MCS and applies the BRDF ward model using the parameters pixelwise. Finally, a new TIFF file is created with the estimated XYZ values for the given incidence and viewing angles.

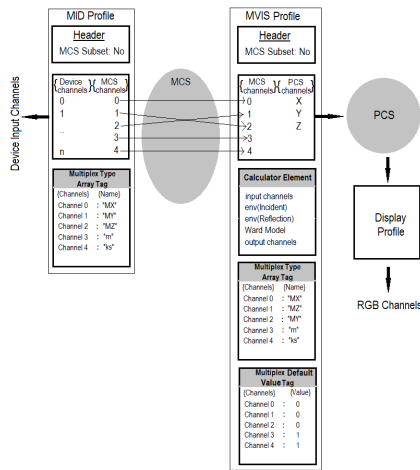


Figure 2. MID-MVIS to encode Ward Model workflow.

Custom PCS

The measured radiance of the source light used to illuminate the samples [5], after normalization, was (0.97, 1, 0.484). Since this is different from the standard D50 PCS used in ICC colour management, a *customToStandardPccTag* has to be defined with the tag signature ‘c2sp’ as a *multiProcessElementType*. This tag converts from the custom colorimetry to standard D50 colorimetry. The matrix to be included inside this tag is the chromatic adaptation transform matrix from custom white point as the source to D50 white point as the destination. Similarly, a *standardToCustomPccTag* using tag signature ‘s2cp’, is required to define the inverse of this chromatic adaptation transform matrix. The linear Bradford chromatic adaptation transform was used to create the 3x3 transform matrix from custom source white point to D50, as recommended in the ICC specification. A *spectralViewingConditions* tag is also defined to include the spectral power distribution of the illuminant, colour matching functions (CMFs) of the observer and the lighting levels of the surround [16].

Results and discussion

The profiles created were applied to TIFF files containing BRDF parameters to obtain XYZ values for different pairs of (incidence, reflection) angles, for each sample. A summary of

the results is given in Table 1, a selection of reflectance functions for cyan and magenta are compared with measured values In Figures 3-8, and a visualization of the results is shown in Figures 9-12.

Performance of profiles relative to Ward model predictions

Table 1. shows the ΔE_{2000} calculated between the estimated XYZ obtained by applying the ICC profile and the estimated XYZ obtained by Sole et. al. [5] and ΔE_{2000} calculated between the estimated XYZ obtained by applying the ICC profile and the estimated XYZ obtained by isotropic Ward model implemented in MATLAB for cyan sample with incidence and reflection angles as (40°, -10°), (40°, 0°), (40°, 10°) and (40°, 30°). In this paper, reflection angle is synonymous to viewing direction. The ΔE_{2000} calculated between MATLAB is negligible while the ΔE_{2000} with Sole et.al. is less than 1.0.

(θ_i, θ_r)	ΔE_{2000} (a)	ΔE_{2000} (b)
(40°, -10°)	0.6407	0.0011
(40°, 0°)	0.6644	0.0010
(40°, 10°)	0.7157	5.8370e-04
(40°, 30°)	0.8636	1.2928e-04

Table 1. (a) ΔE_{2000} between estimated XYZ obtained by Sole. et. al. and estimated XYZ obtained using ICC profiles and (b) ΔE_{2000} between estimated XYZ obtained using MATLAB and estimated XYZ obtained using ICC profiles for cyan sample with incidence and reflection angles as (40°, -10°), (40°, 0°), (40°, 10°) and (40°, 30°). Performance of Ward model encoded as ICC profile in predicting directional measurements

In Figure 3, Figure 4 and Figure 5 for incidence angles 30°, 45° and 60° respectively of the cyan sample, the Y values of the estimated XYZ using the MVIS profile, estimated XYZ adapted to D50, D65 and A illuminants and the reference XYZ with D50 white point are plotted for reflection angles ranging from 80° to -80° in steps of 5°. The estimated Y curves predict the specular lobe on the left of the y-axis at the correct reflection angles when compared to the reference Y curve. Although in Figures 4 and 5, as the incidence angle increases the Y values near the specular lobe are somewhat underestimated.

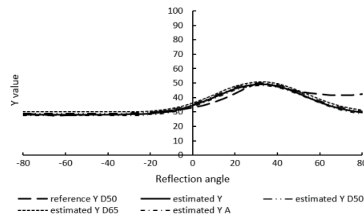


Figure 3. For cyan sample and incidence angle 30°, the reference Y, estimated Y, estimated Y adapted to D50, adapted to D65 and adapted to A values are plotted in the y-axis and reflection angles from -80° to 80° in the x-axis.

Similarly, in Figures 6-8 for the magenta sample and incidence angles 30°, 45° and 60° respectively, the Y values of the estimated XYZ using MVIS profile, estimated XYZ adapted to D50, D65 and A illuminants and the reference XYZ with D50 white point are plotted for reflection angles ranging from 80° to -80° in steps of 5°. Although in Figure 6 the Y values near the

specular lobe are overestimated, in Figures 7 and 8 as the incidence angle increases the Y values near the specular lobe are largely underestimated.

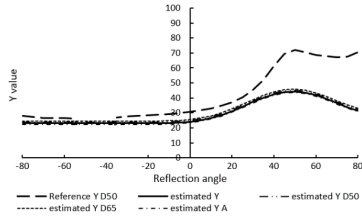


Figure 4. For cyan sample and incidence angle 45°, the reference Y, estimated Y, estimated Y adapted to D50, adapted to D65 and adapted to A values are plotted in the y-axis and reflection angles from -80° to 80° in the x-axis.

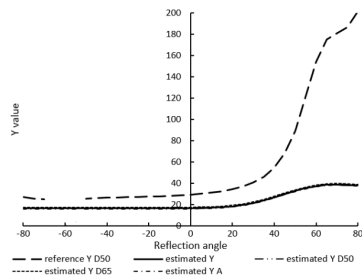


Figure 5. For cyan sample and incidence angle 60°, the reference Y, estimated Y, estimated Y adapted to D50, adapted to D65 and adapted to A values are plotted in the y-axis and reflection angles from -80° to 80° in the x-axis.

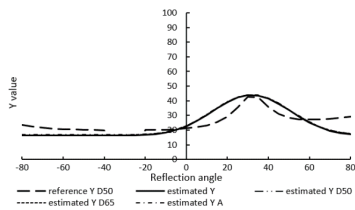


Figure 6. For magenta sample and incidence angle 30°, the reference Y, estimated Y, estimated Y adapted to D50, adapted to D65 and adapted to A values are plotted in the y-axis and reflection angles from -80° to 80° in the x-axis.

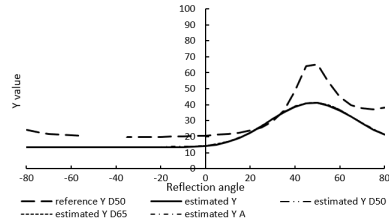


Figure 7. For magenta sample and incidence angle 45°, the reference Y, estimated Y, estimated Y adapted to D50, adapted to D65 and adapted to A values are plotted in the y-axis and reflection angles from -80° to 80° in the x-axis.

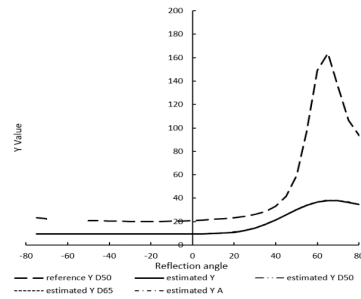


Figure 8. For magenta sample and incidence angle 60°, the reference Y, estimated Y, estimated Y adapted to D50, adapted to D65 and adapted to A values are plotted in the y-axis and reflection angles from -80° to 80° in the x-axis.

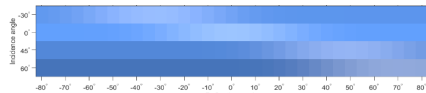


Figure 9. sRGB image of estimated XYZ at incidence angles -30°, 0°, 45° and 60° for reflection angles from [-80°,80°] in steps of 5° of cyan sample.

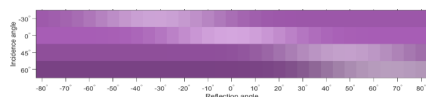


Figure 10. sRGB image of estimated XYZ at incidence angles -30°, 0°, 45° and 60° for reflection angles from [-80°,80°] in steps of 5° of magenta sample.

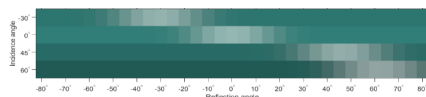


Figure 11. sRGB image of estimated XYZ at incidence angles -30°, 0°, 45° and 60° for reflection angles from [-80°,80°] in steps of 5° of cyan sample.

Figures 9 -12 are sRGB images of estimated XYZ at incidence angles -30°, 0°, 45° and 60° for reflection angles from [-80°,80°] in steps of 5° of cyan, magenta, Pantone 10309C and Pantone 10213C samples respectively, used by Sole et al [5]. These sRGB images are created after adapting the estimated XYZ values to D65 and then converting them to sRGB. From the images the increased reflectance of the specular lobe can be seen, and as the difference between the incidence angle and the normal at 0° increases, the shades become darker.

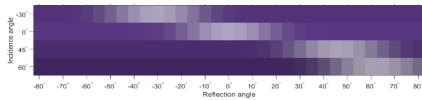


Figure 12. sRGB image of estimated XYZ at incidence angles -30° , 0° , 45° and 60° for reflection angles from $[-80^\circ, 80^\circ]$ in steps of 5° of cyan sample.

The results show that the Ward BRDF model behaves as expected with a smooth Gaussian output when encoded in an ICC profile. These results also show that the performance of an ICC profile encoded BRDF rendering is equivalent to rendering with other computational tools.

Conclusions

Based on a method to obtain fast and low-cost multi angle measurements [5], this paper demonstrates how to extract the BRDF parameters and perform appearance rendering through ICC profiles for any incident light angle and viewing angle pair. Using the MCS connection an efficient reflection model workflow was implemented to render final colorimetric (of device) values for the seven samples with the incident and the reflection angles passed at runtime. The BRDF parameters were passed pixelwise using a TIFF file. This colour-managed workflow gives identical results to the Ward model implementation in Matlab for the equivalent adapted colorimetry, and agrees well with previous results [5].

The Ward model as implemented accurately predicts the reflection angle of the specular lobe. While it performs well in estimating the measured reflectance at different angles of some of the samples, in others it performs less well. This may be due to a failure to take the angular reflectance properties fully into account in deriving the optimized model parameters.

In the future, other reflectance models beyond the isotropic Ward model should be tested. These preliminary results have highlighted some of the limitations and the improvements required. Different metrics could be chosen for optimization of BRDF parameters, with weighting for different appearance parameters such as hue, lightness or chroma, if required. Other BRDF measurement setup should be compared to the one discussed here. For non-planar surfaces the workflow could incorporate incidence and/or viewing angles per pixel in addition to model parameters.

Acknowledgement

This project has received funding from the European Union's Horizon 2020 research and innovation programme under the Marie Skłodowska-Curie grant agreement No. 814158.

References

- [1] D. Guarnera, G. C. Guarnera, A. Ghosh, C. Denk, and M. Glencross, "BRDF representation and acquisition." In Computer Graphics Forum, 2016, vol. 35, no. 2: Wiley Online Library, pp. 625-650
- [2] A. Sole, I. Farup, P. Nussbaum, and S. Tominaga, "Bidirectional Reflectance Measurement and Reflection Model Fitting of Complex Materials Using an Image-Based Measurement Setup."

- Journal of Imaging, vol. 4, no. 11, p. 136, Nov 2018, doi: ARTN 136.
- [3] S. R. Marschner, S. H. Westin, E. P. F. Lafortune, K. E. Torrance, and D. P. Greenberg, "Image-based BRDF measurement including human skin." In 10th Eurographics Workshop on Rendering, pp. 139 – 152, (1999).
- [4] A. Ngan, F. Durand, and W. Matusik, "Experimental analysis of BRDF models." Rendering Techniques, vol. 2005, no. 16th, p. 2, 2005
- [5] A. S. Sole, I. Farup and S. Tominaga, "An image-based multi-directional reflectance measurement setup for flexible objects." In Measuring, Modeling, and Reproducing Material Appearance. International Society for Optics and Photonics. Vol. 9398, p. 93980J (2015).
- [6] A. Sole, I. Farup, P. B. Nussbaum., "Evaluating an image based multi-angle measurement setup using different reflection models." Electronic Imaging, pp. 101-107. (2017).
- [7] R. L. Cook and K. E. Torrance, "A Reflectance Model for Computer Graphics". ACM Trans. Graph., vol. 1, no. 1, pp. 7-24, jan/ 1982. <http://doi.acm.org/10.1145/357290.357293>
- [8] G. J. Ward, "Measuring and Modeling Anisotropic Reflection." SIGGRAPH Comput. Graph., vol. 26, no. 2, pp. 265-272, jul/ 1992. [Online]. Available: <http://doi.acm.org/10.1145/142920.134078>
- [9] A. Sole, "Image-Based Bidirectional Reflectance Measurement of Non-Diffuse and Gonio-Chromatic Materials." ISBN 9788232642847. Doctoral thesis at Norwegian University of Science and Technology (2019:344), 2019
- [10] W. Jakob, "Mitsuba Physically Based Renderer." (2010). <http://www.mitsuba-renderer.org>.
- [11] M. Derhak, P. Green and T. Lianza "Introducing iccMAX – New Frontiers in Colour Management." Proc. SPIE 9395, Colour Imaging XX: Display, Processing, Hardcopy, and Applications, 93950L, (2015).
- [12] A. Sole, I. Farup, S. Tominaga, "Image based reflectance measurement based on camera spectral sensitivities." Electronic Imaging, pp. 1-8. (2016).
- [13] M. Smith, "A simplex method for function minimization." The Computer Journal., 7(4):308-13 (1965).
- [14] ICC.1:2010. "Image technology colour management — Architecture, profile format and data structure." (2010).
- [15] ISO 15076-1:2010 "Image technology colour management - Architecture, profile format, and data structure." (2010).
- [16] ICC.2:2018. Image technology colour management – Extensions to architecture, profile format, and data structure, iccMAX. (2018).
- [17] J. Vogh, "3D Appearance Management using iccMAX." ICC Meeting on Display and 3D Printing, Taipei (2016). http://www.color.org/events/taipei/7-3D_Appearance_Management_using_iccMAX.pdf
- [18] ICC, "iccMAX Reference Implementation." <http://www.colour.org/iccmax/>, accessed January 2020
- [19] ICC, White Paper 45. "iccMAX Multiprocessing Element Calculator Programming." (2019).

Author Biography

Tanzima Habib is a PhD scholar at NTNU. Currently, she is researching on appearance reproduction and colour management system for spectral and 2.5D printing.

Phil Green is Professor of Colour Imaging at the Colour and Visual Computing Laboratory, NTNU, Norway. He is also Technical Secretary of the International Colour Consortium.

Aditya Sole is working as a Project Leader at NTNU and has recently obtained his doctoral degree at the Department of Computer Science. His research interest is to develop and evaluate procedures for measuring the visual appearance of non-diffuse materials.

Article VII

T. Habib, 'Colour Management of Material Appearance,' in *Colour Engineering: Fundamentals and Applications (Under Production)*, P. Green, Ed., John Wiley & Sons, 2023

This article is awaiting publication and is not included in NTNU
Open

Article VIII

T. Habib, P. Green and P. Nussbaum, '2.5D Printing: An Appearance
Reproduction Framework for Printed 3D Surfaces (Under Review),'
Journal of Imaging Science and Technology, 2023

This article is awaiting publication and is not included in NTNU
Open

Article IX

T. Habib, P. Green and P. Nussbaum, 'A weighted goodness-of-fit metric for comparison of spectra,' in *Sensing Colour, Proceedings of the International Colour Association (AIC) Conference 2022*, International Colour Association, 2022, pp. 397–404

COPYRIGHT

Reproduction of this document or parts thereof by any means whatsoever is prohibited without the written permission of the International Colour Association (AIC). All copies of the individual articles remain the intellectual property of the individual authors and/or their affiliated institutions

A Weighted Goodness-of-Fit Metric for Comparison of Spectra

Tanzima Habib ¹*, Phil Green ¹ and Peter Nussbaum ¹

1. Norwegian University of Science and Technology, Gjøvik; syeda.t.habib@ntnu.no, philip.green@ntnu.no, peter.nussbaum@ntnu.no

* Corresponding author: syeda.t.habib@ntnu.no

Abstract

Spectral estimation methods are being increasingly used to create spectral data for colour reproduction applications. Therefore, a good spectral matching metric is required that can minimize colour differences, metamerism as well as errors in the spectral domain. A goodness-of-fit metric is proposed that applies weights to different metrics based on selected criteria and combines them to a single value to assess the fit between two spectra. Acknowledging that for different applications the individual criteria may be more or less relevant, we propose the components of this metric are weighted according to their relative importance in a given application.

Keywords: *Spectral matching, quality metric, spectral estimation, metamerism*

Introduction

Spectral data is of increasing importance in colour reproduction, and in certain cases it is desirable to use spectral data in a workflow when the available source data is colorimetric. In such cases spectral estimation procedures can be used to generate spectral data. When considering such methods, the challenge is to evaluate their ability to predict the original spectra. Neither visual colour difference nor curve fitting approaches can by themselves provide sufficient information, but the relative importance of the two approaches may vary depending on the application, Imai et al. (2002).

Nimeroff, & Yurow (1965) developed a metamerism index which is a weighted sum of the absolute difference between two spectra that correlates well to the chromaticity spread found among observers. Based on similar principles, Viggiano (1990) developed a Spectral Comparison Index (SCI) that derives weights depending on the CIELAB values of the observed spectrum. This metric was further evaluated using non metameric pairs in Viggiano (2004) and it was found that this index assumed values around 2.6 times of total colour difference of CIELAB. According to Imai et al. (2002) the advantage of this metric is that it considers human vision and differences between light and dark colours although the resulting unit could be more intuitive. López-Álvarez (2005) et al. proposed a metric that calculates both the spectral and colorimetric similarity of any pair of

skylights by optimizing with annealing search algorithms which has a specific and limited application.

Our goal is to propose a spectral estimation metric that considers both colorimetric and spectral differences, whose unit is intuitive, and it can be adjusted to minimize attributes depending on the target application. To achieve that, we establish criteria for spectral matches that relate to real-world colour reproduction objectives, including minimization of colour difference, spectral difference, hue difference, metamerism mismatch, non-smoothness, and wavelength inaccuracy for spectral features. We then select or define metrics corresponding to each of these criteria and compute them for a large set of original spectra and their corresponding spectra estimated from tristimulus values using a range of different spectral estimation methods. We observe that most of the metrics tend to rank the estimation methods similarly. These values are then combined to give a single Figure of merit to describe the fit between two spectra. The metric weights are adjusted such that it correlates well to Viggiano's Spectral Comparison Index due to its advantages. The proposed metric provides a useful means of comparing spectra which can be adapted to a wide range of applications.

Spectral and Colorimetric Comparison Indices

For a good spectral match both spectral and colorimetric comparisons have to be carried out. Different metrics are used for spectral and colorimetric comparisons that are discussed as follows.

Mean Absolute error

Mean absolute error (ΔR) is the mean of the sum of the absolute difference between two spectra.

Root mean square error

Root mean square error (RMSE) is the square root of the mean of the squared difference between the reference and test spectra. It measures accuracy of an estimation method however as it is scale dependent it cannot compare results obtained between datasets with different scales.

Metameric Difference

Metameric Difference (ΔM) quantifies the difference in colour between two spectra under a source illuminant and a test illuminant. The squared difference between the L^* , a^* and b^* of the test and reference spectra are calculated under a source illuminant and the same is calculated under a test illuminant. ΔM is given by the square root of the sum of these squared differences.

Colour Inconstancy Index

Colour Inconstancy Index (CII) quantifies the degree to which the colour appearance of a spectrum differs under a source illuminant and a test illuminant, Luo (2003) & Derhak (2020). In manufacturing it is often desired that objects are colour constant i.e. the object does not change its appearance appreciably from one illuminant to another for e.g. illuminant D65 to A, Luo et al (2003).

The tristimulus value of a spectrum is calculated under a source illuminant and then a chromatic adaptation transform is applied to calculate the corresponding colour under a test illuminant. CII is obtained by calculating the colour difference between the corresponding colour and tristimulus value of the spectrum calculated under the test illuminant. ΔCII is the absolute difference between CII obtained for the reference spectra and CII obtained for the estimated spectra.

Smoothness Index

Green (2008) defines a smoothness metric for evaluating the smoothness of a colour transform. The second derivative of the points that lie on a curve is calculated and the median of the second derivative describes the smoothness of a curve. The same can be applied to evaluate the smoothness of a reflectance spectrum and we call it the Smoothness Index (SI). ΔSI is the absolute difference between SI obtained for the reference spectra and SI obtained for the estimated spectra.

Spectral Comparison Index

Viggiano (1990,2002) describes a metric for comparison of radiance ratio spectra based on both spectral and colorimetric principles. It is called the Spectral Comparison Index (SCI) and can be used as a metric to evaluate metamerism between two spectra. A spectral match between two spectra is considered excellent if the SCI is less than 3. SCI is computed as below:

$$M_v = \sum_{\lambda=1}^n w(\lambda) |\Delta\beta(\lambda)| \quad (1)$$

Where, $\Delta\beta(\lambda)$ is the difference between the two spectra and the weights $w(\lambda)$ are computed as below:

$$w(\lambda) = \sqrt{\left(\frac{dL^*}{\Delta\beta(\lambda)}\right)^2 + \left(\frac{da^*}{\Delta\beta(\lambda)}\right)^2 + \left(\frac{db^*}{\Delta\beta(\lambda)}\right)^2} \quad (2)$$

Method

In our experiment, we have selected four different metrics to be combined namely RMSE, ΔM , CII, and SI. RMSE is the most common metric to evaluate two different spectra. ΔM and CII evaluate the colorimetric performance of the estimated spectrum under different illuminants. CII is calculated for each reference and test spectra. The goal is to minimize ΔCII , the difference between the two colour inconsistencies. Smoothness is another desirable property in a surface reflectance spectrum, manipulating which can cost accuracy. Therefore, minimizing ΔSI or SI, one can choose the smoothness of the spectrum to be like that of the reference spectrum or better respectively. We introduce weights to combine each of these metrics into a new goodness-of-fit metric, and we call it the Combined Index (CI). These weights were obtained by adjusting until CI values correlated well to SCI. Thus, CI is made up of RMSE, ΔM , ΔCII and ΔSI as shown in equation 3.

$$CI = 10 * RMSE + (\Delta M_{D65} + \Delta M_E + \Delta M_A + \Delta M_{F12}) + (\Delta CII_{D65} + \Delta CII_E) + 100 * \Delta SI \quad (3)$$

Ten different classical spectral estimation methods were tested to generate spectra from tristimulus values which produce ΔE_{00} of around $1e-13$ i.e. approximately 0 under the same source illuminant (D50) and colour matching functions (CIE 1931 2-degree observer) used for the estimation process. Therefore, the estimated spectra generated by each of these methods are metameric to the reference spectral data. These spectral estimation methods were also evaluated based on their ΔM , RMSE, ΔCII and ΔSI . In this paper, we use the top two performing spectral estimation methods namely, weighted pseudo inverse method (WPI) and third order polynomial (Poly 3) to create the estimated spectra for a reflectance dataset. These estimated spectra are then used to calculate CI and SCI and their correlation with individual metrics ΔR , RMSE, ΔM_{D65} , ΔM_E , ΔM_A , ΔM_{F12} , ΔCII and ΔSI .

The above spectral estimation and evaluation of metrics are carried out using three reflectance datasets, cold-set offset on newsprint (D1), digital print on textile (D2) and web offset on lightweight coated (D3) as shown in Table 1. Three cases are considered, (1) test dataset and training dataset are part of the same reflectance dataset D1, i.e. the estimated spectra are close metamers of the reference, (2) the test dataset is D1, and training dataset is D3 where D1 and D3 have similar spectral curves i.e. the estimated spectra are metamers resembling the spectral characteristics of the training data D3 thereby increasing the degree of metamerism slightly and (3) the test dataset is D2 and training dataset is D3 where D2 and D3 have quite different spectral curves i.e. the estimated spectra are metamers resembling the spectral characteristics of the training data D3 thereby creating a higher degree of metamerism.

Dataset	Range	Description
Cold-set offset on newsprint (D1)	380nm-730nm interval 10 nm	Training and test
Digital print on textile (D2)	380nm-780nm interval 10 nm	Training and test
Web offset on lightweight coated (D3)	380nm-780nm interval 10 nm	Training

Table 1. Reflectance datasets used for spectral estimation from tristimulus value

Results and Discussion

Table 2 lists the different cases of spectral estimation workflow and the overall mean RMSE, ΔM_{D65} , ΔM_E , ΔM_A , ΔM_{F1} , ΔCII , ΔSI , SCI, and CI. A CI of 2 units is a very good spectral match and its value increases gradually as the metamerism under various illuminants and RMSE increases (table 2).

Training	Test	Method	RMSE	ΔM_{D65}	ΔM_E	ΔM_A	ΔM_{F12}	ΔCII	ΔSI	SCI	CI
D1	D1	Poly 3	0.0047	0.1038	0.0197	0.3090	0.4284	0.0910	0.0007	1.6478	1.0829
D1	D1	WPI	0.0056	0.1220	0.0386	0.3569	0.4776	0.0981	0.0009	1.9291	1.2586
D3	D1	Poly 3	0.0120	0.2205	0.1420	0.5660	0.8630	0.1798	0.0018	3.3585	2.4449
D3	D1	WPI	0.0113	0.2777	0.1204	0.8056	1.1078	0.1432	0.0016	3.0770	2.0629
D3	D2	Poly 3	0.0362	0.6468	0.5396	1.6395	2.3409	0.3794	0.0032	13.4026	6.4989
D3	D2	WPI	0.0357	0.6262	0.5627	1.5438	2.2359	0.3182	0.0028	9.8336	6.2093

Table 2. The average metric values for each type of spectral estimation workflow

The correlation values are calculated for SCI and CI with other metrics, viz. ΔR , RMSE, ΔM_{D65} , ΔM_E , ΔM_A and ΔM_{F12} . In Figures 1a,1b and 1c, the graphs show the correlation obtained between SCI and other metrics depicted using bars with slanted lines while the correlation values obtained between CI and other metrics are depicted with solid bars. The blue bars correspond to estimated spectra created using third order polynomials and orange bars correspond to estimated spectra created using weighted pseudo inverse method. The correlations show that the weights chosen for CI makes it correlate to other metrics the same way SCI correlates to those metrics for all the three different cases of metameric spectra generation. SCI and CI showed no correlation with ΔCII and ΔSI .

The results suggest that both CI and SCI can determine metamerism under various illuminants for all the three cases of estimated spectra with different degrees of metamerism. CI can also be used for optimization, where depending on the application the weights can be adjusted to minimize the desired attribute.

In Figure 1a, the results correspond to estimated spectra obtained using dataset D1 as training and test data. In this case, the RMSE and overall ΔM obtained was

very low. Both SCI and CI have a strong correlation with ΔM_{D65} , ΔM_A and ΔM_{F12} i.e., greater than 0.9 and a good correlation with ΔR and RMSE i.e., between 0.8 - 0.9.

In Figure 1b, the results correspond to estimated spectra obtained using dataset D3 as training data and D1 as test data. In this case, the RMSE and overall ΔM obtained was low. Both SCI and CI have a strong correlation with ΔM_{D65} , ΔM_A and ΔM_{F12} i.e., greater than 0.9 and a less than moderate correlation with ΔR and RMSE i.e., between 0.7-0.5.

In Figure 1c, the results correspond to estimated spectra obtained using dataset D3 as training and D2 as test data. In this case, the RMSE and overall ΔM obtained was slightly high. Both SCI and CI have a good correlation with ΔM_{D65} . SCI has good correlation with ΔM_A and CI has moderate correlation i.e. between 0.7-0.8. While CI has good correlation with ΔM_{F12} , and SCI has less than moderate correlation. Both SCI and CI have less than moderate correlation with ΔR and weak correlation with RMSE i.e., less than 0.5. In all the three cases the correlation of SCI and CI with ΔM_E has been weak or less than moderate.

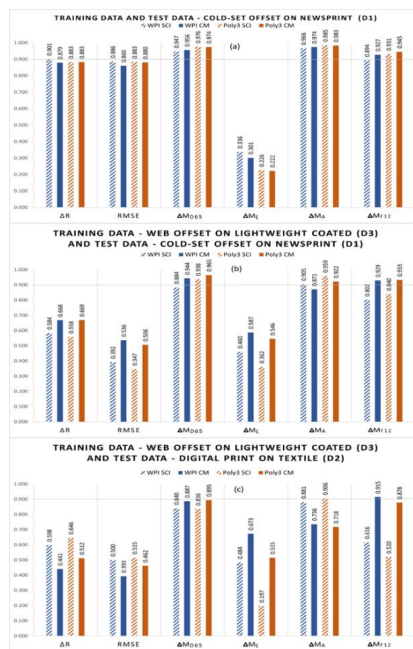


Figure 1. Graph of metric correlations obtained for spectra estimated using (a) D1 as both training and test data, (b) D1 as test data and D3 as training data and (c) D2 as test data and D3 as training data – where spectral estimation methods used WPI (blue) and Poly 3 (orange). Slanted lines depict SCI and solid depict CI correlations to metrics ΔR , RMSE, ΔM_{D65} , ΔM_E , ΔM_A and ΔM_{F12} , respectively.

Figure 2 shows an example of reference spectra vs estimated spectra plot when metric values are (a) low and (b) high.

Conclusions

The new goodness-of-fit metric, CI with adjusted weights behaves like SCI while evaluating estimated spectra with various degrees of metamerism. Both SCI and CI can determine metamerism well between two spectra under source illuminant D50 and test illuminants D65, A and F12. The weights of CI can be adjusted to optimize the outcome to a desired attribute such as smoother spectra, low RMSE, metamerism or colour inconsistency based on the target application.

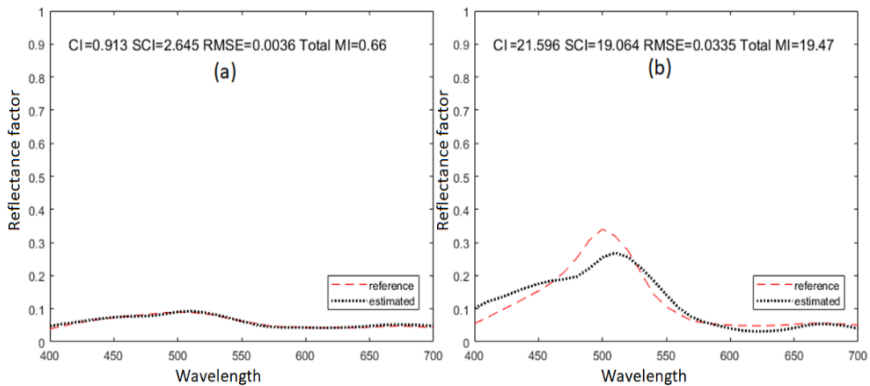


Figure 2. Example of reference vs estimated spectra plot when metric values are (a) low and (b) high.

Acknowledgements

This project has received funding from the European Union's Horizon 2020 research and innovation programme under the Marie Skłodowska-Curie grant agreement No. 814158.

References

- Derhak, M. W. et al. 2020. Wpt (waypoint) shift manifold difference metrics for evaluation of varying observing-condition (observer+illuminant) metamerism and color inconstancy. *Color Research & Application*, 45(6), 1005-1022.
- Green, P. J. 2008. A smoothness metric for colour transforms. In *Color Imaging XIII: Processing, Hardcopy, and Applications* 155-159. SPIE.
- Imai, F. H., Rosen, et al. 2002. Comparative study of metrics for spectral match quality. In *Conference on colour in graphics, imaging, and vision*, 492-496. Society for Imaging Science and Technology.
- López-Álvarez, M. A. et al. 2005. Colorimetric and spectral combined metric for the optimization of multispectral systems. In *Proceedings of the 10th Congress of the International Colour Association*, 1685-1688. USA: Association Internationale de la Couleur.
- Luo, M. R. et al., K. J. (2003). CMC 2002 colour inconstancy index; CMCCON02. *Coloration Technology* 119(5), 280-285.
- Nimeroff, I. & Yurow, J. A. 1965. Degree of metamerism. *JOSA*, 55(2), 185-190.
- Viggiano, J. S. 1990. The comparison of radiance ratio spectra: Assessing a model's "goodness of fit". In *Advanced Printing of Conference Summaries: SPSE's 43rd Annual Conference*, 222-225.
- Viggiano, J. S. 2002. Perception-referenced method for comparison of radiance ratio spectra and its application as an index of metamerism. In *9th Congress of the International Colour Association*, 701-704. International Society for Optics and Photonics.
- Viggiano, J. A. 2004. Metrics for evaluating spectral matches: a quantitative comparison. In *Conference on Colour in Graphics, Imaging, and Vision*, 286-291. Society for Imaging Science and Technology.

Appendix A

Oral Contributions

A.1 Spectral Reproduction

Tanzima Habib. *Spectral Reproduction*. Presented at ICC DEVCON 2020: The Future of Colour Management. https://www.color.org/DevCon/devcon2020/presentations/02-DevCon2020_Habib.pdf

ICC DEVCON 2020

Spectral Reproduction

by
Tazima Habib
NTNU, Gjøvik, Norway
SYGGELE@SIUELE.EE

The Norwegian Center and Visual Computing Laboratory

APPEARS

THE FUTURE OF COLOR MANAGEMENT

ICC MAX

OUTLINE

- Introduction to spectral reproduction
- Spectral acquisition
- Spectral processing
- Spectral reproduction use cases
- Spectral reproduction workflows
- Some metrics for evaluation
- Conclusions

ICC DevCon 2020

TANZIMA HABIB

2

Understanding spectral reproduction

Requirement/Goal	Eg: Spectral Matching
Spectral data acquisition	Eg: Acquire Spectral Data
Spectral processing	Eg: Create model to match spectra
Application	Eg: Apply the workflow to match spot colour to process inks

?

Spectral reproduction is needed!

ICC DevCon 2020

TANZIMA HABIB

3

Driver of spectral reproduction

"Increase in the demand for spectral reproduction workflows"

Reasons:

- Surface reflectance represent material property essential in fields like Cultural heritage, computer graphics
- Intermediate processing in the spectral domain helps in colour accuracy, data hiding etc. important in fields like medical imaging, arts and graphics

Spectral reproduction is needed!

ICC DevCon 2020

TANZIMA HABIB

4

Driver of spectral reproduction

This demand in return has led to:

- technological advancements in spectral acquisition devices and processing hardwares
- availability of spectral and multi-spectral data today

Improvements in spectral acquisition:

- faster, accurate and precise acquisition with available spectrophotometers, TSR, hyperspectral and multispectral imaging systems
- increased repeatability, reproducibility and traceability of devices of spectral and multi-spectral data today

Spectral reproduction is needed!

TANZIMA HABIB
ICCDivCon2020 5

Some spectral acquisition devices

Automatic scanning

Hyperspectral imaging system

- Hyperspectral imaging outputs narrow spectral bands over a continuous spectral range
- Multispectral imaging discrete (3-12) number of channels

Multispectral imaging system

TANZIMA HABIB
ICCDivCon2020 6

Spectral processing

Geometric/multichannel input

↑

Intermediate spectral processing

↑

Geometric/multichannel output

Spectral input

↑

Processing

↑

Geometric/multichannel

Spectral input

↑

Processing

↑

Spectral output

Examples:

- Spectral estimation
- Correcting spectral data
- Spectral BRDF processing
- Colour or other transformation of spectral data

TANZIMA HABIB
ICCDivCon2020 7

Spectral Reproduction use cases

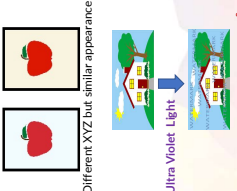
1. Spot colour reproduction
 - Match process colour to spectra of spot colour
2. Printer characterisation when an ink is switched or sequence is changed
 - Spectral printer characterisation

TANZIMA HABIB
ICCDivCon2020 8

Spectral Reproduction use cases

3. Spectral adjustment for substrate colour
 - ✓ Change characterisation data w.r.t the whitepoint in paper
 - ✓ Correct the data spectrally instead of media relative scaling
4. Data hiding
 - ✓ Use ink/meric ink combination to print the watermark

Different XYZ but similar appearance



Ultra Violet Light

9

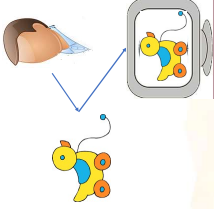
TANZANIA HABIB

ICCDivCon2020

Bala, Bab, and S. "Watermark encoding and detection using normalized illumination." *Color and Imaging Conference, Vol. 2009*, No. 1. Society for Imaging Science and Technology, 2009.

Spectral Reproduction use cases

5. Scene-referred spectral reproduction
 - ✓ Spectral estimation using object specific reflectance database
 - ✓ Match estimated spectra to natural spectra i.e. smooth
 - ✓ Reproduction of accurate colour that resembles the perceived scene (Photorealistic rendering system)



10

TANZANIA HABIB

ICCDivCon2020

Meng, Johannes, et al. "Physically Accurate Color Rendering Using Stimulus Color's Computer Generated Images." In *ICD2015*.

Spectral Reproduction use cases

6. Hi-fidelity colour reproduction and spectral information in medical imaging.
 - ✓ Multispectral images to display (wider colour gamut can display accurately)
 - ✓ Can use spectrum to detect or quantify diseases etc.
7. Spectral BRDF to render synthetic images at different orientations



11

TANZANIA HABIB

ICCDivCon2020

"Research on color reproduction and color image communication based on spectral information: Natural vision system and its application." *Spectral Imaging: Science and Technology*. Color Science, Vol. 0001. International Society for Color and Photocopying, 2006.

Petrovic, Miroslav, and Miroslav. "Modeling the BRDF from spectral reflectance measurements of visible surfaces." *Applied Surface Science* 312 (2014): 87-90.

Spectral Reproduction use cases

8. Minimizing metamorphism under different illuminants
 - ✓ Spectral Input (Target) → Ink combination under illuminant 1 and same ink combination under illuminant 2 should have the lowest colour difference with the target.
9. Softproofing with custom observers
 - ✓ Matching XYZ using custom observer1 to XYZ using custom observer 2



12

TANZANIA HABIB

ICCDivCon2020

L. G. Cohen, S. Le Moan, P. Z. S. K. E. E. and J. P. H. "New generation printing color proofing." *Advanced Imaging and Media Technology*, vol. 41, pp. 38-54, 2014.

Spectral Reproduction workflow

Spectral Proofing:

Spectral to Device colour Profile using a Spectral printer model

13

TANZANIA HABIB

ICC/DCICon2020

Spectral Reproduction workflow

Spectral Proofing:

Ink combinations in Illuminant1 (D50)

Reflectance in Illuminant2 (A, F etc.)

14

TANZANIA HABIB

ICC/DCICon2020

Copyright, Ludovic Gustafsson, et al., "Near generation printing: Towards spectral proofing," *Advanced in Printing and Media Technology*, Vol. 41, 2014, 19-34.
 Ludovic Gustafsson and Ray S. Berns, "Hybrid metameric-based spectral colour matching," *IEEE transactions on image processing*, 20.01.2020

Spectral Reproduction workflow

BRDF encoding:

15

TANZANIA HABIB

ICC/DCICon2020

Metrics to assess spectral reproduction

- ✓ Colour Difference (CIEDE 2000)
- ✓ Root Mean Square Error (RMSE)
- ✓ Goodness of Fit Coefficient (GFC)
- ✓ Smoothness (Green, 2008)
- ✓ Metamerism Index (MI) (CIE, 1986)
- ✓ Special Metamerism Index (CIE, 1989)
- ✓ Color Inconstancy (Luo, Hunt 2003)(Derhak, Luo, Berns, 2020)
- ✓ Hue Constancy (Derhak, Luo, Berns)
- ✓ Spectral Comparison Index (Viggiano, 2002)

16

TANZANIA HABIB

ICC/DCICon2020

Conclusions

- ✓Spectral reproduction workflows can be integrated with colour management
- ✓Possible BRDF rendering using spectral ICC profile
- ✓Possibility of achieving complete spectral colour management
- ✓Need object specific spectral database
- ✓Need metrics to assess the quality of spectral reproduction
- ✓Need increased support for multichannel profiles in existing graphic editors

TANGINA HABIB


17

ICCDWG2020

**THE FUTURE
OF COLOR
MANAGEMENT**

Thank You





TANGINA HABIB

18

ICCDWG2020

A.2 iccMAX BRDF Implementation

Tanzima Habib. *A BRDF Implementation Using iccMAX*. Presented at ICC DEVCON 2020: The Future of Colour Management. https://www.color.org/DevCon/devcon2020/presentations/06-DevCon2020_Habib.pdf

ICC DEVCON 2020

A BRDF Implementation Using iccMAX

by
Tazjima Habib
NTNU, Gjøvik, Norway
SYEFFAH@SIUEHLE.EE

THE FUTURE OF COLOR MANAGEMENT

iccMAX

NTNU

The Norwegian Colour and Visual Computing Laboratory

APPEARS

OUTLINE

- Introduction to BRDF
- BRDF Model and Appearance
- iccMAX
- BRDF Implementation
- Results
- Conclusions

ICC DevCon 2020

TANZJIMA HABIB

2

INTRODUCTION

- Reproducing accurate appearance of a scene has always been the goal of colour imaging or computer graphics.
- Optical properties that contribute to an object's appearance are:
 - colour, gloss, translucency and texture
- Bidirectional Reflection Distribution function (BRDF) is widely used for appearance modelling of materials.
- Appearance reproduction in colour management frameworks

ICC DevCon 2020

TANZJIMA HABIB

3

BRDF

- Represents surface/material reflection characteristics
- Position of the surface
- Direction of incident light
- Amount of light that is reflected

ICC DevCon 2020

TANZJIMA HABIB

4

BRDF MODEL AND APPEARANCE

BRDF Measurements

- Samples : Cyan and magenta
- wax-based inks
- matte coated white paper
- OCE ColorWave 600PP
- The radiance factor of these two samples were measured using a Murakami Goniometer Spectrophotometer GCM5
- Incidence angles (θ_i): 30°, 45° and 60°
- Reflection angles (θ_r): -80° to 80° in intervals of 5°

Kai, W., Jing-Ping, Z., Hong, L. and Kun, H., 2016. Model of bidirectional reflectance distribution function for metallic materials. *Chinese Physics B*, 25(9), pp.09-0301-09-0301.

TANGDIWA HABIB
ICCDivCon2020 5

BRDF MODEL AND APPEARANCE

Analytical models :
Fits measured data and estimate reflectance data
Eg: Ward BRDF model

Phong Model

Physical models:
Use optics and physics to define the function using micro facets
Eg: Cook Torrance Model

Ward BRDF

$$I_p(\theta_i; \theta_r) = \begin{bmatrix} I_{px} \\ I_{py} \\ I_{pz} \end{bmatrix} = \begin{bmatrix} R_{dx} \\ R_{dy} \\ R_{dz} \end{bmatrix} \frac{1}{\pi} + \frac{K_s}{\sqrt{\cos \theta_i \cos \theta_r}} \frac{e^{-\cos^2 \theta_i \cos^2 \theta_r}}{4\pi m^2}$$

Sole, A., Farup, I., Nussbaum, P. and Tominga, S., 2018. Evaluating an image-based bidirectional reflectance distribution function measurement setup. *Applied Optics*, 57(6), pp. 1516-5 1526.

TANGDIWA HABIB
ICCDivCon2020 6

BRDF MODEL AND APPEARANCE

BRDF Model Optimization

- Optimized using the Nelder-Mead downhill simplex
- AE₀₀ colour difference used as the objective function

BRDF Parameters

- K_s , R_{dx} , R_{dy} and R_{dz} and m
- Specular constant
- Diffuse component
- Specular lobe

Ward BRDF

$$I_p(\theta_i; \theta_r) = \begin{bmatrix} I_{px} \\ I_{py} \\ I_{pz} \end{bmatrix} = \begin{bmatrix} R_{dx} \\ R_{dy} \\ R_{dz} \end{bmatrix} \frac{1}{\pi} + \frac{K_s}{\sqrt{\cos \theta_i \cos \theta_r}} \frac{e^{-\cos^2 \theta_i \cos^2 \theta_r}}{4\pi m^2}$$

Sole, A., Farup, I., Nussbaum, P. and Tominga, S., 2018. Evaluating an image-based bidirectional reflectance distribution function measurement setup. *Applied Optics*, 57(6), pp. 1516-5 1526.

TANGDIWA HABIB
ICCDivCon2020 7

BRDF MODEL AND APPEARANCE

BRDF Model Optimization


Peter Peers : There is more to win by improving the fit than improving the BRDF model.

- A major part of BRDF rendering accuracy comes from choosing the right optimization method.
- Should balance the error generated in the diffuse component to error generated in rendering the specular peak
- Better metric to fit the model.
- Adaptive metric

Blerton, J. and Peers, P., 2020, July. An adaptive brdf fitting metric. In *Computer Graphics Forum* (Vol. 39, No. 4, pp. 397-41).

TANGDIWA HABIB
ICCDivCon2020 8

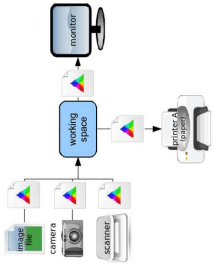
iccMAX



- The ability to use spectral data
- The ability to use different illuminants and observers without the need for chromatic adaptation
- The ability to encode complex transforms, including functional transforms, in the profile
- More support for total colour appearance, including texture and gloss including BRDF

TANZANIA HALBB
ICCDivCon2020 9

BRDF IN COLOUR MANAGEMENT



- ICC.2 (iccMAX) provides a number of options for BRDF implementation
- BRDFStruct tags and external renderer
- BRDF transforms defined by the profile creator
- We use a multiplex connection space (MCS) for BRDF encoding

TANZANIA HALBB
ICCDivCon2020 10

CALCULATOR ELEMENT PROGRAMMING

- ICC.2 (iccMAX) provides calculator element programming
- Stack based programming
- XML representation of iccMAX profiles

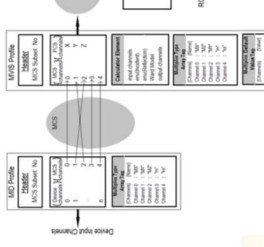
Operator	2	3	add	11	mul	1	add
Stack	3	3	11	11	55	55	56

```

<?xml version="1.0" encoding="UTF-8" standalone="yes" type="text/xml">
  <icc:DeviceMCSProfile>
    <icc:DeviceMCSProfileHeader>
      <icc:DeviceMCSProfileID>1</icc:DeviceMCSProfileID>
      <icc:DeviceMCSProfileName>DeviceMCSProfile</icc:DeviceMCSProfileName>
    </icc:DeviceMCSProfileHeader>
    <icc:DeviceMCSProfileData>
      <icc:DeviceMCSProfileDataElement>
        <icc:DeviceMCSProfileDataElementID>1</icc:DeviceMCSProfileDataElementID>
        <icc:DeviceMCSProfileDataElementName>DeviceMCSProfileDataElement1</icc:DeviceMCSProfileDataElementName>
        <icc:DeviceMCSProfileDataElementValue>1</icc:DeviceMCSProfileDataElementValue>
      </icc:DeviceMCSProfileDataElement>
      <icc:DeviceMCSProfileDataElement>
        <icc:DeviceMCSProfileDataElementID>2</icc:DeviceMCSProfileDataElementID>
        <icc:DeviceMCSProfileDataElementName>DeviceMCSProfileDataElement2</icc:DeviceMCSProfileDataElementName>
        <icc:DeviceMCSProfileDataElementValue>2</icc:DeviceMCSProfileDataElementValue>
      </icc:DeviceMCSProfileDataElement>
    </icc:DeviceMCSProfileData>
  </icc:DeviceMCSProfile>
  
```

TANZANIA HALBB
ICCDivCon2020 11

iccMAX BRDF WORKFLOW



- Input – TIFF file with BRDF coefficients
- An MID profile to read input and pass to the MCS
- An MVIS profile to use MCS as input and apply the encoded BRDF model
- The incidence and viewing angles supplied at runtime
- Output – TIFF containing XYZ values at a new geometry

Implementing directional reflectance in a colour managed workflow. T. Habib, P. Green, A. Sole. LIM2020
TANZANIA HALBB
ICCDivCon2020

MULTIPLEX IDENTIFICATION

- MID profile reads these channels from the TIFF file and passes them to the MCS.

```

midProfileReadChannels(
    &inputChannels,
    &inputModel,
    &outputChannels);
    
```

MID Profile Header	
MCS Subset:	No
Channels X:	MCS
Channels Y:	MCS
Channels Z:	MCS
Channels 0:	0
Channels 1:	1
Channels 2:	2
Channels 3:	3
Channels 4:	4

Multiplex Type Array Tag	
Channel:	Type
Channel 0:	"M"
Channel 1:	"M"
Channel 2:	"M"
Channel 3:	"M"
Channel 4:	"M"

ICC DevCon 2020

MULTIPLEX VISUALIZATION

- MVIS profile then takes the channels from the MCS and applies the BRDF ward model using the parameters pixel-wise
- A new TIFF file is created with the estimated XYZ values for the given incidence and viewing angles

MVIS Profile Header	
MCS Subset:	No
Channels X:	MCS
Channels Y:	MCS
Channels Z:	MCS
Channels 0:	0
Channels 1:	1
Channels 2:	2
Channels 3:	3
Channels 4:	4

Multiplex Type Array Tag	
Channel:	Type
Channel 0:	"M"
Channel 1:	"M"
Channel 2:	"M"
Channel 3:	"M"
Channel 4:	"M"

Calculation Element	
Input Channels:	Output Channels
Channel 0:	0
Channel 1:	1
Channel 2:	2
Channel 3:	3
Channel 4:	4

ICC DevCon 2020

APPLICATION

ICC DevCon 2020

RESULTS

ICC DevCon 2020

BRDF INTERPOLATION METHOD

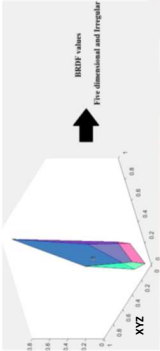
Neugebauer Primaries

Materials: Cyan, Magenta, Yellow, Black

Substrates: Paper, Fabric, Plastic, Wood

Neugebauer primaries: CMYK, RGB, Lab, XYZ

Appearance: Gloss, Matte, Satin, Embossed



BRDF values
Five dimensional and Irregular


Shepard Interpolation

$$Y = \frac{\sum_{i=1}^n Y_i D_i^2}{\sum_{i=1}^n D_i^2}$$


Westland, S., Bagdonaitis, C. and Cheng, V. 2012. *Computational colour science using MATLAB*. John Wiley & Sons.


TANZANIA HABIB
ICCD/Con/2020 17

Application





XYZ in 45°/0°







BRDF Profile






MID Profile





MVS Profile





XYZ in given geometry

TANZANIA HABIB
ICCD/Con/2020 18

CONCLUSIONS

- ✓ Using MCS an efficient rendering framework can be achieved.
- ✓ Framework should be tested on other BRDF models.
- ✓ This lays the ground to develop a more robust framework that can map input XYZ to BRDF coefficients and through MCS to XYZ in another geometry.
- ✓ For this the Interpolation Method can be used
- ✓ Normal map can be used to further decode light and viewing directions and make workflow model robust

Limitations:

- Cannot handle spatial locations

TANZANIA HABIB
ICCD/Con/2020 19

THE FUTURE
OF COLOR
MANAGEMENT

Thank You





TANZANIA HABIB
ICCD/Con/2020 20

A.3 Calculator Element Programming

Tanzima Habib. *Calculator Element Programming*. Presented at ICC DEVCON 2020: The Future of Colour Management. <https://www.color.org/DevCon/devcon2020/presentations/16-DevCon2020Workshop-Tanzima-Calc.pdf>

ICC DEVCON 2020

Calculator Element Programming

THE FUTURE OF COLOR MANAGEMENT

By Tanzima Habib
NTNU, GJEVIK, NORWAY

APPEARS IN THE PROCEEDINGS OF ICC 2020

ICC MAX

OUTLINE

- Introduction
- Operations
- XML Representation
- Types of Operation Encodings
- Extended Structures in XML
- Example 1: Spectral Estimation using Calc elements
- Example 2: BRDF using Calc elements
- Limitations

ICC DevCon 2020

TANZIMA HABIB

2

Important Documents

- iccMAX Specification
<http://color.org/specification/ICC-2-2019.pdf>
- White paper 45: Calculator Element Programming
http://color.org/whitepapers/ICC_White_Paper45_Calculator_Programming-v3.pdf
- ReficcMAX - Win32 executables
<http://color.org/iccmax/index.xalter>
- Examples of Calculator Element Programming in iccMAX
<http://www.color.org/DevCon/devcon2020/index.xalter>
<https://www.ingentaconnect.com/contentone/ist/lim/2020/00002020/00000000/art00028>

ICC DevCon 2020

TANZIMA HABIB

3

Calculator Element Script Programming

A stack-based programming model

Eg:

3
2

Postfix Notation

Eg: 2 3 add or 2 3 mul etc.

Inside multiprocessingElement tag

Eg:

```
<calc>
  <stackElement: <push><push><push><push></stackElement>
  <mul></mul>
</calc>
```

low-level scripting language

Eg: allows more than stack operations

32-bit data parameter

Eg: greater security and predictable behaviour

ICC DevCon 2020

TANZIMA HABIB

4

OPERATIONS

- > take data off the stack
- > directly perform some computational operation
- > apply a processing sub-element
- > get data from a CMM environment variable
- > place data onto the stack
- > get data from input channels
- > store data to output channels
- > store data to indexed memory
- > retrieve data from indexed memory
- > manipulate stack values
- > conditionally select operations to perform

TANZIMA HABIB
ICCDivCon2020

5

XML REPRESENTATION

```

<MultiProcessElements InputChannels="3" OutputChannels="3">
  <SubElements>...</SubElements>
</MultiProcessElements InputChannels="3" OutputChannels="3">
  <Function>
  |
  | <!-- Code using textual representation-->
  |
  </Function>
</MultiProcessElements>
    
```

Calculator elements are encoded in binary structures. (Clause 11 of iccMAX Specification)
Textual representation defined in (Appendix F iccMAX Specification)

TANZIMA HABIB
ICCDivCon2020

6

EXTENDED XML REPRESENTATION

```

<MultiProcessElements InputChannels="3" OutputChannels="3">
  <Imports>...</Imports>
  <Labels>...</Labels>
  <Macros>...</Macros>
  <SubElements>...</SubElements>
</MultiProcessElements InputChannels="3" OutputChannels="3">
  <Function>
  |
  | <!-- Code using textual representation-->
  |
  </Function>
</MultiProcessElements>
    
```

TANZIMA HABIB
ICCDivCon2020

7

VISUAL REPRESENTATION

ICCDivCon2020

Input channel
In (0,3)

1	3	4
---	---	---

ICCDivCon2020

Execution stack

2
4 2 4
3 3 6 6
1 1 2 2

ICCDivCon2020

Output channel
out (0,3)

2	6	4
---	---	---

```

<MultiProcessElements InputChannels="3" OutputChannels="3">
  <CalculatorElement InputChannels="3" OutputChannels="3">
    <Function>
    |
    | In (0,3)
    | 2 6 4
    | 4 2 4
    | 3 3 6 6
    | 1 1 2 2
    |
    | tget (0)
    | out (0,3)
    |
    </Function>
  </CalculatorElement>
</MultiProcessElements>
    
```

TANZIMA HABIB
ICCDivCon2020

8

TYPES OF OPERATION ENCODINGS

1. Floating point constant operations (Push)
2. Channel vector operations
3. CMM environment variable operation
4. Sub-element invocation operations
5. Stack operations
6. Matrix operations
7. Sequence functional operations
8. Functional vector operations
9. Conditional operations
10. Selection operations

TANZIMA HABIB
ICCDivCon2020 9

TYPES OF OPERATION ENCODINGS

1. Floating point constant operations (Push)

```

<MULTIPROCESSELEMENTS InputChannel="1" OutputChannel="3">
  <CALCULATEELEMENT InputChannel="1" OutputChannel="3">
    <MULTIFUNCTION>
      (
        In(0)
        2.5
        3
      )
      out(0,3)
    )
    </MULTIFUNCTION>
  )
  </CALCULATEELEMENT>
</MULTIPROCESSELEMENTS>
  
```

Execution stack

3
2.5
1

Input channel

1

Output channel

1
2.5
3

out(0,3)

TANZIMA HABIB
ICCDivCon2020 10

TYPES OF OPERATION ENCODINGS

2. Channel vector operations

```

<MULTIPROCESSELEMENTS InputChannel="2" OutputChannel="1">
  <CALCULATEELEMENT InputChannel="2" OutputChannel="1">
    <MULTIFUNCTION>
      (
        In(0,2)
        pop(2)
        pop(0)
      )
      out(0)
    )
    </MULTIFUNCTION>
  )
  </CALCULATEELEMENT>
</MULTIPROCESSELEMENTS>
  
```

Temporary memory block

1
2

Input channel

1
2

Output channel

1

out(0)

TANZIMA HABIB
ICCDivCon2020 11

TYPES OF OPERATION ENCODINGS

3. CMM environment variable operation

```

<MULTIPROCESSELEMENTS InputChannel="2" OutputChannel="4">
  <CALCULATEELEMENT InputChannel="2" OutputChannel="4">
    <MULTIFUNCTION>
      (
        In(0,2)
        env(gamma) not.if (pop 2,4)
        env(year) not.if (pop 4,5)
        out(0,4)
      )
      </MULTIFUNCTION>
    )
  )
  </CALCULATEELEMENT>
</MULTIPROCESSELEMENTS>
  
```

Execution stack

3
2.4
2
1

Input channel

1
2

Output channel

1
2
2.4
3

out(0,4)

TANZIMA HABIB
ICCDivCon2020 12

TYPES OF OPERATION ENCODINGS

4. Sub-element invocation operations

```

<MultiProcessElements InputChannel="3" OutputChannel="3">
  <SubElements>
    <SubElement Name="applyGamma" InputChannel="3" OutputChannel="3"></CurrentSubElement>
    <SubElement Name="addSubEl" InputChannel="3" OutputChannel="3"></NextSubElement>
  </SubElements>
  <CalculatorElement InputChannel="3" OutputChannel="3">
    <StartFunction>
      (
        in(0,3)
        copy(3)
        max(0,0,2)
        out(0,3)
      )
    </CalculatorElement>
  </MultiProcessElements>
  
```

TANZANIA HABIB
ICCDivCon2020 13

TYPES OF OPERATION ENCODINGS

5. Stack operations

```

<MultiProcessElements InputChannel="2" OutputChannel="3">
  <CalculatorElement InputChannel="2" OutputChannel="3">
    <StartFunction>
      (
        in(0,2)
        copy(2)
        pop(1)
        flip(3)
        out(0,3)
      )
    </CalculatorElement>
  </MultiProcessElements>
  
```

Execution stack

2
1
2
1

Input channel

1	2
---	---

in (0,2)

Output channel

1	2	1
---	---	---

out (0,3)

TANZANIA HABIB
ICCDivCon2020 14

TYPES OF OPERATION ENCODINGS

6. Matrix operations

```

<MultiProcessElements InputChannel="9" OutputChannel="9">
  <CalculatorElement InputChannel="9" OutputChannel="9">
    <StartFunction>
      (
        in(0,9)
        sum(1)
        out(0,9)
      )
    </CalculatorElement>
  </MultiProcessElements>
  
```

TANZANIA HABIB
ICCDivCon2020 15

TYPES OF OPERATION ENCODINGS

7. Sequence functional operations

```

<MultiProcessElements InputChannel="2" OutputChannel="1">
  <CalculatorElement InputChannel="2" OutputChannel="1">
    <StartFunction>
      (
        in(0,2)
        sum(1)
        2 prod(1)
        3 max(2)
        out(0)
      )
    </CalculatorElement>
  </MultiProcessElements>
  
```

Input channel

1	3
---	---

in (0,2)

Execution stack

1	4	32	32
---	---	----	----

sum(1)
2 4 prod(3)
3 max(2)

Output channel

out(0)

TANZANIA HABIB
ICCDivCon2020 16

TYPES OF OPERATION ENCODINGS

8. Functional vector operations

```

<MultiProcessElement InputChannel="3" OutputChannel="2">
  <CalculatorElement InputChannel="3" OutputChannel="2">
    <MainFunction>
      in(0,3)
      out(0,2)
    </MainFunction>
  </CalculatorElement>
</MultiProcessElement>
  
```

2
4 2
3 3 6
1 1 2

Execution stack

2 2 mul(2)

out(0,2)

1 3 4

Input channel

in(0,3)

4

Temporary memory block

tpout(0)

Output channel

out(0,2)

ICCDevCon2020

TANZIMA HABIB

17

TYPES OF OPERATION ENCODINGS

9. Conditional operations

```

<MultiProcessElement InputChannel="4" OutputChannel="2">
  <CalculatorElement InputChannel="4" OutputChannel="2">
    <MainFunction>
      in(0) >= if (
        in(0,4) mul(2)
      )
      out(0,2)
    </MainFunction>
  </CalculatorElement>
</MultiProcessElement>
  
```

ICCDevCon2020

TANZIMA HABIB

18

EXTENDED STRUCTURES

1. IMPORTS

```

<MultiProcessElement InputChannel="3">
  <Imports>
    <Import File="myVar">
      <Import File="myVector">
        <Import File="myStruct">
          <Import File="myFunc">
            <MainFunction>
              in(0,3)
              out(0,2)
            </MainFunction>
          </Import>
        </Import>
      </Import>
    </Imports>
  </MultiProcessElement>
</MultiProcessElement>
  
```

ICCDevCon2020

TANZIMA HABIB

19

EXTENDED STRUCTURES

3. MACROS

```

<MultiProcessElement InputChannel="1">
  <Macro Name="odd">
    <Macro Name="even">
      <Macro Name="sum">
        <Macro Name="mul">
          <MainFunction>
            in(0)
            call(evo(odd))
            out(0)
          </MainFunction>
        </Macro>
      </Macro>
    </Macro>
  </Macro>
</MultiProcessElement>
  
```

4. SUB ELEMENTS

```

<MultiProcessElement InputChannel="3">
  <SubElement>
    <SubElement Name="apply">
      <SubElement Name="pgbl">
        <SubElement Name="F">
          <MainFunction>
            in(0,3)
            call(apply)
            out(0,3)
          </MainFunction>
        </SubElement>
      </SubElement>
    </SubElement>
  </MultiProcessElement>
  
```

ICCDevCon2020

TANZIMA HABIB

20

EXAMPLE 1: SPECTRAL ESTIMATION

1. Spectral Estimation using classical PCA [Fairman and Brill]

$$R = E_0 + E((A^T E)^{-1}(T - A^T E_0))$$

Average Training Principal Components Mean Centred Coefficients

- E – the three principal components corresponding to the first three highest number of eigen values.
- E₀ – the average spectral reflectance of the training data
- A – weight set for tristimulus integration (XYZ)
- A – weight set for tristimulus integration
- C – coefficients of principal components, R – reflectance

ICC DocCon 2020 TANZIMA HABIB 21

EXAMPLE 1: SPECTRAL ESTIMATION

```

<CalculatorElement InputChannelId="3" OutputChannelId="31">
  <Import FileId="SpectralEstimationDataReport.xml"/>
  <MathFunction>
    in(0,3)
    1. E0
    2. E(E0)
    3. E(A^T E)
    4. T - A^T E0
    5. (T - A^T E0) / (E(A^T E))
    6. E0 + E((T - A^T E0) / (E(A^T E)))
  </MathFunction>
</CalculatorElement>
  
```

ICC DocCon 2020 TANZIMA HABIB 22

EXAMPLE 1: SPECTRAL ESTIMATION

```

iccApplyProfiles RGB_D65_2deg.tif D65_2deg_Reflectance.tif 2 0 1 0 1
argb2xyz66Storer.icc 3
  
```

ICC DocCon 2020 TANZIMA HABIB 23

EXAMPLE 1: SPECTRAL ESTIMATION

iccApplyProfiles RGB_D65_2deg.tif D65_2deg_Reflectance.tif 2 0 1 0 1
argb2xyz66Storer.icc 3

sRGB image
↓
XYZ (E.g. illuminant D65)
↓
apply classical PCA
↓
icc profile
↓
Estimated Reflectance image (31 channels)

ICC DocCon 2020 TANZIMA HABIB 24

Appendix B

iccMAX Profiles in XML

B.1 iccMAX Profiles for Spectral Estimation

Code listing B.1: A2B and B2A Tags of an iccMAX Profile for Spectral Estimation using PCA

```
<AToB3Tag>
  <multiProcessElementType>
    <TagSignature>A2B3</TagSignature>
    <MultiProcessElements InputChannels="41" OutputChannels="3">
      <CalculatorElement InputChannels="41" OutputChannels="3">
        <Imports>
          <Import Filename="PCAMatrixImportData.xml"/>
        </Imports>
        <Macros>
          <Macro Name="RefToXYZ">mtx{Ref2XYZ}</Macro>
        </Macros>
        <MainFunction>
          {
            in(0,41)
            call{RefToXYZ}
            out(0,3)
          }
        </MainFunction>
      </CalculatorElement>
    </MultiProcessElements>
  </multiProcessElementType>
</AToB3Tag>
<BToA3Tag>
  <multiProcessElementType>
    <TagSignature>B2A3</TagSignature>
    <MultiProcessElements InputChannels="3" OutputChannels="41">
      <CalculatorElement InputChannels="3" OutputChannels="41">
        <Imports>
          <Import Filename="PCAMatrixImportData.xml"/>
        </Imports>
        <MainFunction>
          {
            in(0,3)
            1 mtx{AVo}
            sub(3)
            mtx{AV}
            1 mtx{Vo}
            add(41)
          }
        </MainFunction>
      </CalculatorElement>
    </MultiProcessElements>
  </multiProcessElementType>
</BToA3Tag>
```

```

                                out(0,41)
                                }
                                </MainFunction>
                                </CalculatorElement>
                                </MultiProcessElements>
                                </multiProcessElementType>
                                </BToA3Tag>

```

Code listing B.2: A2B and B2A Tags of an iccMAX Profile for Spectral Estimation using Third Order Polynomial

```

<AToB3Tag>
  <multiProcessElementType>
    <TagSignature>A2B3</TagSignature>
    <MultiProcessElements InputChannels="41" OutputChannels="3">
      <CalculatorElement InputChannels="41" OutputChannels="3">
        <Imports>
          <Import Filename="polynomialMatrixImportData.xml"/>
        </Imports>
        <Macros>
          <Macro Name="RefToXYZ">mtx{Ref2XYZ}</Macro>
        </Macros>
        <MainFunction>
          {
            in(0,41)
            call{RefToXYZ}
            out(0,3)
          }
        </MainFunction>
      </CalculatorElement>
    </MultiProcessElements>
  </multiProcessElementType>
</AToB3Tag>

<BToA3Tag>
  <multiProcessElementType>
    <TagSignature>B2A3</TagSignature>
    <MultiProcessElements InputChannels="3" OutputChannels="41">
      <CalculatorElement InputChannels="3" OutputChannels="41">
        <Imports>
          <Import Filename="polynomialMatrixImportData.xml"/>
        </Imports>
        <Macros>
          <Macro Name="Poly3Expansion">
            1
            tget(0,1)
            tget(1,1)
            tget(2,1)
            tget(0,1) 2 gama(1)
            tget(1,1) 2 gama(1)
            tget(2,1) 2 gama(1)
            tget(0,1) tget(1,1) prod(2)
            tget(0,1) tget(2,1) prod(2)
            tget(1,1) tget(2,1) prod(2)
            tget(0,1) 3 gama(1)
            tget(1,1) 3 gama(1)
            tget(2,1) 3 gama(1)
            tget(0,1) 2 gama(1) tget(1,1) prod(2)
            tget(0,1) 2 gama(1) tget(2,1) prod(2)
            tget(1,1) 2 gama(1) tget(0,1) prod(2)
            tget(2,1) 2 gama(1) tget(0,1) prod(2)
            tget(1,1) 2 gama(1) tget(2,1) prod(2)
            tget(2,1) 2 gama(1) tget(1,1) prod(2)
          </Macro>
        </Macros>
      </CalculatorElement>
    </MultiProcessElements>
  </multiProcessElementType>
</BToA3Tag>

```

```

        tget(0,1) tget(1,1) tget(2,1) prod(3)
    </Macro>
</Macros>
<MainFunction>
{
    in(0,3)
    tput(2,1) tput(1,1) tput(0,1)
    call{Poly3Expansion}
    mtx{M}
    out(0,41)
}
</MainFunction>
</CalculatorElement>
</MultiProcessElements>
</multiProcessElementType>
</BToA3Tag>

```

B.2 iccMAX Profile for BRDF Rendering

Code listing B.3: M2B Tag of an MVIS iccMAX Profile for encoding isotropic inplanar BRDF model

```

<multiProcessElementType>
  <TagSignature>M2B0</TagSignature>
  <MultiProcessElements InputChannels="5" OutputChannels="3">
    <CalculatorElement InputChannels="5" OutputChannels="3">
      <SubElements/>
      <MainFunction>
        {
          in(0,5)
          env(tI) not if {pop 0}
          env(tR) not if {pop 45}
          tput(1,1)
          tput(0,1)
          tput(2,1)
          tget(0,2)
          pi pi mul(2)
          180 180 div(2)
          cos(2)
          prod(2)
          0.5 gama(1)
          div(1)
          tput(3,1)
          tget(0,1)
          tget(1,1)
          sub(1)
          2 div(1)
          pi mul(1)
          180 div(1)
          tan(1) 2 gama(1)
          tget(2,1) 2 gama(1)
          div(1)
          -1 mul(1)
          exp(1)
          4 pi mul(1)
          tget(2,1) 2 gama(1)
          mul(1)
          div(1)
          tget(3,1)
          mul(1)
          tput(4,1)
          1 1 1 pi pi pi div(3) mul(3)
        }
      </MainFunction>
    </CalculatorElement>
  </MultiProcessElements>
</multiProcessElementType>

```

```

        tget(4,1) tget(4,1) tget(4,1) add(3)
        tget(0,1) tget(0,1) tget(0,1)
        pi pi pi 180 180 180 div(3) mul(3)
        cos(3)
        mul(3)
        0.97 1 0.484 mul(3)
        out(0,3)
    }
</MainFunction>
</CalculatorElement>
</MultiProcessElements>
</multiProcessElementType>

<tagArrayType>
  <TagSignature>mcta</TagSignature>
  <ArraySignature>utf8</ArraySignature>
  <ArrayTags>
    <utf8TextType><TextData>MX</TextData></utf8TextType>
    <utf8TextType><TextData>MY</TextData></utf8TextType>
    <utf8TextType><TextData>MZ</TextData></utf8TextType>
    <utf8TextType><TextData>Mks</TextData></utf8TextType>
    <utf8TextType><TextData>Mm</TextData></utf8TextType>
  </ArrayTags>
</tagArrayType>

```

Appendix C

Additional Documents

C.1 Requirements Document of the 2.5D printed targets

2.5D Printer Target Samples

The description of the target samples to be printed are discussed below. The FOGRA Media Wedge TIFF V3.0 has to be printed. Each colour patch should be at least 1 cm x 2.7 cm in size.

The FOGRA Media Wedge and its CMY values are given in ANNEXURE 2. The size of the triangular side of each wedge is given in fig: 1. The length of each wedge must be 32.4 cm having 12 colours printed on it. Two wedges will share the height axis as shown in figure 1.

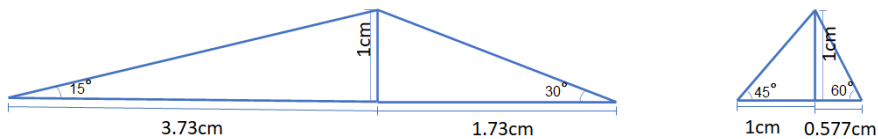


Figure 1: The measurements of the triangular side of wedges to be printed.

The chart must be printed in 5 different angles and height.

1. **15° wedge sample:** In this case a wedge must be printed on the substrate with slope angle = 15°, height = 1 cm, depth = 3.73 cm, length = 32.4 cm. 12 colour patches must be printed on the sloped surface with width of each colour patch being 2.7 cm. Therefore, 6 wedges must be printed to print all the 72 colours in the chart.
2. **30° wedge sample:** In this case a wedge must be printed on the substrate with slope angle = 30°, height = 1 cm, depth = 1.73 cm, length = 32.4 cm. 12 colour patches must be printed on the sloped surface with width of each colour patch being 2.7 cm. Therefore, 6 wedges must be printed to print all the 72 colours in the chart.
3. **45° wedge sample:** In this case a wedge must be printed on the substrate with slope angle = 45°, height = 1 cm, depth = 1 cm, length = 32.4 cm. 12 colour patches must be printed on the sloped surface with width of each colour patch being 2.7 cm. Therefore, 6 wedges must be printed to print all the 72 colours in the chart.
4. **60° wedge sample:** In this case a wedge must be printed on the substrate with slope angle = 60°, height = 0.577 cm, depth = 1 cm, length = 32.4 cm. 12 colour patches must be printed on the sloped surface with width of each colour patch being 2.7 cm. Therefore, 6 wedges must be printed to print all the 72 colours in the chart.

The 45° wedge and the 60° wedge can be printed together where they share the height axis and the same surface colour (colour patches). Similarly, the 15° wedge and the 30° wedge can be printed together where they share the height axis and the same surface colour (colour patches). An example of 45° wedge and 60° wedge sample is given in ANNEXURE 1.

GLOSS SAMPLES

Only flat samples are required to be printed with different gloss. The FOGRA media wedge should be printed on the substrate directly completely flat, slope angle = 0° , with 72 colour patches of size 1.5cm x 2.5 cm each. The media wedge can be rearranged to form 6 rows as shown in the figure 2 below. Each such chart must be printed with different gloss. If possible, it will be good to have four different gloss at least.



Figure 2: Example of gloss sample print requirement.

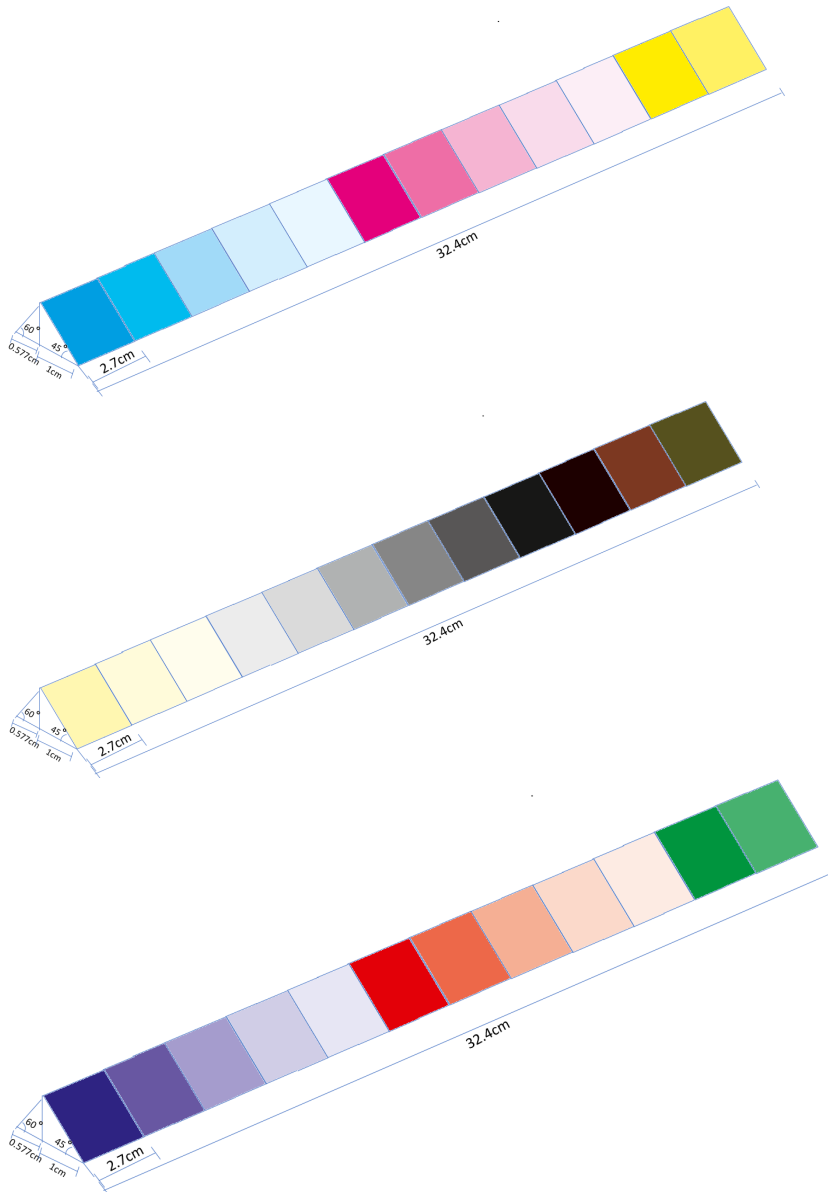
ANNEXURE 1 - AN EXAMPLE OF 45° WEDGE SAMPLE

Figure2: FOGRA Media Wedge Tiff V3.0 printed on 45° and 60° wedges height 1cm, sharing the height axis and the same surface colour.

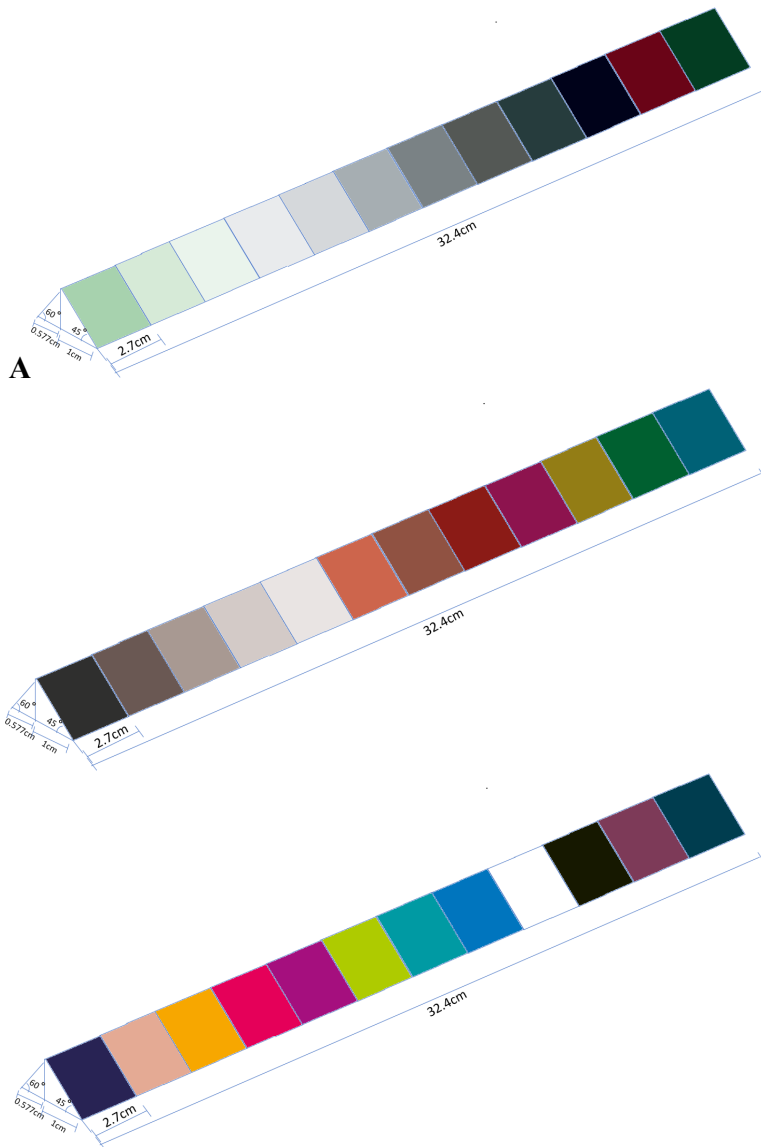


Figure2: FOGRA Media Wedge Tiff V3.0 printed on 45° and 60° wedges height 1cm, sharing the height axis and the same surface colour.

ANNEXURE 2 - FOGRA MEDIA WEDGE TIFF V3.0

Table 1: CMYK Values of FOGRA Media Wedge Tiff V3.0

No.	C	M	Y	K	No.	C	M	Y	K
1	100	0	0	0	37	40	0	40	0
2	70	0	0	0	38	20	0	20	0
3	40	0	0	0	39	10	0	10	0
4	20	0	0	0	40	10	6	6	0
5	10	0	0	0	41	20	12	12	0
6	0	100	0	0	42	40	27	27	0
7	0	70	0	0	43	60	45	45	0
8	0	40	0	0	44	80	65	65	0
9	0	20	0	0	45	100	85	85	0
10	0	10	0	0	46	100	0	0	100
11	0	0	100	0	47	20	100	70	60
12	0	0	70	0	48	70	0	70	80
13	0	0	40	0	49	100	100	100	0
14	0	0	20	0	50	70	70	70	0
15	0	0	10	0	51	40	40	40	0
16	0	0	0	10	52	20	20	20	0
17	0	0	0	20	53	10	10	10	0
18	0	0	0	40	54	20	70	70	0
19	0	0	0	60	55	40	70	70	20
20	0	0	0	80	56	40	100	100	20
21	0	0	0	100	57	40	100	40	20
22	0	100	0	100	58	40	40	100	20
23	0	70	70	60	59	100	40	100	20
24	0	0	70	80	60	100	40	40	20
25	100	100	0	0	61	100	100	40	20
26	70	70	0	0	62	10	40	40	0
27	40	40	0	0	63	0	40	100	0
28	20	20	0	0	64	0	100	40	0
29	10	10	0	0	65	40	100	0	0
30	0	100	100	0	66	40	0	100	0
31	0	70	70	0	67	100	0	40	0
32	0	40	40	0	68	100	40	0	0
33	0	20	20	0	69	0	0	0	0
34	0	10	10	0	70	0	0	100	100
35	100	0	100	0	71	0	70	0	60
36	70	0	70	0	72	70	0	0	80

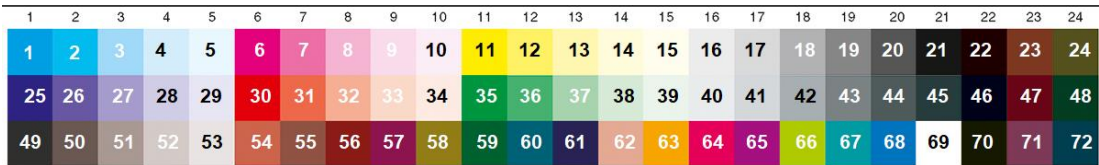


Figure 3: FOGRA Media Wedge Tiff V3.0

ISBN 978-82-326-7242-4 (printed ver.)
ISBN 978-82-326-7241-7 (electronic ver.)
ISSN 1503-8181 (printed ver.)
ISSN 2703-8084 (online ver.)



NTNU

Norwegian University of
Science and Technology